University of Messina

Department of Engineering

PhD Course in Engineering and Chemistry of Materials and Constructions

(XXIX cycle, 2014-2016)

Energy valorization of Sicilian agro-industrial residues by steam gasification

Doctoral Dissertation
(Messina – 2017)

PhD Candidate:

Mauro Prestipino

Coordinator

Prof. Signorino Galvagno

Supervisor

Prof. Lucio Bonaccorsi

Table of contents

ABSTRACT

Among the renewables primary energy sources, biomasses are promising candidates that are able to ensure programmable and constant energy production, while providing energy security, especially in rural areas where the access to energy infrastructures is limited. Agro-industrial activities represent important source of residual biomass that could be used as renewable feedstocks for energy purpose, enhancing local economies, while reducing residues/wastes landfilling. Among the different thermochemical biomass conversion technologies, gasification allows to produce a gas mixture (syngas), used for electricity generation, synthesis of liquid fuels and chemicals. Furthermore, it is also considered a preferable route for electricity production from small plants in remote areas, where gasification coupled with internal combustion engine systems are more convenient than combustion coupled with steam engine.

In order to realize and encourage the development of local bioenergy economies, further contributions to increase technical data and information about the feasibility of sustainable projects are of fundamental importance. From the above, the intent of this dissertation is to supply fundamental information and tools for the design of steam gasification reactors and systems fed by agro-industrial residues that are typical of the Sicilian economic network and residues from 2nd generation bioethanol production.

The first approach used for facing this issue consisted in the study of gas-solid reactions kinetics of steam gasification of different chars obtained from residual biomass. In addition, the kinetic parameters were also determined. The knowledge of steam-char kinetics is of fundamental importance in the design of efficient gasification reactors, since it results to be the controlling reaction when steam is used as gasifying medium. Thermogravimetric analysis showed that the different chars are characterized by different reaction profiles and different reactivity. The influence of ash-forming elements with catalytic (Ca, K) and inhibiting (Si, P) character was evaluated by introducing the *Inorganic Composition Ratio* (*ICR = (Ca+K)/(Si+P)*), in order to include in one index both catalytic and inhibiting elements. A good correlation was found between *ICR* and time of half conversion. It has been noticed that samples with similar *ICR* show similar reaction profiles and comparable time of conversion. In particular, the samples with *ICR* < 1 showed marked decelerating reaction profiles, while samples with *ICR* > 1 exhibited sigmoidal reaction mode.

It was further determined that, unlike to other authors, the presence of calcium could not be neglected in order to find an acceptable correlation between kinetic behavior and ash composition, which is the biomass characteristic that has the most influence on the char gasification kinetics. The kinetic study of various feedstocks is not only interesting for reactor design optimization, but it is also a useful tool for planning a proper supply chain for steam co-gasification of local residual biomass.

For instance, it was highlighted that in terms of conversion kinetic, the best feedstock integration for co-gasification could be made with orange peels and grape pomace. In addition, both residues from second-generation bioethanol showed a very similar reactivity.

The second approach consists in the development of a simulation tool that is able to supply preliminary information for the design of Combined Heat and Power (CHP) systems for energy valorization of agro-industrial residues. The study has been developed using Aspen Plus simulation software, which allows to develop evaluations about process feasibility and optimization of process parameters, in order to maximize the efficiencies, without the necessity to involve commercial-scale facilities. With this approach, it is possible to obtain useful data for the proposed system optimization, while evaluating its sustainability and the potential of the application in a real context. The CHP system that has been studied consisted in the combination of Solid Oxide Fuel Cell (SOFC) with a citrus peel gasificator (using air and steam as oxidants), which used residues from the citrus juice production as fuel. The scope of the feasibility study was to determine the energy balance of the process and verifying the possibility of self-producing the heat required for the drying step, being this the most energy-demanding one. A zero-dimensional simulation model, using Aspen Plus simulation software, was used to analyze the combined system. Mathematical model of the gasification unit was experimentally validated by lab-scale experiments, while the SOFC model was validated with data available in literature. After the stand-alone models validation, the two units' models were integrated in order to simulate the scale-up of the CHP system, which was able to generate an output of 120 kW DC. Hence, the required feedstock flow-rate and the system energy performances were evaluated. Results showed that 77.2 kg/h of dry biomass (0% H_2O) are required in order to produce the syngas necessary to feed the 120 kW DC SOFC unit. If 7,000 h of operational year are considered, the total amount of wet citrus peel with 82% of water content (as it comes out from the extraction process and before the mechanical drying) will be about 429 kg/h and 3,003 t/year, with the possibility to produce 580 MWhe. This information revealed the potential of energy production from a single citrus juice company, which is about 0.193 MWhe/t. Furthermore, it was also possible to find the amount of CO_2 savings, that is 189 t/year, considering biomass as a carbon neutral fuel.

It can be concluded that by using a simulation model, it was possible to understand the potential of citrus residues energy valorization through the integration of gasification process with a solid oxide fuel cell, the process sustainability, while some of the operative conditions were optimized.

SOMMARIO

Tra le fonti di energia primaria rinnovabile, le biomasse risultano essere candidati promettenti in grado di garantire una costante e programmabile produzione di energia, provvedendo al contempo alla sicurezza energetica, in particolare nelle aree rurali dove l'accesso alle infrastrutture energetiche può essere limitato. Le attività manifatturiere del settore agro-industriale rappresentano una importante risorsa di biomasse residuali da poter utilizzare come materie prime rinnovabili a scopi energetici, favorendo lo sviluppo di economie locali, riducendo al contempo la quantità di rifiuti da destinare a discarica. Tra le diverse tecnologie di conversione termochimica delle biomasse, la gassificazione permette di produrre una miscela di gas (syngas) che può essere impiegata per la produzione di energia elettrica, la sintesi di combustibili liquidi e chemicals per l'industria chimica. Inoltre la gassificazione è da preferirsi per la produzione di energia elettrica in impianti di piccola scala, per i quali la gassificazione accoppiata a motori a combustione interna risultano essere più efficiente rispetto alla combustione diretta della biomassa accoppiata a mini turbine a vapore.

Allo scopo di incoraggiare lo sviluppo di bio-economie locali, è di fondamentale importanza la produzione di contributi tecnici utili alla valutazione della sostenibilità di nuovi progetti. Da quanto sopra esposto, l'obiettivo del presente lavoro di tesi è fornire informazioni e strumenti base per la progettazioni di reattori e sistemi di gassificazione con vapore acqueo, alimentati da scarti agro-industriali tipici del tessuto economico siciliano e residui della produzione del bioetanolo di seconda generazione.

Il primo approccio a questo argomento ha riguardato lo studio della reazione gas-solido di steam gasification di char ottenuti da differenti biomasse residuali, ottenendo in fine i parametri cinetici del processo globale. Lo studio della cinetica della reazione steam-char è di fondamentale importanza per il design di reattori efficienti, in quanto questa risulta essere la reazione che controlla il processo quando viene utilizzato vapore come mezzo di gassificazione. Le analisi termogravimetriche hanno mostrato che differenti char sono caratterizzati da differenti profili di reazione e differenti reattività. L'influenza dei metalli costituenti le ceneri, sia con azione catalitica (Ca e K) che con azione inibente (Si e P), è stata valutata grazie all'introduzione dell'*Inorganic Composition Ratio* (*ICR* = *(Ca+K)/(Si+P)*), in grado di considerare contemporaneamente in un unico indice gli elementi ad azione catalitica ed inibente. E' stata riscontrata una buona correlazione tra l'indice *ICR* e il tempo necessario a raggiungere il 50% della conversione, notando simili profili di reazione e un comparabile tempo di conversione tra char con simili valori di *ICR*. In particolare, i char con *ICR* < 1 hanno mostrato una evidente modalità di conversione di tipo decelerativo, mentre i campioni con *ICR* > 1 hanno mostrato un profilo di tipo sigmoidale. Al contrario dell'approccio usato da altri autori, è stato inoltre evidenziato come il contributo del calcio non possa essere trascurato per poter ottenere una

correlazione accettabile tra comportamento cinetico e composizione delle ceneri. Quest' ultima risulta infatti essere la caratteristica dei char che più influenza la cinetica di reazione.
L'interesse dello studio della cinetica di reazione di diverse biomasse non è solo legata alla progettazione dei reattori, ma risulta anche di primaria importanza per la pianificazione del più opportuno programma di approvvigionamento, soprattutto nel caso di co-gassificazione di più biomasse residuali locali. Per esempio, nel presente studio è stato evidenziato che la migliore integrazione per la co-gassificazione, tra le biomasse residuali studiate, si può ottenere tra il pastazzo di agrumi e le vinacce, almeno in termini di comportamento cinetico. Inoltre, entrambi i residui della produzione del bioetanolo di seconda generazione hanno mostrato una reattività molto simile.

Il secondo approccio utilizzato nello svolgimento di questo lavoro consiste nella realizzazione di uno strumento di simulazione in grado di fornire informazioni preliminari per la progettazione di sistemi di cogenerazione per la valorizzazione di residui agro-industriali. Lo studio è stato svolto attraverso l'utilizzo del software di simulazione Aspen Plus, il quale permette di svolgere valutazioni sulla fattibilità e l'ottimizzazione di diverse tipologie di processi, al fine di massimizzare le efficienze senza la necessità di coinvolgere impianti di grande scala. Con questa tipologia di approccio è possibile ottenere dati utili per l'ottimizzazione del sistema proposto, valutarne la sostenibilità e le potenzialità dell'applicazione in contesti reali. Il sistema di cogenerazione che è stato studiato consiste nella combinazione di fuel cells ad ossido solido (SOFC) con un gassificatore, utilizzante aria e vapore come agenti gassificanti ed alimentato da pastazzo di agrumi ottenuto dal processo di estrazione dei succhi di agrumi. Lo scopo dello studio di fattibilità è stato quello di determinare il bilancio energetico del processo di valorizzazione energetica di tali scarti e verificare la possibilità dell'autoproduzione del calore richiesto per la fase di essiccazione della biomassa, essendo questo lo step più energivoro dell'intero processo. Un modello di simulazione zero dimensionale è stato utilizzato per l'analisi del sistema combinato proposto. Il modello matematico dell'unità di gassificazione è stata validata sperimentalmente tramite un impianto in scala laboratorio, mentre il modello della SOFC è stato validato tramite dati di letteratura. Dopo la validazione dei singoli modelli separati, questi sono stati integrati al fine di simulare lo scale-up del sistema proposto, in grado di produrre 120 kW DC (direct current) di output elettrico. Dunque, sono state valutate la portata della biomassa necessaria ad alimentare il gassificatore e le performance energetiche delle singole unità e del sistema integrato. I risultati hanno mostrato che sono necessari circa 77.2 kg/h di biomassa secca (0% H_2O) per poter produrre il syngas necessario ad alimentare l'unità SOFC da 120 kW DC. Se si prendono in considerazione 7,000 h di funzionamento annue, la quantità totale di scarto di produzione con l'82% di umidità (così come si ottiene dal processo produttivo priva dell'asciugatura meccanica e termina) è circa

429 kg/h e 3,003 t/anno, con una potenzialità di produzione di circa 580 MWhe. Dunque, lo strumento di simulazione ha dimostrato le potenzialità di valorizzazione energetica degli scarti di produzione di un'azienda che produce succhi di agrumi, il cui potenziale energetico specifico risulta circa 0.193 MWhe/t. E' stato inoltre possibile valutare la quantità di CO_2 risparmiata, risultando circa 189 t/anno, considerando la biomassa come un combustibile *carbon neutral*.

Acknowledgments

I would like to thank my supervisor, Prof. Lucio Bonaccorsi, and Dr. Antonio Galvagno for guiding me through the PhD course, supporting the research activity and my ideas with their experience.
Special thanks to the PhD course coordinator, and former Faculty Dean, Prof. Signorino Galvagno, who always was a reliable guide for all the students.
I gratefully acknowledge Prof. Anders Brink, my supervisor at Åbo Akademi University in Finland, who gave me the opportunity to spend three very important months of my PhD course, working in an international environment.
I would also like to thank the BCT research group led by Dr. Vitaliano Chiodo, at CNR – ITAE in Messina, where I carried out the research activities related to the fluidized bed gasification.

In addition, I would like to thank my parents, who supported my choices and gave me the possibility to achieve my goals. They also taught me the importance of hard work and I am very grateful for this.

The last but not the least, special thanks to my beloved Emy. She is my partner in studies, in work and life. Her invaluable support and comprehension have been of fundamental importance.

Mauro Prestipino

1. Introduction

The global population growth is closely linked with the economic growth in developing countries [1.1]. This phenomenon leads to the increase of global primary energy demand and environmental issues. For these reasons, especially in the last two decades, public sensitivities are focused on finding sustainable pathways for energy production, trying to reduce fossil fuels dependency. Among the renewables primary energy sources, biomass are promising candidates able to ensure programmable and constant energy production, while providing energy security to rural areas where the access to energy infrastructures is limited [1.2; 1.3]. Moreover, biomass use is a very versatile solution for conversion of primary energy. In fact, different sources of biomass, such as forest maintenance materials, dedicated crops and residues from agriculture, can be converted in different forms of fuels (liquid, solid and gas), using different technologies (thermochemical or biological) [1.4]. Despite several advantages, some issues have to be considered when assessing biofuel and bioenergy production, such as (i) land use change impact, (ii) water consumption and (iii) food security. Possible pathways that should be followed for a sustainable bioenergy production are marginal lands use for energy crops, exploitation of residues from wastes and forest maintenance [1.5].

Agro-industrial activities represent important source of residual biomass that could be used as renewable feedstocks for energy purpose, enhancing local economies and being a good path for reducing residues/wastes landfilling. Among the different thermochemical biomass conversion technologies, gasification allows to produce a gas mixture (syngas), used for electricity generation, synthesis of liquid fuels and chemicals [1.6; 1.7]. Furthermore, it is also considered a preferable route for electricity production from small plants in remote areas, where gasification coupled with internal combustion engine systems are more convenient than combustion coupled with steam engine [1.6; 1.7]. In particular, air/steam gasification allows to obtain higher syngas heating values because of the reduced amount of nitrogen and the higher hydrogen percentage through the enhancement of steam-carbon, water-gas shift and hydrocarbons steam reforming reactions [1.7]. Furthermore, the producer gas composition can be tuned varying the steam to biomass ratio (S/B) and Equivalence Ratio (ER) [1.7-1.12].

A further efficiency improvement in power production from biomass is syngas utilization in high temperature fuel cells [1.10]. These electrochemical devices directly convert chemical energy of fuels (such as mix of hydrogen, carbon monoxide and methane) in electrical energy. Such features make these devices, especially Solid Oxide Fuel Cells (SOFC), particularly suitable for syngas utilization in an efficient way without involving combustion. One limitation of traditional fuel cells utilization is that hydrogen is often produced from fossil fuels reforming [1.13-1.15]. On the opposite, through

residual biomass gasification it is possible to produce hydrogen rich syngas, which powers the fuel cell, while exploiting a renewable and sustainable source.

In order to make a preliminary study about the feasibility and sustainability of biomass valorisation projects, simulation models are of great interest, allowing time and costs savings while providing qualitative and quantitative information on processes [1.7]. Many authors using ASPEN Plus as simulation software [1.16-1.18] extensively discussed the usefulness of the process modelling in the field of bio-fuels or bio-chemicals production. There are different approaches for modelling thermochemical processes. Steady state models are the most used in literature because of their simplicity, mainly using approaches based on equilibrium and Gibbs free energy minimization methods [1.19-1.23]. Other authors use steady state approaches based on kinetic models [1.24-1.26] in order to predict gas composition after a finite time. A further detailed approach makes use of computational fluid dynamics (CFD) calculations for predicting temperature, composition and other parameters inside the reactor [1.27].

1.1. Italian renewable and bioenergy framework

Italy is the largest importer of electricity among the IEA European countries [1.28], so its energy security is still an important issue to be faced. In addition, the natural gas imports, mainly from North Africa and Eastern Europe, have a significant impact on this topic. For this reasons, the efforts of the Italian energy policies were also focused on the improvement on systematic energy savings programs and promotions of renewable energy production, especially for electricity generation. In fact, in 2015 the IEA estimation about the share of renewable energy was 18.2 % for total primary energy supply (TPES) and 40.2% for electricity generation [1.28], while the IEA average is 10% and 23.5%, respectively. The largest contribution to the renewable electricity generation is addressed to hydro and solar, being 15.6% and 9.3%, respectively. Biofuels and wastes contribute for 7.8 %, while wind and geothermal shares are 5.2% and 2.2%, respectively. Solar photovoltaic (PV) energy has registered a very rapid increase in the last decade because of dispensing of very generous incentives. This rapid increase in PV energy production implies a proper electrical grid balance. Bioenergy may play an important role among the renewable energy forms that are able to generate electricity in a predictable, constant and distributed way. Despite the relevant efforts in the last years for enhancing renewable energy, according to the IEA, "*it remains unclear what strategic direction policy making will take with the imminent expiration of economic support for a large part of renewable electricity technologies* [1.28]".

Regarding bioeconomy and biofuels in Italy, it seems that for the first time a systemic planning on bioeconomy strategy will be faced. On November 22nd 2016, a public consultation was opened on

the adoption of the Italian Bioeconomy Strategy, promoted by the Italian Presidency of Council Ministers. From the "Bieconomy in Italy" (BIT) consultation draft, what is apparent is that the potential of waste management in agricultural, forestry and municipal sectors are considered as fundamental to enable circular economy [1.29]. It stresses the importance of "locally routed value chains" for promoting sustainable growth in Europe and in the Mediterranean basin. The bieconomy strategy encompasses the conversion of bioresources and biowastes into added value products such as food, feed, bio-based products and bioenergy. The BIT draft underlines the relevant role that agriculture and agrifood industry play in the Italian economy context. As a consequence, the valorization of agricultural residues and wastes could take on a relevant role in a bioenergy national and international strategy. The huge variety of agricultural products and byproducts in the Italian territory implies that relevant efforts have to be done in the direction of a diversified bioresource exploitation, with the aim of the efficient integration of different bioproducts and biowastes. The biowastes from the principal agrofood industries in Italy is about 1.2 Mt/year of solid matter [1.30], referred to the residues of the transformation of tomatoes, potatoes, legumes, olives for oil production, citrus, and grapes for wine production. With a particular focus on the Sicilian case, about 99% of its share of agrifood industries wastes is represented by grape, citrus and olive pomaces, while they represent 93% of the Italian agrifood industries wastes [1.30; 1.31]. It is important to underline that the above data are referred only to the residues of raw materials processing. Grasses and woody residues from Italian agriculture activities are quantified in 10 Mt/year [1.30; 1.31].

With regard to biofuel, the global scenarios for alternative fuels by 2030 indicate that alternative fuels could represent 10-30% share of transport fuels. Italy is the fourth-largest producer of biodiesel and bioethanol in the EU [1.28]. In this field, the new decree for biofuels (October 2014) introduced the definition of "advanced biofuels", intending those fuels produced from residues and wastes. This, once again emphasizes the importance of wastes valorization and answers to the global concerns about the sustainability of biofuels production, being bioethanol the fastest growing biofuel [1.32]. Bioethanol can be produced by non-food lignocellulosic biomass, called 2nd generation bioethanol, such as wood, straw and reed, which substitute 1st generation bioethanol obtained from food biomass. If the target of biofuel incorporation at 10% of the energetic content will be pursued by 2020, the amount of lignin rich residues will be substantial. Moreover, the development of processes based on the principle of green chemistry and focused on the exploitation of polysaccharides, can be another large source of lignin-rich residues.

1.2. Scope of work

The reasons behind this research study come from both environmental and economic considerations. The development of local bioenergy economies, based on residues valorization, is a viable way for the reduction of waste production and landfilling. From the economic point of view, this approach can boost local enterprises and give additional incomes to rural areas from residues, the management of which often imply additional cost. Furthermore, the spread of energy valorization of local agro-industrial residues, coming from small and medium enterprises, enhances distributed renewable energy production, reduces centralized energy production from fossil fuels and favors energy security. In order to realize and encourage the development of local bioenergy economies, further contributions to increase technical data and information about the feasibility of sustainable projects are of fundamental importance. In accordance to the above mentioned reasons, the scope of this dissertation is to supply fundamental information and tools that are necessary for the design of steam gasification reactors and efficient CHP systems, fed by agro-industrial residues that are typical of the Sicilian economic network and residues from 2nd generation bioethanol production, which makes use of agricultural residues and non-food biomass. In particular, the selected agro-industrial residues were obtained from food processing, such as Citrus Peel (CP), Grape Pomace (GP), Olive Pomace (OP) and Reed. In addition, Reed Lignin (RL) and Straw Lignin (SL) from bioethanol production process has been used. The main reason beyond the selection of these residues relies in the fact that they are not still exploited enough, especially for power generation through thermochemical gasification.

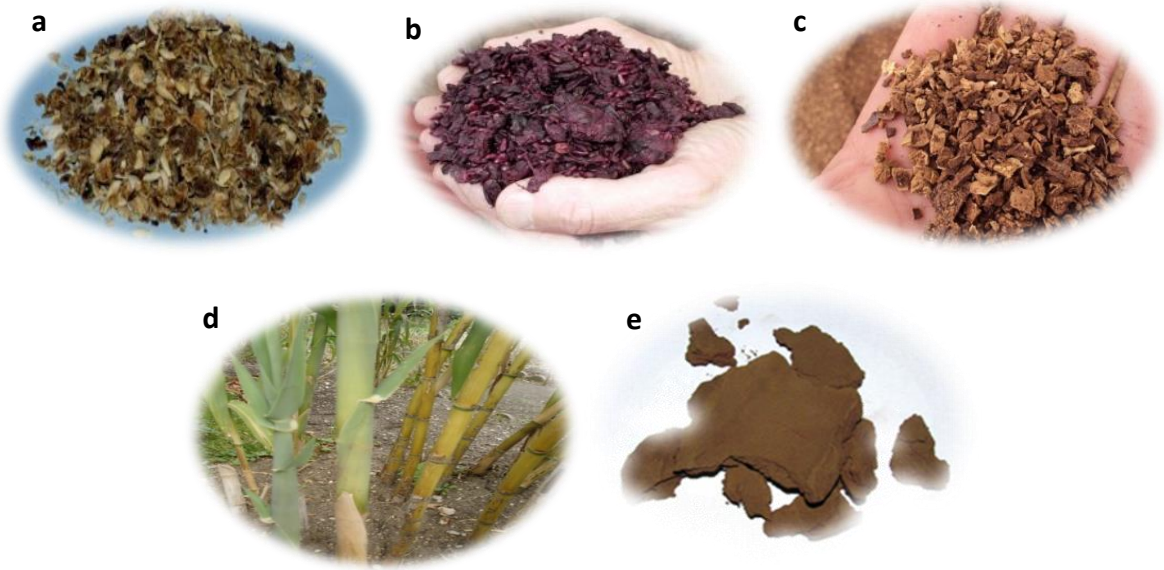

Figure 1. 1 Agro-industrial residue from Sicilian industries: Citrus Peel (a), Grape Pomace (b), Olive Pomace (c), Reed (d), Reed Lignin and Straw Lignin (e).

The first approach to the issue was to compare the gas-solid reaction kinetics of steam gasification of chars obtained from the above mentioned residual biomass, obtaining the kinetic behaviors and parameters. The knowledge of steam-char kinetics is of fundamental importance in the design of efficient gasification reactors, since it results to be controlling reaction [1.7; 1.33] when steam is used as gasifying medium. Various authors [1.33; 1.34] verified that kinetics of char steam gasification may vary considerably with the biomass even when chars are prepared with the same methods. The interest of kinetic study of various feedstock is not only related to reactor design optimization, but it is also of primary importance for planning a proper supply chain for steam co-gasification of local residual biomass. The topic of the kinetic study is further discussed in Chapter 2.

The second approach was to verify the potential application and the feasibility of a Combined Heat and Power (CHP) systems for energy valorization of agro-industrial residues, by means of a reliable and useful simulation model. Hence, the object of Chapter 3 is the investigation of the energy sustainability of a CHP system, in which a Solid Oxide Fuel Cell (SOFC) unit has been combined with a citrus pomace gasificator (using air and steam as oxidants). Indeed, operative conditions and syngas composition of the gasification process make air/steam gasification attractive in CHP generation systems with high temperature fuel cells, as SOFCs are. The study has been developed using Aspen Plus as simulation software, which allows developing evaluations about process feasibility and optimization of process parameters, in order to maximize the efficiencies, without the necessity to involve commercial-scale facilities. With this approach, it was possible to obtain useful data for process optimization and for the assessment of sustainability and potential of green technology application.

1.3. Thermochemical biomass conversion technologies

Biomass conversion processes for energy or fuel production consist in breaking down biomass molecules in into smaller ones, and further upgrading. These processes can be classified in two main categories: biochemical and thermochemical. The first category is characterized by slow conversion rates, low temperatures, while the molecules decomposition is made by means of bacteria or enzymes. As reported in Figure 1.2, typical biochemical processes are fermentation and digestions, both aerobic and anaerobic. The main products of anaerobic digestion are carbon dioxide and methane, forming the Biogas, while the main product of aerobic digestion (composting) is a solid digestate. Fermentation is a biochemical process which convert biomass into sugars through the action of enzymes or acid solutions. The sugar is further converted in alcohols or other chemicals by the action of yeasts. Thermochemical conversions are driven by thermal energy [1.35]. In fact, these processes take place in a range from medium to high temperatures (300-1200°C), either in absence or in presence of reactive gases.

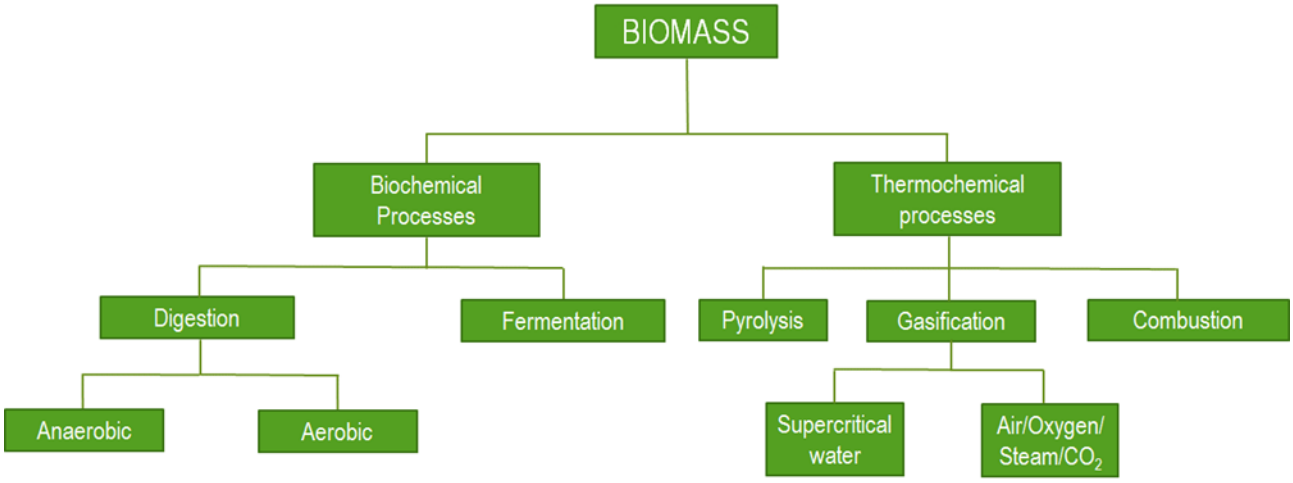

Figure 1. 2 Biomass conversion technologies

Pyrolysis conversions occur in absence of oxygen, at temperatures between 300°C to 600°C, obtaining a combustible gas, a carbonaceous solid (char) and a condensate as products. The global process results to be endothermic, whereby it is heated electrically or by mean of external burner fed by the produced gas. The latter is also known as syngas, and it is composed of H_2, CO, CO_2, CH_4 and other hydrocarbons. The yields of the different pyrolysis products can be tuned by acting on the process temperature and heating rate. Combustion is the thermochemical conversion that take place at high temperatures (800-1400°C) using excess of oxygen, obtaining thermal energy as main product. The products of complete combustion, H_2O and CO_2, are the main components of the product gas. In this case, the solid products of combustion is made by ash, that is the inorganic fraction of biomass. Unlike combustion, gasification takes place in an oxygen deficient environment [1.7], and

the main product is the syngas. This can be used in order to produce chemicals (e.g. Fischer-Tropsch synthesis of fuels) or for direct use in engines or fuel cells. Other products are obtained, such as tar and ash, being the condensate and the solid product. Within the ash, some carbon is also present because of the not complete conversion that may occurs. The tar is in many cases an undesired product, which can cause clogging problems of the lines or damages in the final user (internal combustion engines, gas turbines, fuel cells, etc.). Gasification process occur in the range of 600-1200°C, and the syngas composition can be tuned acting on the gasification agents (O_2, Air, CO_2, Steam) and the process temperature. The reactor type can also affect products yields and composition.

1.3.1. Biomass gasification

As mentioned above, gasification takes place in presence of a gasification medium. Usually, oxygen is fed within the gasification medium, in order to supply the heat required for the endothermic reactions. The amount of oxygen is defined by means of the equivalence ratio, ER, which is the ratio between the oxidant actually used in the process and the stoichiometric amount for biomass combustion [1.7]. The ER can be calculated according to the following equation [1.7]:

$$ER = \frac{O_{2,actual}}{O_{2,stech.}}$$

where $O_{2,stech.}$ and $O_{2actual}$ are the stoichiometric oxygen required for complete combustion and the oxygen actually used in the gasification process, respectively. Typically, in gasification process $0.2 < ER < 0.4$, while $ER > 1$ in case of combustion.

Since the biomass is fed at low temperatures (<100°C), biomass is subjected to a heating process with a finite heating rate. Hence, biomass moves through different conversion steps that occurs sequentially. These conversion steps are illustrated in Figure 1.3 [1.7] and listed below:

1) Drying.
2) Thermal decomposition (Pyrolysis).
3) Gasification of char and gas phase reactions.
4) Char combustion.

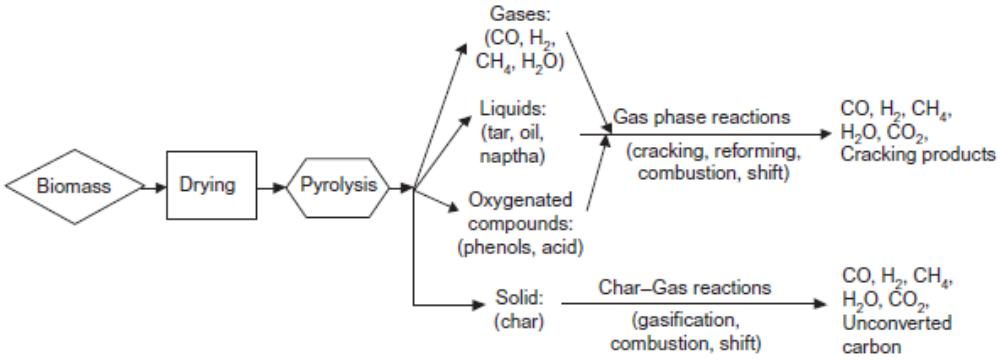

Figure 1. 3 Biomass conversion steps during gasification process [1.7]

Drying

Drying is the first step of conversion because it happen when the biomass enters the reactor, or it is going to enter. This consists in moisture evaporation, which takes place in the range between 70-150°C, and it is highly endothermic. In order to reduce the heat required for drying and to ensure sufficient heating values of syngas, the moisture content should be 10-20%$_{wt}$ [1.7].

Pyrolysis

Pyrolysis is a complex step that, like drying, takes place without the interaction with the gasification medium. This step involves the thermal breakdown of larger hydrocarbons molecules, obtaining a solid product, the char, and a mix of permanent gases and condensable vapors. The first are mainly hydrogen, carbon monoxide, carbon dioxide, methane and other light hydrocarbons. The seconds are made of heavy and complex hydrocarbons that form the tar. The pyrolysis step takes place starting from about 200°C, following various steps, until the gasification reactions start (~650-700°C). Globally, pyrolysis is considered as an endothermic process, whose heat is supplied by the exothermic reaction in the combustion step.

Gasification

The gasification of biomass occurs actually between the chars produced during pyrolysis and the gasifying medium. This step is characterized by heterogeneous reaction between char, steam, oxygen and carbon dioxide. The latter can be fed by the gasifying medium or can be the product of the following combustion step. Moreover, homogenous reaction in gas phase takes place, but the heterogeneous reaction are the most important for reactor design. Since char's reaction are the slower of the entire process, they result to be the controlling reactions of the gasification process.

The following reactions are the most important in the gasification step:

$C + CO_2 \leftrightarrow 2CO$	$\Delta H = 172.6$ kJ/mol	(r1)
$C + H_2O \leftrightarrow CO + H_2$	$\Delta H = 131.4$ kJ/mol	(r2)
$C + 2H_2 \leftrightarrow CH_4$	$\Delta H = -74.9$ kJ/mol	(r3)
$CO + H_2O \leftrightarrow CO2 + H2$	$\Delta H = -41.2$ kJ/mol	(r4)
$CH_4 + H_2O \leftrightarrow CO + 3H_2O$	$\Delta H = 201.9$ kJ/mol	(r5)

It can be noticed that there are some exothermic reactions. However, the process can be globally considered endothermic. Reactions 1 (Boudouard reaction) and 2 (water-gas) are the slowest reactions in the gasification step. When only air is fed into the reactor, the Boudouard reaction is the most important in the char gasification step. The CO formation from the Boudouard reaction is favored at higher temperature. As opposite, carbon dioxide and carbon deposition is favored at lower temperatures. It is important to underline that the rate of char gasification reaction in CO_2 is irrelevant below 700-725°C [1.7; 1.36; 1.37].

When steam is used as gasifying medium, the reaction with steam (r2 and r4) are of primary importance, and water-gas reaction results to be dominant with respect the Boudouard reaction [1.7; 1.36]. The presence of high hydrogen concentration (>30%) in the gasification atmosphere, could have a strong inhibiting effect on steam gasification reaction rates. Hence, it is recommended to continuously remove hydrogen from the reaction bed [1.7; 1.36]. Reaction r4 (shift reaction) occurs in gas phase between steam and carbon monoxide, giving hydrogen and carbon dioxide as products. The equilibrium yields of this reaction decrease as the temperature increase [1.7; 1.38], shifting the equilibrium towards reactants. This implies that lower temperatures give higher hydrogen content.

Combustion

The combustion step occurs in the reactor area that is close to the air entrance, where the temperature is also the highest (800-1200°C). The oxidative reactions that involves oxygen are the most exothermic. For this features they supply the required heat for the other endothermic steps. It follows that in an industrial scale gasifier, the reactor temperature is controlled by means of the ER, i.e. air flow rate. The higher is the ER, the higher is the reactor temperature.

Table 1.1 [1.7] gives a detailed overview of the reactions that occur in the whole gasification process, encompassing both combustion and gasification steps. During combustion step, both R4 and R5 in Table 1.1 takes place. Since their extent depends on the temperature , a partition coefficient was found in order to determine which reaction "is selected" by oxygen [1.7; 1.39]. Hence, the combustion equations of char may be combined as follow [1.7]:

$$C + O_2 \longrightarrow 2(\gamma - 1)CO + (2 - \gamma)CO_2 \qquad \text{(r1.6)}$$

where γ is a partition coefficient that was related to kinetic parameters and temperature through the following relation proposed by Laurendau [1.40].

$$\gamma = \frac{2\left(Ae^{\frac{-E}{RT}} + 1\right)}{Ae^{\frac{-E}{RT}} + 2}$$

Reaction Type	Reaction
Carbon Reactions	
R1 (Boudouard)	$C + CO_2 \leftrightarrow 2CO + 172$ kJ/mol[a]
R2 (water–gas or steam)	$C + H_2O \leftrightarrow CO + H_2 + 131$ kJ/mol[b]
R3 (hydrogasification)	$C + 2H_2 \leftrightarrow CH_4 - 74.8$ kJ/mol[b]
R4	$C + 0.5\ O_2 \rightarrow CO - 111$ kJ/mol[a]
Oxidation Reactions	
R5	$C + O_2 \rightarrow CO_2 - 394$ kJ/mol[b]
R6	$CO + 0.5O_2 \rightarrow CO_2 - 284$ kJ/mol[c]
R7	$CH_4 + 2O_2 \leftrightarrow CO_2 + 2H_2O - 803$ kJ/mol[d]
R8	$H_2 + 0.5\ O_2 \rightarrow H_2O - 242$ kJ/mol[c]
Shift Reaction	
R9	$CO + H_2O \leftrightarrow CO_2 + H_2 - 41.2$ kJ/mol[c]
Methanation Reactions	
R10	$2CO + 2H_2 \rightarrow CH_4 + CO_2 - 247$ kJ/mol[c]
R11	$CO + 3H_2 \leftrightarrow CH_4 + H_2O - 206$ kJ/mol[c]
R14	$CO_2 + 4H_2 \rightarrow CH_4 + 2H_2O - 165$ kJ/mol[b]
Steam-Reforming Reactions	
R12	$CH_4 + H_2O \leftrightarrow CO + 3H_2 + 206$ kJ/mol[d]
R13	$CH_4 + 0.5O_2 \rightarrow CO + 2H_2 - 36$ kJ/mol[d]

Table 1. 1 Typical reactions of gasification processes [1.7]

From the above steps description it is clear that every step is characterized by a specific temperature range. This imply that inside the reactors there is a temperature gradient and that the different zones can be identified, especially for the fixed bed reactors. Figure 1.3 makes clear the steps stratification in an updraft reactor, underlining the reactions for each step and the temperature variation along the reactor. It is evident how the inert environment of the pyrolysis step is ensured by the relatively low

temperature and by the presence of gasification and combustion hot gases, which are the products of complete oxygen conversion. The steps stratification and the characteristics of the other types of reactor will be explained in the following sections.

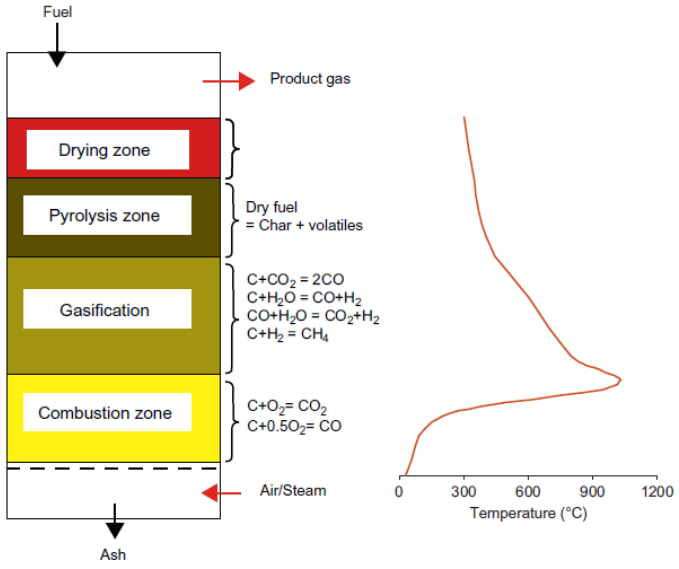

Figure 1. 4 Schematic of gasification steps and temperature profile in updraft reactor [1.7]

The gasifying medium reacts with the char and volatiles formed during the pyrolysis step, converting them into gases with low molecular weight like H_2, CO, CO_2 and CH_4. Since oxygen is almost always required in order to ensure the exothermic reactions, and considering that air is cheaper than pure oxygen, air is used as gasifying medium in most of commercial scale application of biomass gasification. This implies that N_2 is another important component of the syngas outlet stream. Nitrogen in the syngas has the effect of diluting the syngas and lower the heating value. If steam is used as gasifying agent, the water-gas and the shift reactions will become dominant, so the hydrogen production is enhanced. Usually, in commercial scale reactors, steam is fed in combination with air, with effect to increase the syngas heating values with respect to the sole air gasification. It follows that gasifying medium composition and its amount strongly affect the syngas composition. As the oxygen amount in the reactor's inlet stream increase, the CO_2 increases at the expenses of CO, while an increase of steam concentration leads to higher H_2 and CO_2 content, reducing CO concentration because of the shift reaction. Table 1.2 reports the effects of using different gasifying medium on syngas heating values [1.7; 1.41]. It has been already discussed that the equivalence ratio, ER, is a parameter that indicates the operating conditions of a biomass gasifier when air or oxygen are used. For steam gasification processes the steam to biomass ratio, S/B, is the parameter used to describe the operating conditions. S/B indicates the ration between steam and dry biomass mass rates. It should

pointed out that an excess of steam causes to the reduction of reactor's temperature and increases the heat required for steam generation, impacting negatively on the process energy balance.

Table 1. 2 Syngas heating values at different gasifying medium

Gasifying medium	Heating Value [MJ/Nm^3]
Air	4-7
Steam	10-18
Oxygen	12-28

1.3.2. Reactors for biomass gasification

Gasification of biomass makes use of a variety of chemical reactors, most of them were adapted from coal gasification technologies. The reactors can be classified according to the movement of the reactor bed and the direction of gas flow [1.42]:

- Fixed bed: updraft or countercurrent, downdraft or concurrent, and cross-draft
- Fluidized bed: bubbling bed, circulating and dual bed.
- Entrained flow

1.3.2.1. Fixed bed reactors

Fixed bed reactors are the oldest and the most reliable reactors because of their simplicity in management and construction [1.35; 1.43]. This type of reactors are also classified as moving bed reactor, because the biomass bed moves down in the reactor as a plug flow [1.7]. The particular attraction of fixed bed gasifier is the possibility to build them cheaply in small size [1.7; 1.41; 1.44], making them particularly attractive for distributed local energy production. The different gasification steps are clearly stratified along the reactor and can be clearly identified by mean the temperature profile of the reactor. Figure 1.5 [1.41] shows the simplified schematic of fixed bed gasifiers.

In updraft gasifiers (left side in Figure 1.5) biomass and gas flow in opposite direction. Biomass moves from the top to the bottom, while gasifying medium and syngas moves towards the top of the reactors.

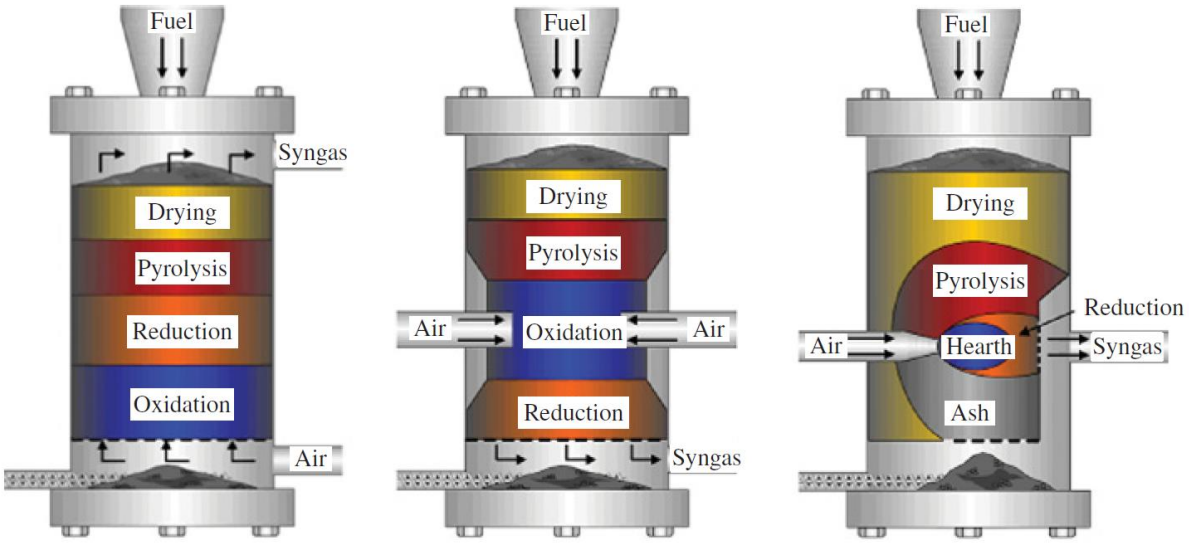

Figure 1. 5 Fixed bed gasification reactors, Updraft (left), Downdraft (middle), Crossdraft (right) [1.41]

Updraft reactor is suitable for biomass with high ash content (up to 25%) and high moisture (up to 60%). The main drawback is the very high tar yield (30-150 g/Nm^3) [1.7]. In addition to the isssues related to syngas cleaning, the high tar content involve the reduction of gasification efficiency, because it has been reported that more than 20% of energy content of the syngas is kept in tar [1.45; 1.35]. The higher tar content is due to the specific design that entails syngas cooling in the pyrolysis section, where tar are produced.

In downdraft gasifiers (middle in Figure 1.5), this drawback is overlapped because pyrolysis products pass through zones at higher temperatures, with the effect of tar cracking. The tar amount is between 0.01 g/Nm^3 and 6 g/Nm^3 [1.7]. In this reactor, both biomass and syngas flow downward. As opposed to updraft reactor, in downdraft the air is supplied at a certain height by means of a set of nozzles, placed around the gasifiers [1.7; 1.44; 1.46]. For this particular configuration, the reduction zone, i.e. gasification zone, is in a lower level than combustion. Another advantage of downdraft gasifiers is the very short start-up time (about 20-30 minutes). The main drawback of this reactor is the high ash and particles content in the outlet stream, because of the gas outlet position. For this reason low-ash biomass are preferred, as well as too much smaller particle size is not desirable. Downdraft gasifier can be further classified in throated and throatless. The first present a reduced cross sectional area at a certain height in order to realize combustion in the narrowest part of the reactor, in order to achieve a uniform temperature distribution and to enhance the conversion of pyrolysis products by forcing them to pass through this narrow passage. An efficient design for downdraft gasification reactors consists in the building of an annular jacket around the reactor where hot syngas passes before leaving the rector. Flowing externally from the bottom to the top of the

reactor, the hot syngas transfer the heat to the vertical reactor's walls [1.44]. With this design, biomass with high moisture content can be treated more efficiently, enhancing drying and pyrolysis steps.

In Cross-draft gasifiers (right side of Figure 1.5) biomass and gasification agent flow in a perpendicular direction each other [1.41] and it releases the syngas from the sidewall. Because of the small reaction zone, this gasifier has a shorter start-up time (5-10 minutes) than downdraft. This features implies that it is suitable for fuels with low volatiles, while the position of syngas outlet needs low ash content. In fact, it is primarily used for gasification of charcoal.

Fixed bed reactors results to be not attractive for very big scale gasification (> 10 MW_{th} of biomass thermal input) [1.7; 1.41]. One reason could be addressed to the poor uniformity of temperature distribution inside these reactors in big scale applications.

1.3.2.2. Fluidized Bed reactors

Fluidized bed reactors has been widely exploited in the field of coal conversion, both for combustion and gasification. Then has proved to be suited also for biomass gasification. They consists in bed of inert or catalytic particles that are moved under the action of a fluidization agent, coinciding with the gasification agent, which passes through the bed with a specific velocity. The latter is calculated in order to be enough to keep the bed material in a semi-suspended condition [1.7; 1.35]. Fluidized bed are well known for their excellent mixing and temperature uniformity, which represent their majors advantages [1.7; 1.41]. This type of reactor can be of three basic types: Bubbling Fluidized Bed (BFB), Circulating Fluidized Bed (CFB) or Dual Fluidized Bed (DFB). Figure 1.6 gives a schematic representation of the three reactors types [1.41].

In BFB gas velocity is above the minimum fluidization velocity, but below the maximum terminal velocity, with typical gas velocity are in the range 0.5-3 m/s [1.41]. Biomass is fed from the side, in the lower part of the reactor, while the fluidization medium is fed from the bottom of the reactor. The syngas leaves the reactor from the top and passes through a cyclone that removes ash and particles from the syngas stream. In BFB, the majority of gasification reaction occur in the reactor's core, that is the area with constant cross sectional area and where the reactor bed is moving. Other gas-phase and cracking reactions take place in the free board, the reactor zone with higher cross sectional area. In this part, almost all particles fall back down in the bubbling bed.

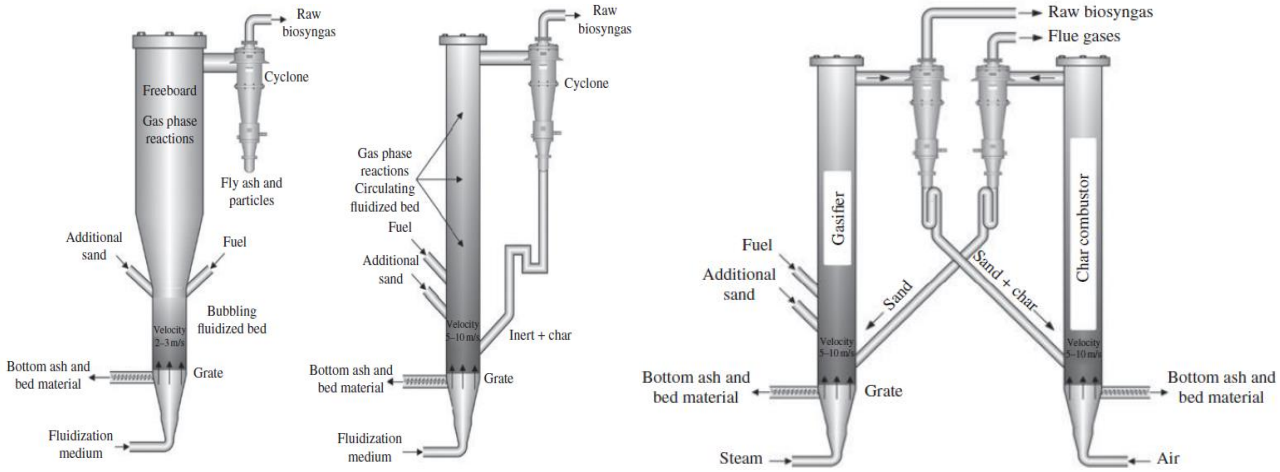

Figure 1. 6 Schematic of fluidized bed gasifiers: bubbling fluidized bed (left), circulating fluidized bed (middle), dual fluidized bed (right) [1.41].

CFB reactors (middle of Figure 1.6) make use of a recirculation system that allows recirculating the unconverted char, ash and particles that are removed from the gas stream thorough the cyclone. In this case, particles recirculation is obtained with gas velocity higher than in BFB, aiming for higher carbon conversion degree.

Dual fluidized bed reactors (right side of Figure 1.6), also known as interconnected reactors, are attracting a lot of interest because they separate the gasification step from the combustion one. The gasification reactor is fed with fuel and steam, while the combustion reactor is fed with air and with unconverted char from the gasification reactor. Flues gases from combustion chamber leave the reactor without mixing with the syngas, avoiding syngas dilution by nitrogen and achieving very high heating values. The char combustor reactor recirculate the hot sand into the gasification reactor, in order to provide the required heat.

Tar production in fluidized bed reactors is typically between downdraft and updraft gasifiers (~1g/Nm^3).

1.3.2.3. Entrained flow reactors

Entrained flow gasifiers are concurrent plug-flow reactors where gas and fuels moves together with very short resident time. In order to ensure the entrained conditions, the fuel must be in pulverized form. These reactors are only used for very large scale applications (>100 MWth). The typical gasification temperature is above 1000°C, allowing almost tar free syngas and carbon conversions very close to 100% [1.7]. The high temperature further implies that ashes are melted and produced as slag and methane concentration is almost negligible because of the enhancement of cracking reactions. The drawbacks are related to the sustainability of the process, because high temperature means high oxygen flow rates. Furthermore, pulverization of fibrous materials, like

lignocellulosic biomass, is not easy and requires a lot of energy. In addition molten ash from biomass can corrode the gasifier because of the presence of alkali compounds [1.7]. At the light of these shortcomings, entrained flow reactors are not popular for biomass gasification.

1.3.2.4. Reactor selection

Figure 1.7 [1.41] shows the different gasification technologies and the respective scales. The proper gasification technology evaluation with regard to the scale is the first step in the process for gasification technology selection. For small and decentralized plants, fixed bed reactors could be the best choice because they are easy to handle and cheap. If the biomass input is > 4 MW_{th}, BFB could be also selected. Then, it is necessary to consider the physical and chemical properties of biomass, such as water and ash content, and the feasibility of optional pretreatments that could be necessary with some gasifiers. Additionally, biomass gasifiers should be able to manage eventual changes in fuel supply [1.41]. Biomass with high moisture content could be handled by updraft gasificator, while if the moisture content is < 20% also downdraft gasifiers could be considered for small size plant.

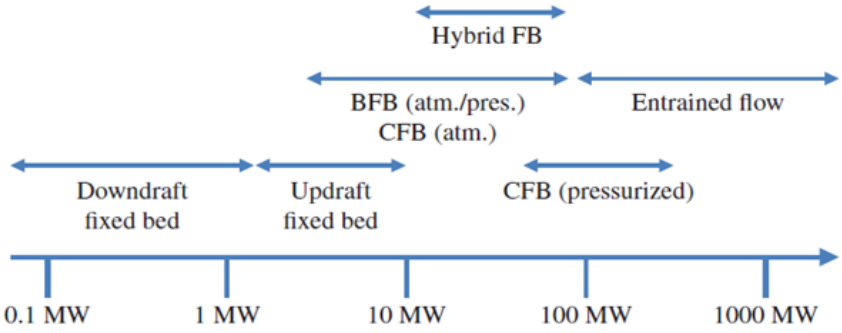

Figure 1. 7 Gasification reactors and scale of application (in terms of biomass input) [1.41]

Besides to moisture, also ash content could play an important role in reactor selection. Agricultural residues are often characterized by high ash content with high amount of alkali metals (K, Na), which may cause ash agglomeration [1.7; 1.41]. Fixed bed reactors could be more sensitive to this problems because of the static condition of the bed, which favors particle agglomeration, even if agglomeration in fluidized bad can cause serious problems, like bed de-fluidization [1.47]. On the other hand, some solution to control ash and bed agglomeration can be applied, like a proper bed material selection [1.47]. While facing ash handling issues, temperature is another process variable that should be considered. In fact, it is well known that higher temperatures favors ash agglomeration.

Furthermore, according to the final use of syngas, the gasifier should be selected according to the desired syngas composition and purity. In this sense, tar in the syngas stream is the major issue that needs to be faced. The allowed tar levels are 0.05 g/Nm^3 for gas engines, 0.005 g/Nm^3 for gas

turbine, and 0.001 g/Nm^3 for fuel cells. It follows that updraft is not the best suited reactor for direct syngas utilization for power production. Otherwise, extensive and expensive syngas cleaning steps are needed.

1.3.3. Syngas end use and power generation

The first use of biomass gasification (BG) was for fuel gas or chemical feedstock production [review brit], in order to substitute or integrate petrochemical processes. Afterwards, progress in gasification technology and the increased potential of poly-generation concept made it very suitable for co-generation of electricity and other useful products (SNG, biofuels…) and/or heat. This approach allowed optimizing energy and economical performances and sustainability, increasing the interest in these technologies.

In recent years, BG reduced the gap with conventional combustion for power generation. According to Sikarwar et al. these advances are due to legislation changes and the simplicity of the application rather than economic advances [1.44]. The syngas stream clean-up is still the most costly step of biomass gasification, thereby limiting the application of syngas for those reactors that have high tar yields. Combustion of syngas within a boiler could be a viable option in case of low quality product gas. However, electricity production through this system are characterized by low efficiency (~ 20%) [1.44; 1.48]. Conventional gas engines has been proven as affordable and reliable technologies for decentralized energy production, due to their compact structure and the possibility to easy heat recovery from the engine cooling section and from the exhaust gases. The adaptation of this technology to syngas utilization made biomass gasification for combined heat and power (CHP) very attractive. Nevertheless, the syngas heating value is lower than that of natural gas, leading to a power loss, since the cylinder volume remains constant. In order to overcome this problem, some authors suggested to enhance the compression ratio. This solution is limited by the increase potential for vibrations and knocking [1.44] that could damage the engine. In fact, very high hydrogen content in the engine's combustion chamber is the favors these phenomena. Some gas engine manufacturer, introduced modifications to the engine control system in order to reduce the knocking effect, allowing for pushing the maximum hydrogen content limits.

The good efficiency of CHP systems drove the development of biomass gasification technologies. This implicates that plants should be placed close to an end user of the produced heat, limiting the location of cogeneration systems. Hence, small and medium decentralized plants result to be the best choice. Of course, the plant size is also dependent on a sustainable supply chain. Table 1.3 shows some examples of installed CHP plants,in which internal combustion engines are fed by biomass

syngas. It is interesting to notice that the plant that has dual fluidized bed reactor shows a very low nitrogen content, allowing the enhancement of lower heating value.

Table 1. 3 Some examples of experienced CHP plant fed by syngas

Plant	Harboøre (DK)	Yamagata (JP)	Nidwalden (CH)	Güssing (A)
Reactor type	Updraft (air)	Updraft (air)	Downdraft (air)	DFB (air/steam)
Electrical Output (kWe)	1500	1200	1200	2300
H_2 (%)	15-18	15-18	15	40
CH_4 (%)	3-5	3-5	2	10
CO (%)	25-28	25-28	18	24
CO_2 (%)	7-10	7-10	12	23
N_2 (%)	50-55	50-55	47	3
LHV (MJ/Nm^3)	6.8	6.8	5.4	10.5

Fuel cells (FC) are devices that are able to directly convert the chemical energy of fuel into electrical energy [1.41]. Several types of FC have been developed up to date, each of which operates with different fuels and at different temperatures. Molten Carbonate Fuel Cells (MCFCs) and Solide Oxide Fuel Cells (SOFCs), which operates at high temperatures (>600°C), admit mix of H_2, CO and CH_4 as fuel, while carbon dioxide is also admitted as inert gas, without compromising the cells functionality. However, SOFC type showed higher resistance to gas contaminants than MCFC, which is a critical point when is fueled by syngas from biomass [1.41]. It must be clarified that intensive syngas cleaning procedures are required to meet the requirements of a SOFC. The fuels enters the porous anode where is dispersed over the anode-oxide electrolyte and electrochemically oxidized. The anode is able to catalyze the chemical and electrochemical reactions while conducts the electrons towards an external circuit connected to the cathode. The latter distributes the oxygen at its interphase with the electrolyte while conducts the electrons from the external circuit in order to reduce oxygen molecules into oxides ions, which move to the anode thorough the anode. A schematic operation of a SOFC is shown in Figure 1.8.

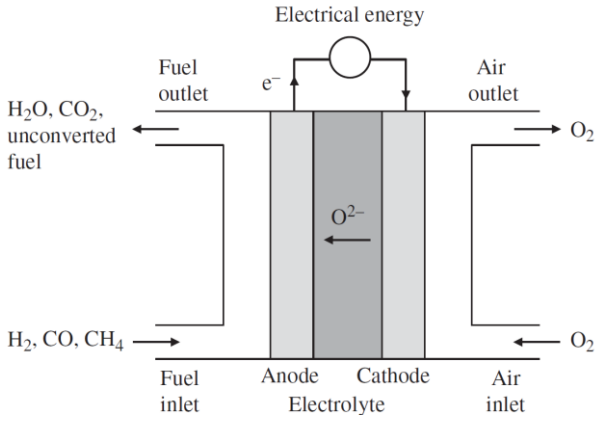

Figure 1. 8 Schematic of a Solid Oxide Fuel Cell [1.41]

Solid oxide fuel cell is a technology that already attracted high interest for efficient conversion of syngas from biomass. A SOFC typically work at temperatures between 600 and 100°C. The high operative temperature and the high tolerance towards contaminates, makes this type of fuel cells particularly suitable for integration with biomass gasifiers. Furthermore, SOFC can be used from very small applications (1 kW) up to some MW. The high temperatures of flue gases are useful for using the system in CHP mode. Different studies showed that the combination of biomass gasification with solid oxide fuel cells can give electrical efficiencies from 34% to 45% and CHP efficiencies from 74% to 80% [1.48 – 1.53].

Further increase of electrical efficiency can be achieved through the combination of biomass gasification-solid oxide fuel cells and gas turbine (GT) or micro gas turbine (MGT). The latter, can be fed by the unconverted fuel that is present the exhaust gas from the SOFC. The BG-SOFC-(M)GT system offers very efficient solutions also for small scale decentralized combined heat and power production.

References

[1.1] Population and sustainable development, UNITED NATIONS POPULATION INFORMATION NETWORK (POPIN), UN Population Division, Department of Economic and Social Affairs, with support from the UN Population Fund (UNFPA), INTERNATIONAL CONFERENCE ON POPULATION AND DEVELOPMENT, Cairo, Egypt, 1994. (http://www.un.org/popin/icpd/infokit/infokit.eng/6interre.html).

[1.2] S. Mazzola, M. Astolfi, E. Macchi, The potential role of solid biomass for rural electrification: A techno economic analysis for a hybrid microgrid in India, Applied Energy 169 (2016) 370-383.

[1.3] J. Schneider, C. Grubea, A. Herrmanna, S. Rönsch, Atmospheric entrained-flow gasification of biomass and lignite for decentralized applications, Fuel Processing Technology 152 (2016) 72-82.

[1.4] A. Demirbaş, Biomass resource facilities and biomass conversion processing for fuels and chemicals, Energy Conversion and Management 42 (2001) 1357-1378.

[1.5] M. Patel, X. Zhang, A. Kumar, Techno-economic and life cycle assessment of lignocellulosic biomass thermochemical conversion technologies: A review, Renewable and Sustainable Energy Reviews 53 (2016) 1486-1499.

[1.6] F. Pinto, R. N. Andrè, C. Carolino, M. Miranda, P. Abelha, D. Direito, J. Dohrup, H.R. Sorensen, F. Girio, Effects of experimental conditions and addition of natural minerals on syngas production from lignin by oxy-gasification: Comparison of bench and pilot scale gasification, Fuel 140 (2015) 62-72.

[1.7] P. Basu, Biomass Gasification, Pyrolysis and Torrefaction - Practical Design and Theory – Second Edition, (Oxford: Academic Press Elsevier 2013)

[1.8] M.Formica, S.Frigo, R.Gabbrielli, Development of a new steady state zero-dimensional simulation model for woody biomass gasification in a full scale plant, Energy Conversion and Management, 120 (2016) 358-369

[1.9] F. Wang, X. Zeng, Y. Wang, J. Yu, G. Xu, Characterization of coal char gasification with steam in a micro-fluidized bed reaction analyzer, Fuel Processing Technology 141 (2016) 2–8.

[1.10] Z.U. Din, Z.A. Zainal, Biomass integrated gasification-SOFC systems: Technology overview.

[1.11] A. Gomez, M. Vargas, N. Mahinpey, A theoretical model to estimate steam and CO_2 gasification rates based on feedstock characterization properties, Fuel Processing Technology 149 (2016) 187–194.

[1.12] J. H. Kihedu, R. Yoshiie, I. Naruse. Performance indicators for air and air–steam auto-thermal updraft gasification of biomass in packed bed reactor, Fuel Processing Technology 141 (2016) 93–98.

[1.13] G. Italiano, C. Espro, F. Arena, A. Parmaliana, F. Frusteri, Doped Ni Thin Layer Catalysts for Catalytic Decomposition of Natural Gas to produce hydrogen, Applied Catalysis A: General 365 (2009) 122–129.

[1.14] F. Frusteri, G. Italiano, C. Espro, C. Cannilla, G. Bonura, H_2 production by methane decomposition: Catalytic and technological aspects, International Journal of Hydrogen Energy, 37 (2012) 16367 - 163374

[1.15] Th. Damartzis, S. Michailos, A. Zabaniotou, Energetic assessment of a combined heat and power integrated biomass gasification–internal combustion engine system by using Aspen Plus, Fuel Processing Technology 95 (2012) 37–44

[1.16] H. Zheng, N. Kaliyan, R. V. Morey, Aspen Plus simulation of biomass integrated gasification combined cycle systems at corn ethanol plants, Biomass and Bioenergy 56 (2013) 197-210

[1.17] J. Matthew, R. De Kama, R. V. Morey, G. D. Tiffany, Biomass Integrated Gasification Combined Cycle for heat and power at ethanol plants, Energy Conversion and Management 50 (2009) 1682–1690

[1.18] C. Chen, Y.-Q. Jin, J.-H. Yan, Y. Chi , Simulation of municipal solid waste gasification in two different types of fixed bed reactors, Fuel 103 (2013) 58–63

[1.19] Babu BV, Sheth PN. Modeling and simulation of reduction zone of downdraft biomass gasifier: effect of char reactivity factor. Energy Conversion Management, 2006 ; 47:2602–11.

[1.20] Giltrap DL, McKibbin R, Barnes GRG. A steady state model of gas–char reactions in a downdraft gasifier. Sol Energy 2003; 74:85–91.

[1.21] Shabbar S, Janajreh I. Thermodynamic equilibrium analysis of coal gasification using Gibbs energy minimization method. Energy Conversion Management, 2013;65:755–63.

[1.22] Sharma AK. Equilibrium modeling of global reduction reactions for a downdraft (biomass) gasifier. Energy Conversion Management 2008; 49:832–42.

[1.23] Melgar A, Pe´rez JF, Laget H, Horillo A. Thermochemical equilibrium modeling of a gasifying process. Energy Convers Manage 2007; 48:59–67

[1.24] Nikoo MB, Mahinpey N. Simulation of biomass gasification in fluidized bed reactor using ASPEN PLUS. Biomass Bioenergy 2008;32:1245–54.

[1.25] Saravanakumar A, Hagge MJ, Haridasan TM, Bryden KM. Numerical modeling of a fixed bed updraft long stick wood gasifier. Biomass Bioenergy 2011;35:4248–60.

[1.26] Inayat A, Ahmad MM, Abdul Mutalib MI, Yusup S. Process modeling for parametric study on oil palm empty fruit bunch steam gasification for hydrogen production. Fuel Process Technol 2012;93:26–34

[1.27] D. Baruah, D.C. Baruah, Modeling of biomass gasification: A review. Renewable and Sustainable Energy Reviews; 39 (2014) 806-815.

[1.28] International Energy Agency, Energy Policies of IEA Countries – Italy- 2016 Review (2016), https://www.iea.org/publications/freepublications/publication/energy-policies-of-iea-countries---italy-2016-review.html, (20.12.2016)

[1.29] Bioeconomy in Italy – Consultation Draft, (2016), http://www.agenziacoesione.gov.it/opencms/export/sites/dps/it/documentazione/NEWS_2016/BIT/BIT_EN.pdf, (20.12.2016)

[1.30] Studio sull'utilizzo di biomasse combustibili e biomasse rifiuto per la produzione di energia, ISPRA – Istituto Superiore per la protezione e la ricerca ambientale, Roma, 2010, http://www.isprambiente.gov.it/it/pubblicazioni/rapporti/studio-sull2019utilizzo-di-biomasse-combustibili-e-biomasse-rifiuto-per-la-produzione-di-energia (18.03.2016).

[1.31] Censimento ISTAT Agricoltura 2010, http://dati.istat.it/Index.aspx?DataSetCode=DCSPCOLTIVAZ/, (16.04.2016).

[1.32] N.-O. Nylund, P. Aakko-Saksa, K. Sipilä, Status and outlook for biofuels, other alternative fuels and new vehicles. VTT – Research notes 2426, (2008).

[1.33] Dupont, C., Nocquet, T., Da Costa, J.A., Verne-Tournon, C., 2011. Kinetic modelling of steam gasification of various woody biomass chars: influence of inorganic elements. Bioresour. Technol. 102, 9743–9748.

[1.34] Moilanen, A., 2006. Thermogravimetric characterizations of biomass and waste for gasification processes. VTT, Espoo.

[1.35] W. Doherty, Modelling of Biomass Gasification Integrated with a Solid Oxide Fuel Cell System, DIT, Ireland, 2014.

[1.36] C. Di Blasi, Combustion and Gasification rates of lignocellulosic chars, Progress in Energy and Combustion Science 2009; 35; 121-140.

[1.37] C. Di Blasi, Modeling and simulation of combustion processes of charring and non-charring solid fuels. Prog. Energ. Combust. Sci. 1993, 19 (1), 71-104.

[1.38] G. K. Reddy, P. G. Smirniotis, Water Gas Shift Reaction: Research Developments and Applications, Elsevier, 2015.

[1.39] J.R. Arthur, Reactions between carbon and oxygen. Trans. Faraday Soc. 1951, 47, 164-178.

[1.40] N.M Laurendeau, Heterogeneous kinetics of coal char gasification and combustion, Progress in Energy and Combustion Science,Volume 4, Issue 4, 1978, Pages 221–270.

[1.41] Biomass as a sustainable energy source for the future : fundamentals of conversion processes, edited by Wiebren de Jong and J. Ruud van Ommen. Published by John Wiley & Sons, Inc., Hoboken, New Jersey (2014).

[1.42] Brown RC. Thermochemical Processing of Biomass: Conversion into Fuels, Chemicals and Power. Chichester (UK): John Wiley & Sons; 2011.

[1.43] Olofsson I, Nordin A, Söderlind U. Initial review and evaluation of process technologies and systems suitable for cost-efficient medium-scale gasification for biomass to liquid fuels. Umeå: Energy Technology & Thermal Process Chemistry, University of Umeå; 2005.

[1.44] V. Sikarwar,a M. Zhao, P. Clough, J. Yao, X. Zhong, M. Z. Memon, N. Shah, E. J. Anthonyf, P. S. Fennell, An overview of advances in biomass gasification, Energy & Environmental Science, 2016.

[1.45] Austermann S, Whiting K. Commercial Assessment: Advanced Conversion Technology (Gasification) for Biomass Projects. Juniper; 2007.

[1.46] E.B. Machin, D.T. Pedroso, N. Proenza. J.L. Silveira, L. Conti, L. Bollini Braga, A.B. Machin; Tar reduction in downdraft biomass gasifier using a primary method; Renewable Energy 78 (2015) 478-483.

[1.47] T. Lu, K.-Z. Li, R. Zhang, J.-C. Bi, Addition of ash to prevent agglomeration during catalytic coal gasification in a pressurized fluidized bed, Fuel Processing Technology 134 (2015) 414–423.

[1.48] S. Heidenreich, P. U. Foscolo, New concepts in biomass gasification, Progress in Energy and Combustion Science 46 (2015) 72-95.

[1.49] Bang-Møller C, Rokni M, Elmegaard B, Ahrenfeldt, Henriksen UB. Decentralized combined heat and power production by two-stage biomass gasification and solid oxide fuel cells. Energy 2013; 58:527-37.

[1.50] Doherty W, Reynolds A, Kennedy D. Computer simulation of a biomass gasification-solid oxide fuel cell power system using Aspen plus. Energy 2010; 35:4545-55.

[1.51] Nagel FP, Schildhauer TJ, McCaughey N, Biollaz SMA. Biomass-integrated gasification fuel cell systems e part 2: economic analysis. Int J Hydrogen Energy 2009;34:6826e44.

[1.52] Colpan CO, Hamdullahpur F, Dincer I. Solid oxide fuel cell and biomass gasification systems for better efficiency and environmental impact. In: Stolten D, Grube T, editors. Proceedings of the 18th World Hydrogen Energy Conference; 2010. pp. 305e13. ISBN 978-3-89336-651-4.

[1.53] Wongchanapai S, Iwai H, Saito M, Yoshida H. Performance evaluation of an integrated small-scale SOFC biomass gasification power generation system. J Power Sources 2012; 216:314-22.

2. Kinetic study of char steam gasification

2.1. Chapter Introduction

The importance of carrying out kinetic studies of biomass gasification is related to the absence of repeatability of biomass structure and composition [2.1,2.2], so it is necessary to investigate the conversion rate of each type of biomass that have to be used in thermochemical processes, aiming for efficiency. In a steam gasifier, the steam-char reaction is dominant with respect the other heterogeneous reactions. Hence, a good knowledge of this reaction is of fundamental importance for reactors using steam as gasifying agent. In this Chapter, the kinetic study of char gasification reaction in a steam/nitrogen atmosphere is presented for chars obtained from six agro-industrial residues. As mentioned in the Introduction Chapter, the residual biomass object of this study were Citrus Peel (CP), Grape Pomace (GP), Olive Pomace (OP), Reed (*Arundo Donax*) and residues from 2nd generation bioethanol industry, named as Reed Lignin and Straw Lignin. Hence, the kinetic behavior of chars obtained from these residues have been investigated. Thermogravimetric analysis (TGA), that is a common technique for carrying out kinetic studies of solid-gas reactions, has been used in this research activity. The first part of the Chapter introduces the chars' gasification rates and its dependences on biomass/chars characteristics. Then, a detailed theoretical background about methods and approaches to kinetics studies, through thermal analysis, has been realized in order to find the most reliable methods for the evaluation of kinetic parameters (activation energy, pre-exponential factor and reaction order) from thermogravimetric data. Since TG analysis gives integral data, the integral isoconversional (model free) method has been applied to this study. In the second part of the Chapter the experimental procedures are detailed. The study has been developed by mean of a TG analyzer after that characterizations of the parent residual biomass and respective chars were performed. Materials characterizations consisted in proximate and ultimate analysis of biomass, morphological analysis of chars through scanning electron microscopy (SEM) and gas adsorption isotherm analysis for the specific surface area determination through the BET (Brunauer-Emmett-Teller) equation. The main ash-forming elements were also determined in order to detect and quantify the presence of catalytic and inhibiting elements towards the solid-gas gasification reactions. With regard to thermogravimetric analysis, isothermal thermogravimetric runs were carried out in steam/nitrogen atmosphere. The effect of steam partial pressure was also evaluated by fixing the temperature and varying the steam concentration in gas stream. The third section shows the results of experimental activities and TGA data elaboration.

2.1.1. Introduction on biomass gasification rates

Solid particle conversion of biomass in gasification processes follows pyrolysis, when char is forming, and heterogeneous reactions of char. The latter step represents the gasification steps. The kinetic study of solid particles conversion is of fundamental importance in order to obtain data about the conversion rates for design purpose. Heterogeneous gasification reactions of char, being the slowest steps, are of particular interest. The gas phase reactants are mainly steam and carbon dioxide, which are responsible for the following reactions [2.2]:

$C_f + CO_2 \longrightarrow C(O) + CO$ (r1)

$C(O) + CO \longrightarrow C_f + CO_2$ (r2)

$C(O) \longrightarrow CO$ (r3)

The above reactions are related to the CO_2 gasification of char (Bouduard reaction), which takes place in the active carbon sites, C_f, and involves the formation of intermediate carbon-oxygen complex C(O). Reaction (2) shows the inhibiting effect of CO by lowering the C(O) concentration, and it has been studied in few research works [2.3,2.4,2.5,2.7]. When modeling the CO_2 gasification, the inhibiting effect is often neglected and the following global model is applied:

$C_f + CO_2 \longrightarrow 2\ CO$ (r4)

Steam – carbon reactions are of primary importance when assessing the gasification kinetics. Steam gasification involves even more complex mechanism than CO_2 gasification, because of the combined inhibiting action of hydrogen and carbon monoxide. The following reactions compose the complete steam gasification mechanism [2.2]:

$C_f + H_2O \longrightarrow C(O) + H_2$ (r5)

$C(O) + H_2 \longrightarrow C_f + H_2O$ (r6)

$C(O) \longrightarrow CO$ (r7)

$C_f + H_2 \longrightarrow C(H_2)$ (r8)

$C(H_2) \longrightarrow C_f + H_2$ (r9)

$C_f + ½\ H_2 \longrightarrow C(H)$ (r10)

$$C(H) \longrightarrow C_f + \tfrac{1}{2} H_2 \quad \text{(r11)}$$

The previous reactions show how the steam gasification of char is basically driven by oxygen exchange and hydrogen inhibition mechanisms [2.6, 2.7]. As same as for CO_2 gasification, for char steam gasification a simplified global mechanism is used:

$$C + H_2O \longrightarrow CO + H_2 \quad \text{(r12)}$$

In this work, both the CO_2 and steam global gasification reactions have been taken into account in order to describe the global conversion rates of solid particles.

The combined effects of different processes that involves the interaction between the gasifying agents and the solid particles may affect the char reactivity. The most relevant process are mass transfer of the gaseous reactants to the external surface of the particles, mass transfer inside the porous structure of particles, and the intrinsic kinetics of reactions [2.2, 2.8]. Hence, three different regimes can occur [2.9,2.10,2.11]. The regime I takes place when the temperature and particles are so small that the kinetic rate is much slower than the diffusion rate. Small particles (0.1 mm) and temperatures typically below 800°C [2.11] or 900°C [2.12] should be considered in order to neglect the diffusion effects. In this case, the particles conversion is kinetically controlled. Once the rate of gaseous species diffusion become comparable to the reaction rate, the limited penetration of the reactants leads to the intra-particle mass transfer controlled mechanism, the so-called regime II. In this case, the conversion occurs mainly on the external surface of the particle because the intra-particle mass transfer is the controlling step and consequently the reaction rate is proportional to the external surface of the particle [2.2]. Regime III is established when the controlling mechanism is the mass transfer from the bulk gas to the external surface of the particle. Low operating temperatures and low heating rates are also of fundamental importance in order to reduce the effects of heat transfer. It follows that in order to evaluate the intrinsic kinetics, this must be separated from mass and heat transfer effects, and conversion should occur in the regime I conditions.

Char reactivates and conversion rates are influenced by different intrinsic factors that are related to the inorganic matter composition (catalytic active sites), char structure (i.e. surface area and accessibility) and char composition (carbon active sites). The synergetic effects of all these features are not easy to be managed and considered together when assessing the kinetics models of particles conversion, even because of the variation of char properties during conversion. Hence, the most common approach is based on the evaluation of the global reactivity of the heterogeneous reactions [2.2], obtaining kinetic data and parameters that should be considered as global. Biomass structure and composition anyway have to be considered during the understanding process of different kinetic behaviors of different biomass source. For instance, the importance of catalytic action of inorganic

matter should not be overlooked, because it may considerably affect the biomass gasification rates. Alkaline (Na, K) and alkaline earth (Ca, Mg) metals, in forms of oxides or salts are considered as good catalyst for steam gasification of carbon [2.1, 2.13, 2.14]. A further confirmation of the catalytic activity of these metals can be found in literature where the effects of char demineralization thorough water or acid leaching were examined [2.15-2.21]. According to literature data, it seems like the inorganic matter has higher influence on reactivity then morphology the surface area [2.1].
The effect of morphology on gasification rates are related to the accessibility of the internal carbon through the porous channels of chars. It is to understand that higher surface areas leads to higher active sites availability and thus higher reaction rate. It has to be underlined that the gasification reactions occurs mainly on the surface of macro and mesopores [2.2], so the surface area measurements that include microporosity are not always correlated to a specific reactivity, despite it is largely adopted in char characterization. This has been confirmed also in this work. The surface area and porosity of chars are mainly affected by heating rate and temperature during pyrolysis. It has been verified that very high heating rates leads to high reactive chars.

2.1.2. Theoretical background on kinetic computations

Thermogravimetric analysis are useful routes to assess the rates of solid particle conversion. In fact, these methods are widely used for detailed kinetics studies of biomass and char conversion under different atmospheres.

Char reactivity is usually expressed according to the following expression:

$$r = -\frac{1}{m}\frac{dm}{dt} = \frac{1}{1-\alpha}\frac{d\alpha}{dt} \quad (1)$$

$$\alpha = \frac{m-m_t}{m_0-m_f} \quad (2)$$

where m is the actual mass, α the degree of conversion (or converted fraction), m_0 is the initial mass, m_t is the sample mass at time t, and m_f is the final value of sample mass when 100% of conversion is achieved. From the previous equations, it is trivial to understand the potential of thermogravimetric analysis for studying biomass and char reactivity.

The conversion rate can be expressed as a function of three major variables that are: temperature (T), degree of conversion (α) and partial pressure of gaseous reactants (P), according to the following equation:

$$\frac{d\alpha}{dt} = k(T)f(\alpha)h(P) \quad (3)$$

The temperature dependence, k(T), is known as reaction rate constant, and it is typically parametrized through the Arrhenius equation:

$$k(T) = Aexp\left(-\frac{E}{RT}\right) \quad (4)$$

where A and E are the pre-exponential factor and activation energy, respectively, and both are kinetics parameters, while R is the universal gas constant. The equation of Arrhenius dependence on temperature is often used in several kinetic studies on biomass gasification [2.1-2.22]. The pressure dependence h(P) expresses the correlation between the gaseous reactants concentration and the reaction rate, which may be strongly influenced by this parameter, especially for the reaction of oxidation and reduction [2.22], as in the case of biomass gasification. This variable is expressed in the form of power law:

$$h(P) = P^n \quad (5)$$

were n is considered as the reaction order, which is also the third kinetic parameter. The so called kinetic triplet (A, E and n) that are obtained experimentally, should be named "effective", "apparent" or "global", in order to underline that they might be different from those values that are strictly correlated to the intrinsic kinetics [2.22, 2.23]. This happens because of the difficulty to avoid the influences of thermal and mass diffusion or the interference of other conversion steps characterized by different kinetic behavior. The dependence of the process rate on the extent of conversion is expressed by f(α), which is the reaction model. This variable takes into account the mechanism by which the reaction rates varies with the extent of conversion. During biomass or char conversion, also the kinetic parameters could vary. The reaction model parameter includes the effects related to structural changes of chars, without making explicit the pore properties. In fact, the sole variable introduced in almost all the models is α [2.2]. For this features, the f(α) parameter, is also defined as the structural term of the conversion rate. A wide variety of reaction models has been proposed for describing the conversion dependence of conversion rate. The most frequently used for solid-state kinetics were reported by Vyazovkin et al. [2.22], shown in Table 2.1, where g(α) is the integral form of the reaction model, expressed as follow:

$$g(\alpha) = \int_0^{\alpha} \frac{d\alpha}{f(\alpha)} = AP^n \int_0^t \exp\left(\frac{-E}{RT}\right) dt \quad (6)$$

Table 2. 1 Set of reaction model use to describe thermal decomposition in solids [22]

	Reaction model	$f(\alpha)$	$g(\alpha)$
1	Power law	$4\alpha^{3/4}$	$\alpha^{1/4}$
2	Power law	$3\alpha^{2/3}$	$\alpha^{1/3}$
3	Power law	$2\alpha^{1/2}$	$\alpha^{1/2}$
4	Power law	$2/3\alpha^{-1/2}$	$\alpha^{3/2}$
5	One-dimensional diffusion	$1/2\alpha^{-1}$	α^{2}
6	Mampel (first-order)	$1-\alpha$	$-\ln(1-\alpha)$
7	Avrami–Erofeev	$4(1-\alpha)[-\ln(1-\alpha)]^{3/4}$	$[-\ln(1-\alpha)]^{1/4}$
8	Avrami–Erofeev	$3(1-\alpha)[-\ln(1-\alpha)]^{2/3}$	$[-\ln(1-\alpha)]^{1/3}$
9	Avrami–Erofeev	$2(1-\alpha)[-\ln(1-\alpha)]^{1/2}$	$[-\ln(1-\alpha)]^{1/2}$
10	Three-dimensional diffusion	$2(1-\alpha)^{2/3}(1-(1-\alpha)^{1/3})^{-1}$	$[1-(1-\alpha)^{1/3}]^{2}$
11	Contracting sphere	$3(1-\alpha)^{2/3}$	$1-(1-\alpha)^{1/3}$
12	Contracting cylinder	$2(1-\alpha)^{1/2}$	$1-(1-\alpha)^{1/2}$
13	Second-order	$(1-\alpha)^{2}$	$(1-\alpha)^{-1}-1$

All the reaction models can be grouped in three major classes, according to the reaction profile of α *vs* t (Figure 2.1) [2.22]: accelerating, decelerating and sigmoidal models. Accelerating models describe processes whose reaction rate increases with conversion (curve 1), reaching the maximum at the end of conversion process. This type of models are usually described by a power-law model:

$$f(\alpha) = m\alpha^{(m-1)/m} \tag{7}$$

The decelerating models represent reactions whose conversion rate reaches the maximum at the beginning of the process and it decelerates continuously, according to the common expression:

$$f(\alpha) = (1-\alpha)^{m} \tag{8}$$

The reaction models belonging to the sigmoidal group represent process that are composed by the combination of both accelerating and decelerating processes at the initial and final stages, respectively. The Avrami-Erofeev models typically represent the sigmoidal kinetic behavior:

$$f(\alpha) = m(1-\alpha)[-\ln(1-\alpha)]^{(m-1)/m} \tag{9}$$

When assessing kinetic behavior of solid particles conversion with thermal analysis, some precise requirement should be addressed in order to have high quality and reliable data. One issue in data processing is the choice between integral or differential data. This choice should as much as possible be dependent on the specific analysis. For instance, integral data are most suitable for TG analysis, while differential data should be selected for DSC analysis [2.22]. Starting from integral data, differentiation could amplify the noise, so that this option should be avoided. A typical example is represented by steam gasification TGA tests that are usually affected by noise in the TG data, suggesting that using differential data may not be the best solution. Data smoothing could be an option, but it should be used carefully in order to avoid the introduction of systematic errors.

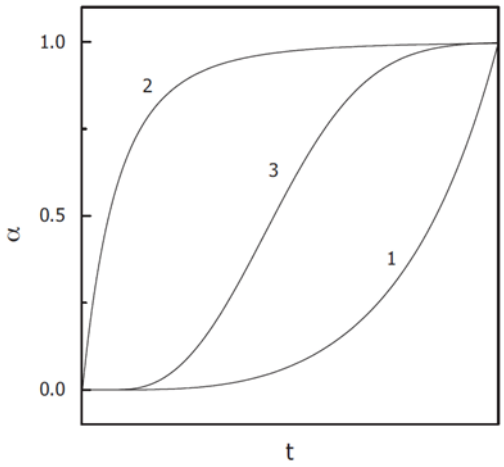

Figure 2. 1 *α vs t* reaction profiles for (1) accelerating, (2) decelerating, (3) sigmoidal models

Another key issue that has to be pointed out is the use of isothermal or constant rate run for kinetics studies. In the field of thermochemical biomass conversion, isothermal runs can not be applied to any situation. As an example, for biomass pyrolysis studies the heating time to a fixed temperature involves the loss of information related to the mass loss, even in inert atmosphere. Furthermore, pyrolysis process could involve several steps that are impossible to cover with isothermal runs. When assessing the kinetic mechanism of char gasification reactions through thermal analysis, the carbonaceous material tends to stabilize the mass under inert atmosphere until the operating temperature is reached. At this time the gasifying agent is send to the balance and the isothermal reaction can occur. In most of these processes the thermochemical conversion takes place in one step, as in the case when char is gasified in the presence of carbon dioxide or steam, so isothermal runs can be performed. It is important to stress the concept that during isothermal runs non-zero extent of conversion is reached during the non-isothermal step, involving unavoidable computational errors. Hence, the effects of these errors must be taken into account and carefully assessed. In case of constant heating rate experiments, the main disadvantage is represented by the difficulty to identify the different models [2.22]. The general suggestion of the ICTAC kinetic committee [2.22] is to consider the combination of isothermal and non-isothermal experiments, in order to exploit advantages of both methods.

Isoconversional methods are kinetic approaches that allow understanding how the kinetics behavior varies with the extent of conversion. These approaches are particularly useful for biomass gasification process, whose overall reaction mechanism involves complex processes within the same decomposition step [2.24]. Isoconversional methods starts from the application of the isoconversional principle to Eq.(3), stating that the reaction rate at constant extent of conversion is only function of temperature [2.22, 2.23, 2.25]. According to this principle, from Eq.(3) follows that:

$$\left[\frac{dln(d\alpha/dt)}{dT^{-1}}\right]_{\alpha} = \frac{-E_{\alpha}}{R} \quad (10)$$

These methods are further defined as "model-free", because from Eq.(10) it follows that isoconversional values of activation energy can be determined through the isoconversional rate without assuming any particular reaction model.

It is possible to distinguish two different isconversional methods: the differential and the integral ones. The most common differential isoconversional method applies the isoconversional principle to Eq. (3), so that the following equation is obtained:

$$\ln\left(\frac{d\alpha}{dt}\right)_{\alpha,i} = ln[f(\alpha)A_{\alpha}] - \frac{E_{\alpha}}{RT_{\alpha,i}} \quad (11)$$

In Eq.(11) the subscripts α and *i* indicates a specific extent of conversion and a specific temperature program, respectively. For isothermal experiments, *i* is referred to an individual temperature, while for linear non-isothermal temperature programs it identifies an individual heating rate. Eq. (11) can be rearranged in the following expression, useful for non-isothermal experiments:

$$\ln\left(\beta_i \frac{d\alpha}{dT}\right)_{\alpha,i} = ln[f(\alpha)A_{\alpha}P^n] - \frac{E_{\alpha}}{RT_{\alpha,i}} \quad (12)$$

where β_i is the constant heating rate, and the activation energy (E_α) for the individual extent of conversion can be calculate from the slope of the plot $t_{\alpha,i}$ vs. $1/T_i$.

Eq. (6) have the following analytical solution only for isothermal temperature programs [2.22]:

$$g(\alpha) = AP^n exp\left(\frac{-E_{\alpha}}{RT_i}\right) \quad (13)$$

the application of the isoconversional principle to the above equation leads to:

$$\ln t_{\alpha,i} = \ln\left[\frac{g(\alpha)}{A_{\alpha}P^n}\right] + \frac{E_{\alpha}}{RT_i} \quad (14)$$

Similarly to Eq. (12), it is possible to obtain the activation energy at a certain extent of conversion from the slope of the plot $t_{\alpha,i}$ vs. $1/T_i$. When performing constant heating rate temperature program, Eq.(6) do not have an analytical solution. Hence, there are various approximation of the temperature integral for integral isoconversional methods. Most of the approximated equations are in a linear form, and can be generically expressed as follow [2.22]

$$ln\left(\frac{\beta_i}{T_{\alpha,i}^B}\right) = Const - C\left(\frac{E_{\alpha}}{RT_{\alpha}}\right) \quad (15)$$

One of the simplest and more accurate approximation was proposed by Murray and White, which considered B = 2 and C = 1. This solution of the temperature integral was adopted by Kissinger-Akahira-Sunose, which gives rise to the homonymous famous equation [2.26,2.27]:

$$\ln\left(\frac{\beta_i}{T_{\alpha,i}^2}\right) = Const - \left(\frac{E_\alpha}{RT_\alpha}\right) \quad (16)$$

Differential isoconversional methods are considered as more accurate than integral ones, because they do not use any approximation. However, isoconversional integral methods applied to isothermal processes do not need approximated solution of temperature integral (Eq.(14)). Moreover, differential data methods that are used to handle integral data introduce inaccuracies due to the numerical differentiation, which often implies noise in differential data. This background leads to the conclusion that isothermal isoconversional methods should be considered as reliable and accurate solutions when performing kinetic studies through thermogravimetric analysis (integral data). This idea has been applied to this research work in order to develop a kinetic study of the overall reactions of biomass char.

As mentioned before, the isoconversional methods are also known as model-free methods, because it allows to calculate the activation energy without making any assumption about the reaction model. This definition should not be interpreted literally, because it is possible to calculate both the reaction model and the pre-exponential factor, by using the so-called *compensation effect*. This method is based on the assumption that A and E are strongly correlated. It follows that, even though the substitution of various models $f_i(\alpha)$ yields various pairs of E_i and A_i, it is possible to find the following relationship:

$$\ln A_i = aE_i + b \quad (17)$$

Eq.(17) implies that a and b can be found by applying different reaction models in order to find the A_i and E_i pairs. Then, by substituting the activation energy obtained with a model-free method, it is possible to calculate the actual isoconversional pre-exponential factor. As a consequence, the latter can be determined even if the reaction model is not selected but the correct activation energy is known.

The application of the compensation effect was originally proposed for single-step process [2.28] but it has been proven later also for multi-step process [2.29].

A method to obtain the kinetic pairs for different reaction models is rearranging Eq.(3), in the following form [2.30]:

$$ln\left(\frac{1}{f_i(\alpha)}\frac{d\alpha}{dt}\right) = ln(A_i P^n) - \frac{E_i}{RT} \quad (18)$$

With this method, also known as single-heating-rate method [2.30], the activation energy and pre-exponential factor pairs can be estimated by using various *i* reaction model and plotting the left side of Eq.(18) vs. 1/T values obtained at one heating rate. From the intercept and the slope of the line, the A_i and E_i values are obtained. The above reaffirms the importance of using both isothermal and constant heating rates temperature programs, aiming at the best possible understanding of the kinetic behavior. As summarized by Vyazovkin [2.30], the method of estimating the pre-exponential factor consists in four fundamentals steps. An isoconversional method is applied to determine the model-free activation energy and reaction order. This can be applied through isothermal or non-isothermal runs. A single-heating-rate analysis is performed in order to determine A_i and E_i pairs. The latter values are applied to the compensation effect method in order to obtain a and b coefficients in Eq.(17). Then, the isoconversional activation energy values (at various α) are substituted in Eq.(17) for getting the isoconversional valued of pre-exponential factor. With such approach the main drawback is related to the necessity of using differential equations to integral data (e.g. TGA) as it is the case of the present study. To this regard, an integral approach for the application of the compensation effect has been chosen. In order to avoid using approximated results of integral data, isothermal temperature program should recommended. In such conditions Eq.(1) can be rearranged as follow:

$$g_j(\alpha) = k_j(T_i, P)t \qquad (19)$$

Where the subscript j indicates the various reaction models. In Eq.(19) the rate constant incorporates the partial pressure dependency of reaction rate because it is a constant of the integral in the right side of Eq.(6). For each reaction model, the corresponding rate constant, can be determined from the slope of the plot of $g_j(\alpha)$ *vs. t*. Furthermore, various rate constants can be obtained at various T_i temperatures, in order to obtain the kinetic parameters using the typical Arrhenius equation [2.31]:

$$lnk_j(T_i) = ln\left(A_j \cdot P^n\right) - \frac{E_j}{RT_i} \qquad (20)$$

Despite the use of Eq. (19) and Eq. (20) involves a model-fitting-like approach, it should be stressed that according to the compensation effect it is not necessary to find the best fitting model. Indeed, after obtaining the *a* and *b* constant in Eq.(17), the isoconversional (i.e. model-free) pre-exponential factors can be obtained by substituting the isoconversional values of activation energy.

Furthermore, the effect of the gasifying medium partial pressure has been evaluated rearranging Eq.(14) in the following expression, in order to determine the isoconversional kinetic parameter *n:*

$$\ln t_{\alpha,i} = \ln\left[\frac{g(\alpha)}{A} + \frac{E_\alpha}{RT}\right] - nlnP \qquad (21)$$

In this thesis work an integral isoconversional approach has been applied in order to determine the activation energy at various extent of conversion (α) from the slope of lnt_i vs $1/T_i$ lines, obtained at each extent of conversion, as follows from Eq.(14). The isothermal data were obtained from thermogravimetric analysis in steam/nitrogen environment. The compensation effect has been applied using the integral expression of the reaction model according to Eq.(19) and Eq.(20), in order to determine the isoconversional values of the pre-exponential factor.

2.2. Materials and methods

2.2.1. Biomass feedstock and chars

The biomass object of this study are residues of agro-industrial activities that are typical of the Sicilian area, such as citrus, grape and olive pomaces, which are residues obtained from citrus juice, wine and olive oil production, respectively. In addition to these residues, *Arundo Donax* (named as reed) has been chosen because it grows naturally in the Mediterranean Basin, and it could be considered as a good source of feedstock for the integration with agricultural residues in thermochemical processes. Other by-products that have been selected for this study are residues from 2nd generation bioethanol industry, using wheat straw and *Arundo Donax* (reed) as feedstocks. The resulting residues are lignin reach biomass, which can be exploited for energy purpose in thermochemical processes. All the aforementioned biomass were previously characterized in order to determine the proximate and ultimate analysis. The kinetic study of the heterogeneous gasification reaction were conducted using the chars of the above mentioned residual biomass or byproducts. The chars were obtained at 500°C in a dynamic atmosphere of nitrogen for 1h. The parent samples placed in a cold and inert area inside a quartz tubular reactor and were introduced in the hot zone of the reactor when it reached the operating temperature. Then, the chars were crushed and sieved in order to obtain particle size smaller then 100 µm.

2.2.2. Biomass and chars characterization

The ultimate analysis, for determining the CHNS/O composition of parent biomass and the respective chars, were carried out through a Perkin Elmer CHNS/O analyzer, while proximate composition was obtained using a thermogravimetric analyzer (Q 600, TA Instruments). Moisture content in the "as received" samples is reported in Table 2.2. Citrus peel (CP) is usually obtained with water content ranged between 80-85%, and the citrus juice company supplied it after drying in a rotary kiln, reducing the moisture content at about 19.5%. Grape pomace (GP), olive pomace (OP) and reed were supplied after about one month of natural drying, while reed lignin (RL) and straw lignin (SL) were previously dried before being supplied. All the biomass samples were then dried in a furnace at 80 °C for 24 h in order to make the materials easier to handle for the grinding and sizing processes. The ultimate and proximate composition of dried samples, as they were used in the experimental activity, is shown in Table 2.3

Table 2. 2 Moisture content in as received samples

Biomass	M (%)
Citrus Peel (CP)	19.5
Grape Pomace (GP)	55.0
Olive Pomace (OP)	20.7
Reed	41.4
Reed Lignin (RL)	10.1
Straw Lignin (SL)	12.3

Table 2. 3 Ultimate and Proximate analysis of the biomass object of this study

	Ultimate and proximate analysis (%)$_{db}$								
	C	H	N	S	O[a]	Ash	VM	FC	Moisture
Citrus Peel (CP)	39.7	5.6	1.0	0.1	37.2	8.4	66.5	17	8
Grape Pomace (GP)	49.4	5.8	2.3	0.2	34.6	7.7	60.9	25.9	5.5
Olive Pomace (OP)	52.1	6.4	1.2	0.1	36.1	4.2	69.9	23.8	2.1
Reed	46.8	5.6	1.0	0.9	40.3	5.4	72.7	18.6	3.4
Reed Lignin (RL)	48.8	6.0	2.0	0.2	33.9	9.1	64.1	19.0	7.8
Straw Lignin (SL)	46.0	6.0	1.3	0.1	34.8	11.7	61.9	19.5	7.1

The inorganics in char samples were analyzed by an inductively coupled plasma-optical emission spectroscopy (ICP-OES) and an inductively coupled plasma-mass spectroscopy (ICP-MS). Morphological characterizations of chars were performed by mean of a scanning electron microscope (SEM) and BET surface area analysis, performed for non-converted and for chars at 50% of conversion in steam-nitrogen atmosphere (50%v/v Steam).

2.2.3. Experimental procedures

As mentioned before, the kinetic study of the heterogeneous reactions were performed mainly using isothermal temperature programs. The temperatures for the isothermal runs were below 800°C in order to guarantee as much as possible kinetics controlled conditions [2.2]. For each sample, at list four different temperatures were tested, with steps of 25°C, with partial pressure of 50.6 kPa for the reacting gases. The effect of gas partial pressure on chars gasification reactions was evaluated at isothermal conditions and varying the gasifying medium (steam) partial pressure from 10.1 to 50.6 kPa, using nitrogen as complement. The TG apparatus used for the steam gasification kinetic study was not a conventional thermogravimetric analyzer. It consists in a customized reactor that can be heated up to the desired temperature and can use selected reactive atmospheres. In this particular configuration, the sample is kept in an inert area at room temperature area on the top of the apparatus, and then lowered down in the reactor when the desired conditions are reached, in order to perform the tests in isothermal conditions. This thermogravimetric apparatus consists also in a steam generator kept at 250°C, as well as the transfer line, and fed by a HPLC pump. The apparatus scheme is shown in Figure 2.2. About 60 mg of char was loaded in a sample holder made of two concentric hollows cylinders. The external walls of the external cylinder were made by a metallic net reducing impediment to gas diffusion toward the sample.

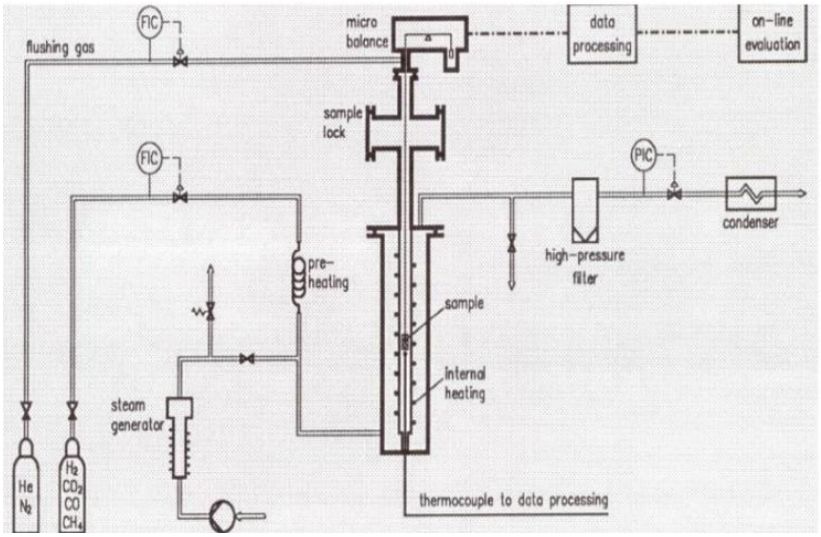

Figure 2. 2 Thermogravimetric apparatus used for the kinetic study of steam-char reactions

The external walls of the external cylinder were made by a metallic net reducing impediment to gas diffusion toward the sample. The isothermal runs at constant partial pressure, were performed at 50.6 kPa of steam partial pressure (nitrogen as complement).

In Table 2.4, the list of operating conditions for the different samples is reported. It can be noticed that in steam atmosphere, the char obtained from residues of 2nd generation bioethanol production (Straw Lignin and Reed Lignin Char) were studied at higher temperature than other samples. These conditions were necessary because the latter showed reaction rates much higher than RLChar and SLChar when steam was used as gasifying medium.

Table 2. 4 Temperatures and steam partial pressures of the isothermal thermogravimetric analysis

Char sample	Temperatures range	Steam Partial pressure
CPChar	650-725°C	10.1-25.2-50.6 kPa
GPChar	650-725°C	10.1-25.2-50.6 kPa
OPChar	650-725°C	10.1-25.2-50.6 kPa
RChar	650-725°C	10.1-25.2-50.6 kPa
RLChar	725-800°C	10.1-25.2-50.6 kPa
SLChar	725-800°C	10.1-25.2-50.6 kPa

2.3. Results

2.3.1. Chars morphological characterization

Results obtained from the scanning electron microscopy are displayed in Figure 2.3, which show char morphology of samples before conversion (a-f) and at 50% of conversion under steam atmosphere at 725°C (a'-f'). It can be noticed the formation of bigger pores due to the coalescence of smaller pores caused by overpressure during volatile release [2.32]. SEM images evidenced the heterogeneous structure of chars. Furthermore, it is possible to observe the evident presence of carbonized fibers in reed char and reed lignin char. The latter also shows the presence of the fibers embedded in an amorphous structures, due to the treatments of the bioethanol production process. Reed Lignin Char (RLChar) and Straw Lignin Char (SLChar) showed a less opened external pore structure, if compared with the others samples.

Table 2. 5 Specific surface areas of chars at different degrees of conversion.

BET Surface area [m^2/g]		
Sample	$\alpha = 0$	$\alpha = 0.5$
CPChar	3	199
GPChar	3	202
ReedChar	2	121
OPChar	4	500
RLChar	5	420
SLChar	20	413

The char's morphology was further investigated through the gas adsorption isotherms, and then followed by the BET (Brunauer–Emmett–Teller) analysis for the surface area calculation. This analysis revealed that the char's have a low surface area, related to its microporosity, before the steam gasification process, which values ranged from 2 to 20 m^2/g , as reported in Table 2.5. When char-steam reaction occurred, the formation of a micro-structured network is evidenced by the significant increase of the BET surface area at $\alpha = 0.5$, reaching values up to 500 m^2/g for Olive Pomace Char (OPChar). As evidenced by the SEM images, this behavior is further accompanied by the formation of large openings on the external surface, except for lignin chars that showed a more recalcitrant

attitude to form larger pores during steam gasification. Comparing the BET surface areas with the SEM images at $\alpha = 0$ and $\alpha = 0.5$, it is possible to conclude that the structure evolution of OPChar, RLChar and SLChar is more oriented to the formation of micropores, being the BET surface at 50% of conversion bigger than the others chars.

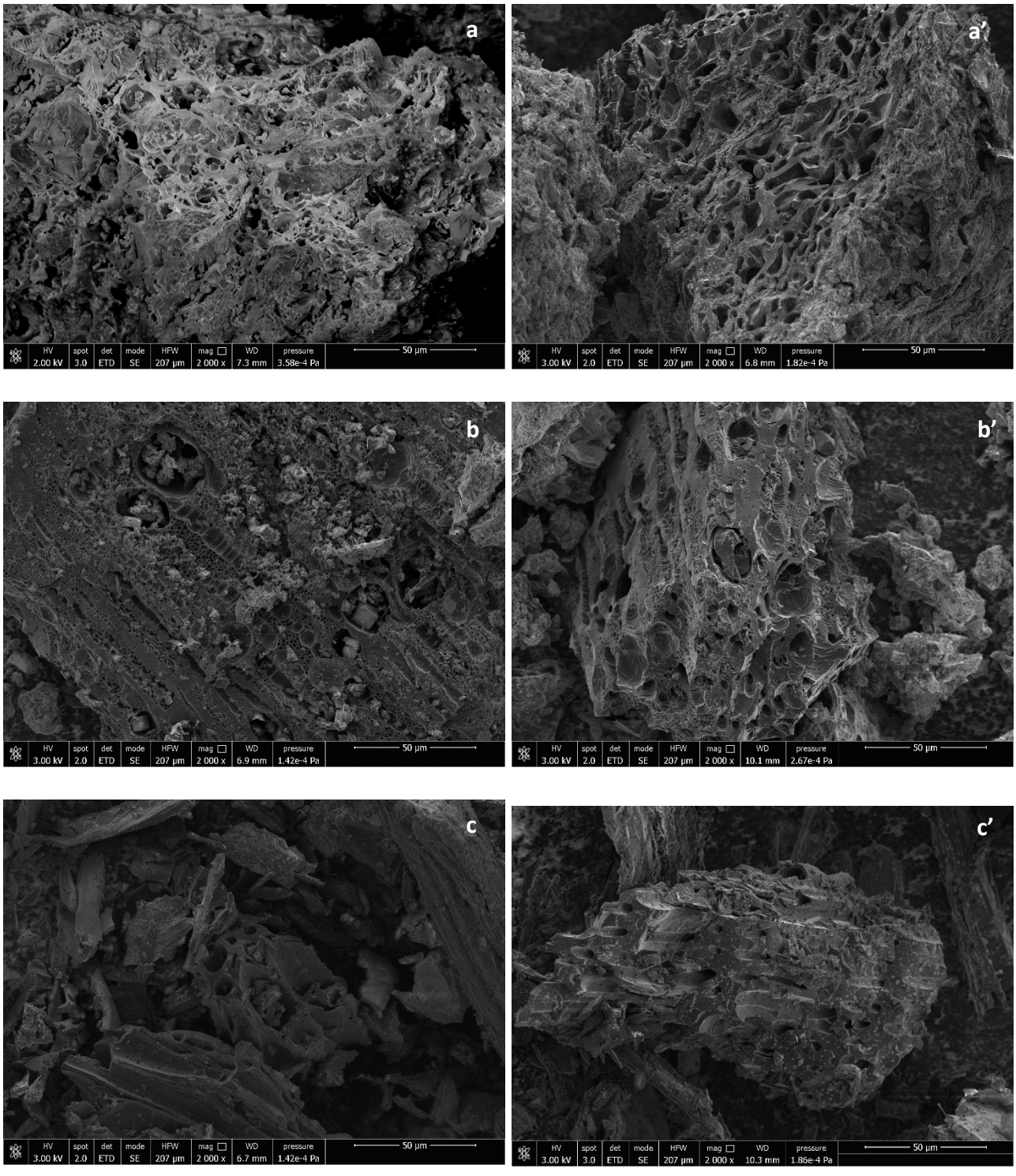

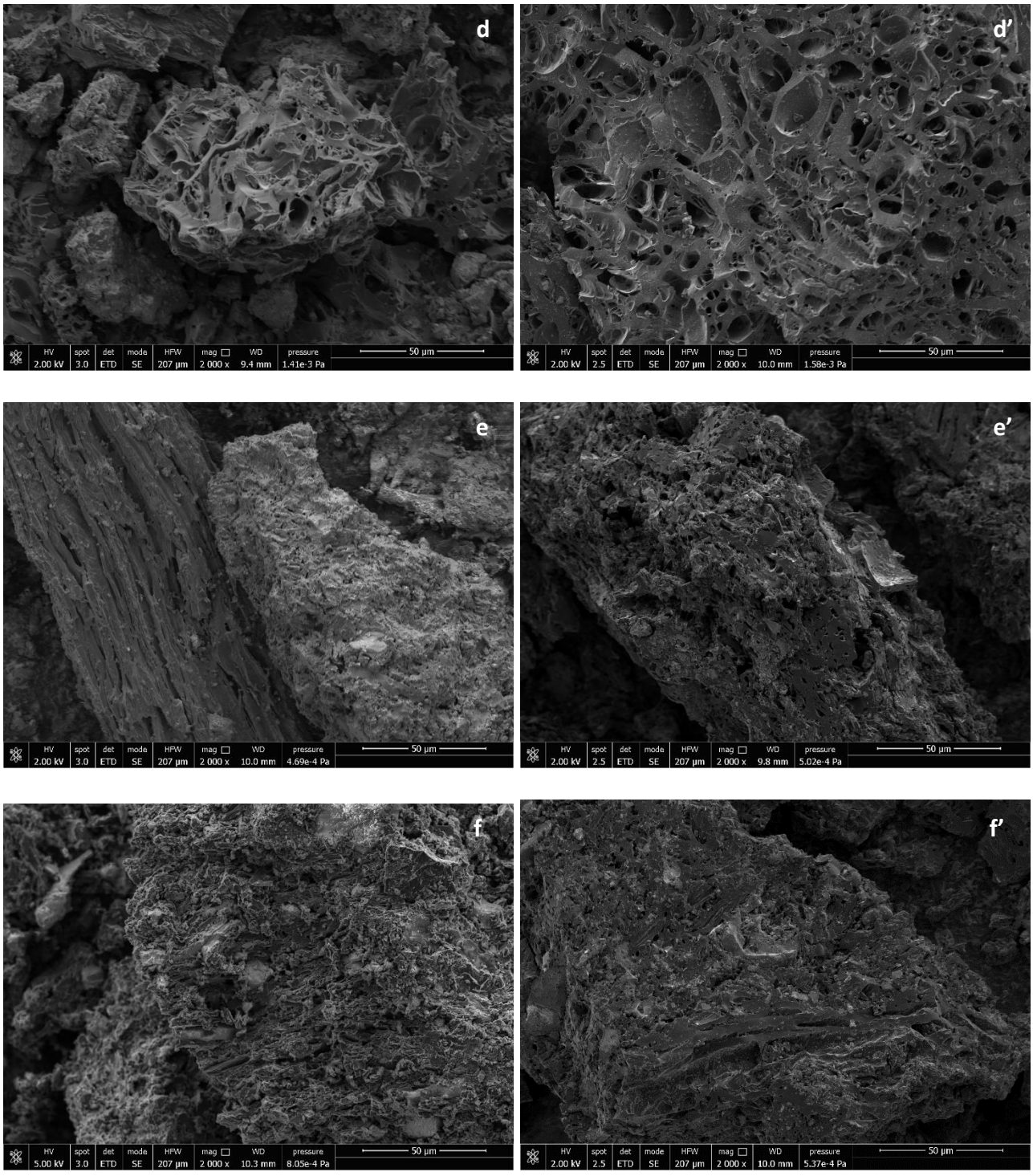

Figure 2. 3 SEM images of (a) CPChar, (b) GPChar, (c) ReedChar, (d) OPChar, (e) RLChar and (f) SLChar, before steam conversion and at 50% of conversion (a'-f').

2.3.2. Ash composition

The inorganic elements in char samples were analyzed by an inductively coupled plasma-optical emission spectroscopy (ICP-OES) and an inductively coupled plasma-mass spectroscopy (ICP-MS). Metals composition is of fundamental importance in understanding or anticipate the kinetic behavior of different biomass, because of their catalytic action that may considerably affect the biomass gasification rates. In particular, in this work the attention was focused on the concentration of Ca and K, which have good catalytic effects on steam gasification reactions. As opposite, it has been found that Si has an inhibiting effect on char-steam reactions [2.1]. In this work, a parameter has been introduced in order to quantify the combined presence of the catalytic and inhibiting effects of the inorganic elements. This parameter, named as *Inorganic Composition Ratio (ICR)*, takes into account the catalytic effect of Ca and K in the char-steam reaction, while considers the inhibiting effect of Si and P in the same reaction. According to this approach, the new parameter has the following expression:

$$ICR = \frac{(Ca+K)}{(Si+P)} \quad (22)$$

Unlike Dupont [2.1] and Hognòn [2.14], the *ICR* also considers the catalytic action of calcium, which effect cannot be ignored in order to make a comprehensive study of the effects of inorganic elements on the gasification kinetic. In Table 2.6, it is worth noting that the Citrus Peel Char (CPChar) is characterized by a very high concentration of Ca. As it is widely described in section 2.3.3, the latter is also the most reactive one and shows the higher *ICR*.

Table 2. 6 Concentration of inorganic components of chars

Element	**CPChar [mg/kg]**	**GPChar [mg/kg]**	**ReedChar [mg/kg]**	**OPChar [mg/kg]**	**RLChar [mg/kg]**	**SLChar [mg/kg]**
K	*13,641*	*65,175*	*70,030*	*23,874*	*20,984*	*22,300*
Ca	*106,159*	*14,730*	*2,026*	*8,620*	*24,991*	*11,800*
Fe	*254*	*1,183*	*450*	*1,432*	*3,150*	*4,400*
Na	*736*	*415*	*168*	*615*	*910*	*1,400*
Mg	*2,893*	*2,604*	*2,210*	*1,502*	*2,119*	*1,500*
Al	*398*	*838*	*310*	*1,569*	*912*	*3,300*
Si	*7,120*	*9,110*	*12,364*	*9,213*	*52,628*	*90,500*
P	*2,981*	*6,320*	*4,136*	*1,347*	*3,262*	*1,600*
ICR	***11.86***	***5.18***	***4.37***	***3.08***	***0.82***	***0.37***

2.3.3. Kinetic data results

The kinetic study was performed mainly using isothermal temperature programs. The first approach for handling the thermogravimetric data was to plot the extent of conversion as function of time for each i^{th} temperature used for each char, as reported in Figure 2.4 (a-f). These graphs explicit the reactivity of the analyzed samples. In fact, the shorter is the time to reach a specific degree of conversion, the higher is the reactivity. Furthermore, the shape of α vs time plot gives important information about the mechanism of reaction. It can be noticed that samples shown in Figure 2.4 a-d follow a sigmoidal like conversion mode, showing both accelerating and decelerating behaviors, reaching the maximum of the reaction rate at an intermediate value of conversion. This reaction profile can be associated to the Avrami-Erofeev models [2.30], as reported in Eq. 9 and Table 2.1. It is worth noting that CPChar shows a conversion curve almost linear up to 90% of conversion, with a constant slope. Reed lignin and straw lignin chars behave differently because they are characterized by a marked decelerating mode, since their rates decrease continuously with the conversion. Reaction-order models reported in Eq. 8 often describe these behaviors. The differences can be made more explicit by the bar chart in Figure 2.5, where the time at half conversion ($t_{0.5}$) is expressed for each sample, showing great differences in reaction rates. In particular, both lignin chars show a very slow reactivity if compared with the others agro-industrial wastes, since the time of half conversion are 15 - 20 times higher than citrus peel char. Figure 2.4 (e-f) further stresses that at 725°C RLChar and SLChar are not able to reach values of conversion as much as 0.9, even after 11,000 seconds. This behavior implies that high conversion efficiency for lignin chars can be reached only at high temperatures, reducing global efficiencies if compared with the others samples.

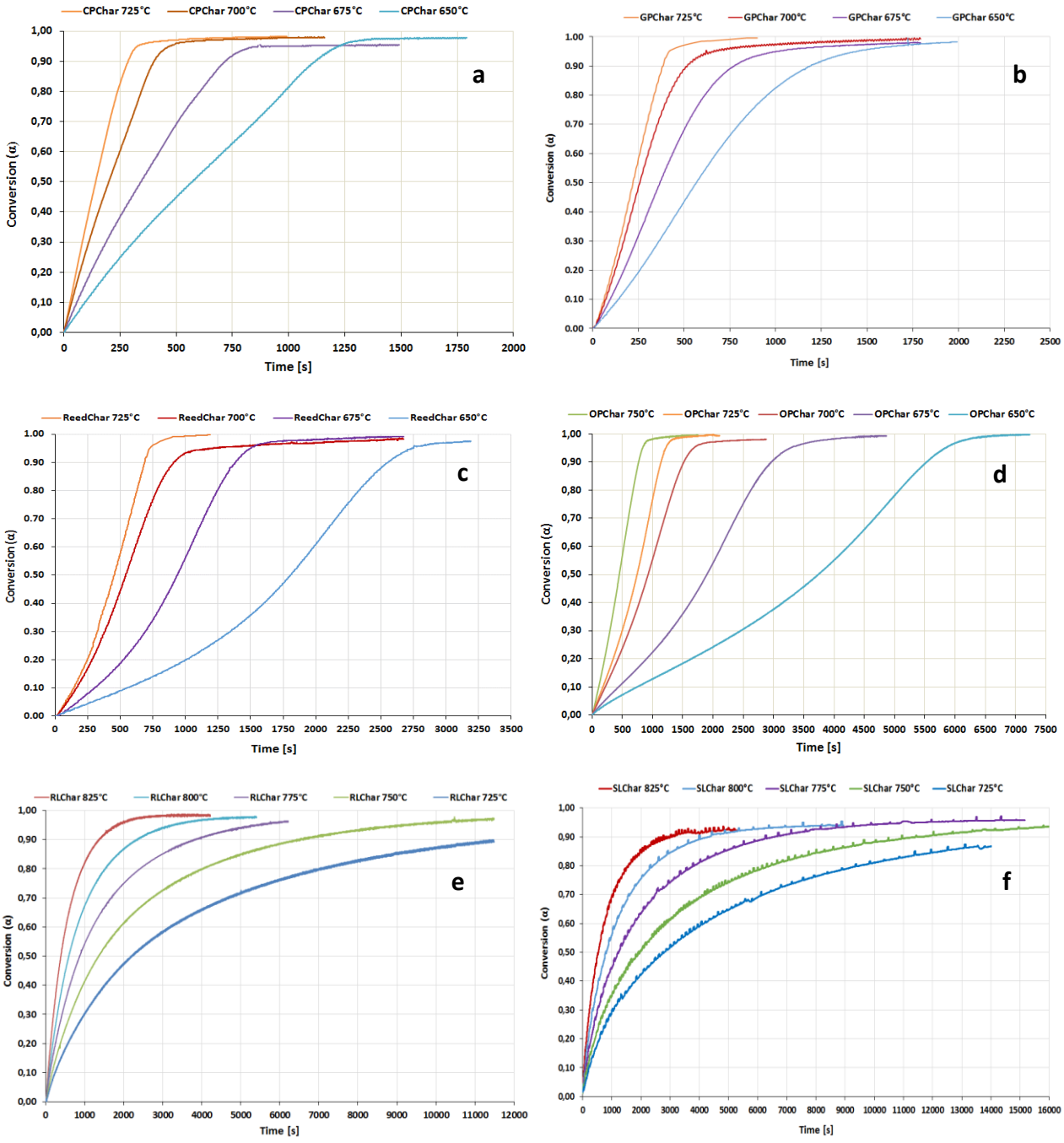

Figure 2. 4 Isothermal α vs t curves of (a) CPChar, (b) GPChar, (c) ReedChar, (d) OPChar, (e) RLChar and (f) SLChar samples at different temperatures and 50.6 kPa steam partial pressure (N_2 as complement)

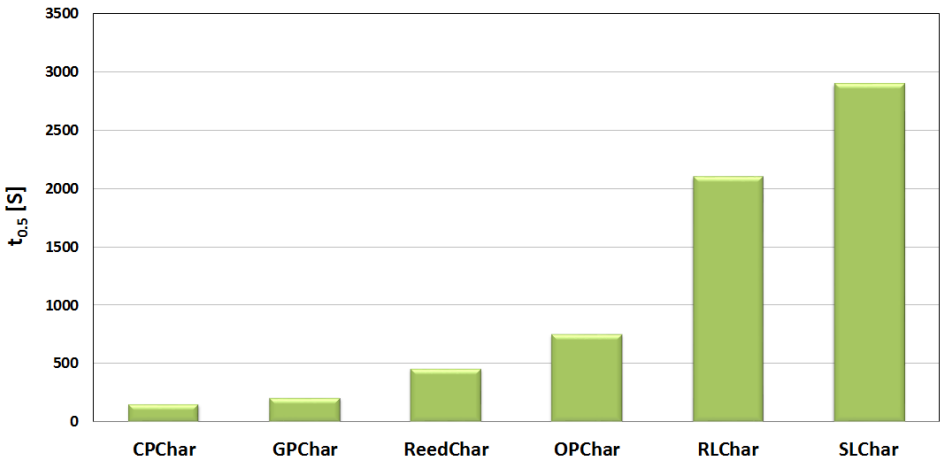

Figure 2. 5 Time of half conversion for char samples at 725°C and 50.6 kPa_{H2O}).

In the light of the kinetic results and chars characterizations, it is possible to state that differences in conversion kinetics can be addressed to the differences found in the inorganic elements composition. In fact, two main characteristics can be correlated to the reactivity: morphology and concentrations of catalytic sites [2.2]. Albeit it was not possible to find a relationship between BET surface area reactivity, Figure 2.6 underline the dependency between reaction time and the inorganic composition ratio (*ICR*). This figure is consistent with the consideration that time of half conversion, which is inversely proportional to reactivity, is highly dependent on the concentration of catalytic elements. The two graphs in Figures 2.6 and 2.7 make use of different parameters in order to consider the effect of the catalytic/inhibiting inorganic elements. In Figure 2.6 the ICR parameter considers both the calcium and potassium catalytic effect, as reported in Eq.22. As opposite, in Figure 2.7 the only potassium contribution has been considered. In the light of the results obtained in this study, it can be argued that the calcium content could not be neglected, contrarily to other authors [2.1, 2.14] who did not consider its contribution. For this reason, it was necessary to introduce the *ICR* parameter. In fact, because of the very high concentration of Ca in CPChar, a correlation with good approximation, can be found making use of *ICR*, as shown in Figure 2.6. From the trend of the time of half conversion it can be further observed that for high *ICR* values, an increase of *ICR* ratio has weak effects on conversion time. The relevant role of calcium in steam gasification of carbon is also confirmed in literature by other authors [2.2, 2.13]. It can be concluded that while studying kinetic behavior of agricultural or food processing residues, which are characterized by high ash and calcium content, the latter's contribution should not be neglected.

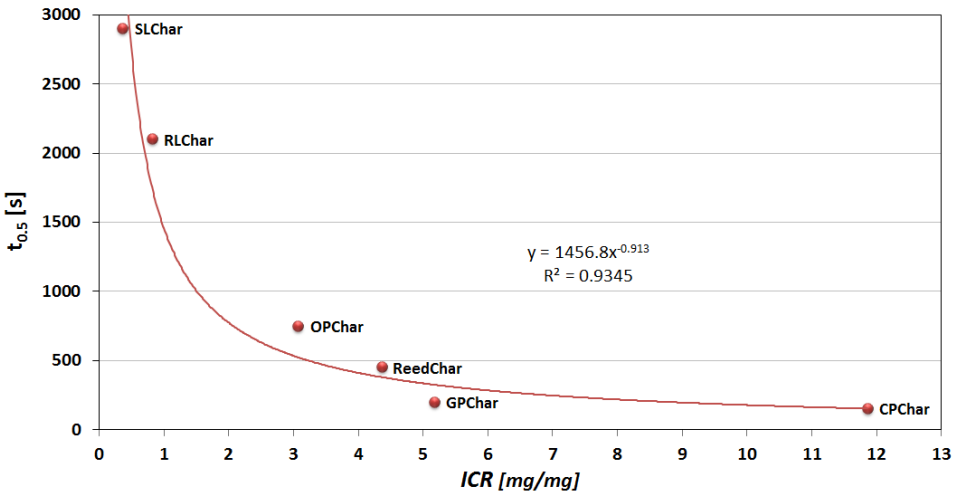

Figure 2. 6 Time of half conversion vs ICR ratio for the different chars (725°C, 50.6 kPa_{H2O}).

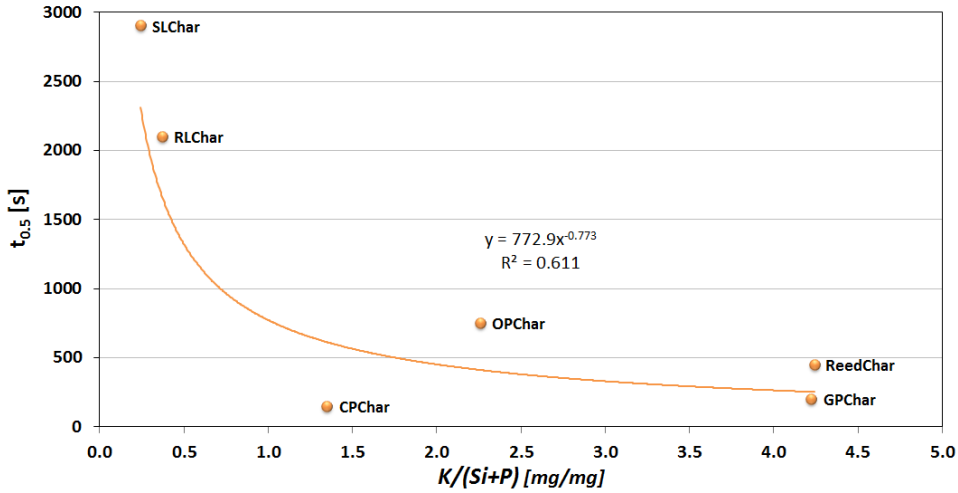

Figure 2. 7 Time of half conversion vs K/(Si+P) ratio for the different chars (725°C, 50.6 kPa_{H2O}).

2.3.3.1. Activation Energy

The plot of $\ln t_{\alpha,i}$ versus 1/T is shown in Figure 2.8 (a-f). It was obtained at different degrees of conversion (from 0.2 to 0.8) for each sample (a-f) with a good linearity of data for the various conversions, being $R^2 > 0.98$. Each line is representative of a specific conversion. Hence, according to Eq.14, from the slope of the straight lines in Figure 2.8 it is possible to calculate the apparent activation energy at various degrees of conversion.

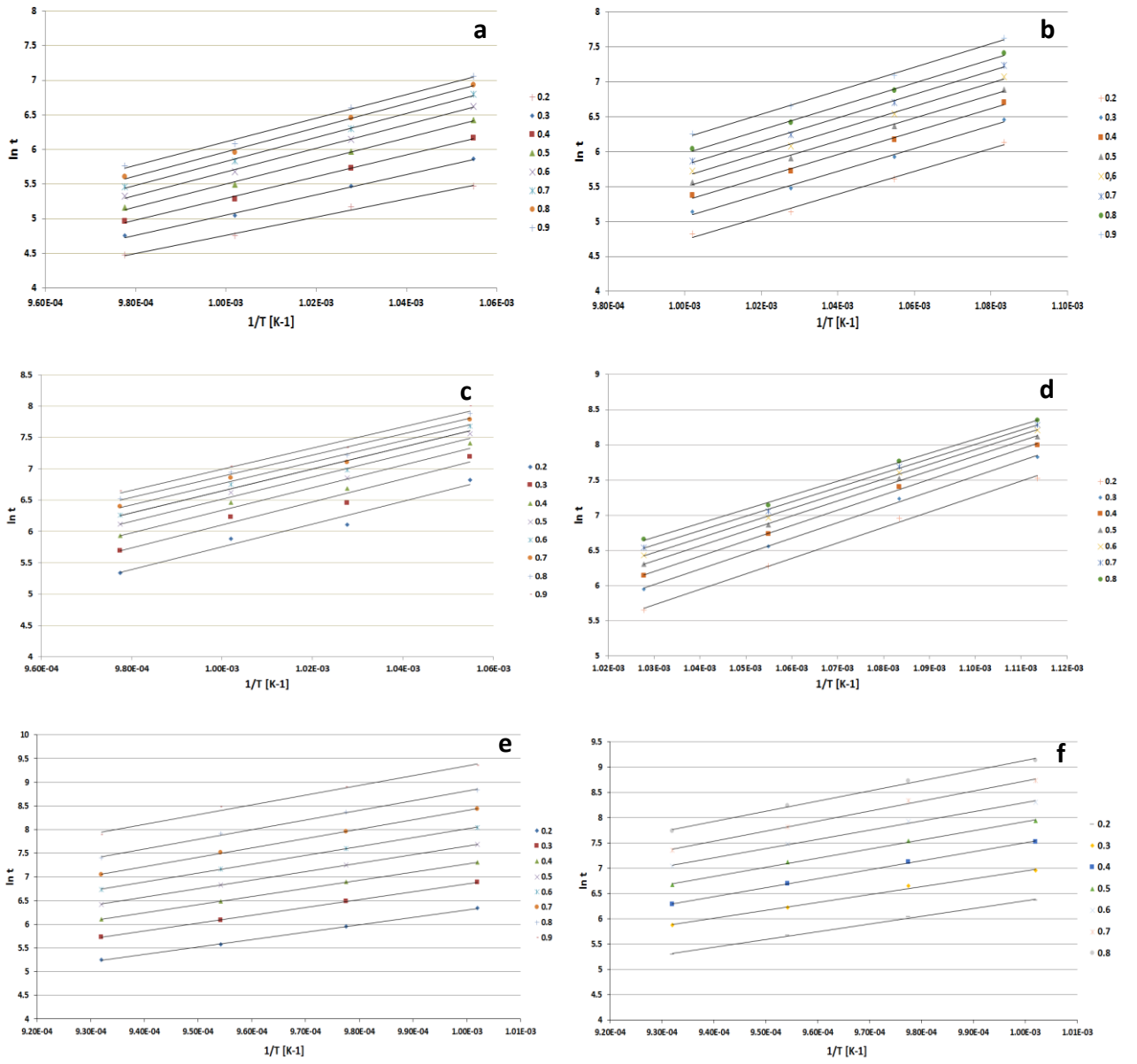

Figure 2. 8 ln t *vs* 1/T lines of of (a) CPChar, (b) GPChar, (c) ReedChar, (d) OPChar, (e) RLChar and (f) SLChar samples at different temperatures and 50.6 kPa steam partial pressure (N2 as complement)

The apparent activation energy dependency on conversion is plotted in Figure 2.9 for all the char samples in the range $0.2 \leq \alpha \leq 0.8$. The rapid increase of activation energy, that is almost linear, is evident for both lignin chars (RLChar and SLChar), which have very similar values, ranging from 134 to 188 kJ/mol for RLChar and from 141 to 176 kJ/mol for SLChar. The larger difference in apparent activation energy for these two samples was observed for the last point, when $\alpha = 0.8$. This behavior is consistent with the marked decelerating mode observed in Figure 2.4 (e-f) and with the residual material becoming increasingly refractory [2.30]. The rapid increase of the activation energy for the lignin chars could be addressed to the rapid consumption of the more active sites, characterized by lower activation energy. On the contrary, the agricultural and ago-food residues have slight variations of activation energy over the conversion range. GPChar and OPChar show E_α roughly

constant, while for ReedChar and CPChar E_α slightly decreases and increases, respectively, as conversion increases. The lowest apparent activation energy is observed for CPChar (128 kJ/mol), while the highest was observed for ReedChar (183 kJ/mol), recorded at $\alpha = 0.2$ for both samples. It is interesting to notice the similar behavior of E_α for citrus peel char (CPChar) and grape pomace char (GPChar), which showed the lowest apparent activation energies and the highest reactivity. The different behaviors observed for the analyzed samples highlight the differences of char thermochemical decomposition.

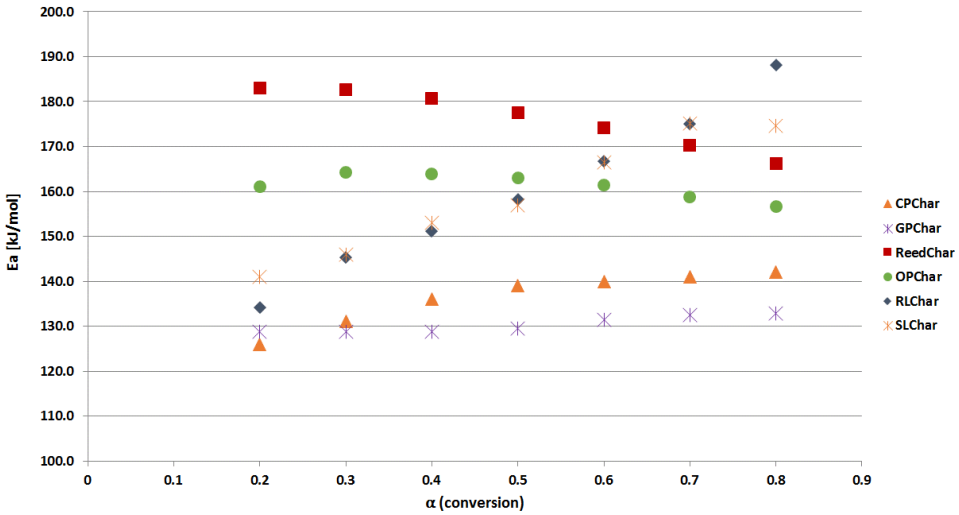

Figure 2. 9 Isoconversional activation energies of char samples

2.3.3.2. *Reaction order*

The effect of gas partial pressure on chars gasification reactions was evaluated at isothermal conditions and varying the gasifying medium partial pressure from 10.1 to 50.6 kPa. With such approach it is possible to calculate the exponent *n* (reaction order) in Eq.(5). Figure 2.10 (a-f) shows the conversion (α) *vs* time plot for all the char's samples. As expected, the reaction modes (i.e. the reaction profiles) remain the same even at lower steam partial pressure, while the reaction rates decreases with the steam concentration. The reaction order has been evaluated by plotting *ln t* as a function of the natual logarithm of steam pratial pressure (*ln P*) at different degrees of conversion. These plots represent straight lines with a good approximation ($R^2 \geq 0.97$), as reported in Figure 2.11 (a-f), whose slope indicates the reaction order *n*, and the effect of steam partial pressure on reactivity, in accordance with Eq. (21). From Figure 2.12, in wich the reaction order variation with conversion is represented, it is possible to observe that the effect of the steam partial pressure on the reaction is almost constant with conversion, except for the citrus peel chars, which shows an increased *n* from 0.11 up to 0.34. This sample is also the one that exhibits the lowest reaction order values, while the

others showed values higher then 0.68. The very low reaction order of CPChar indicates that the reaction mechanism is higly limited by the desorption step, resulting slower than the absorption one.

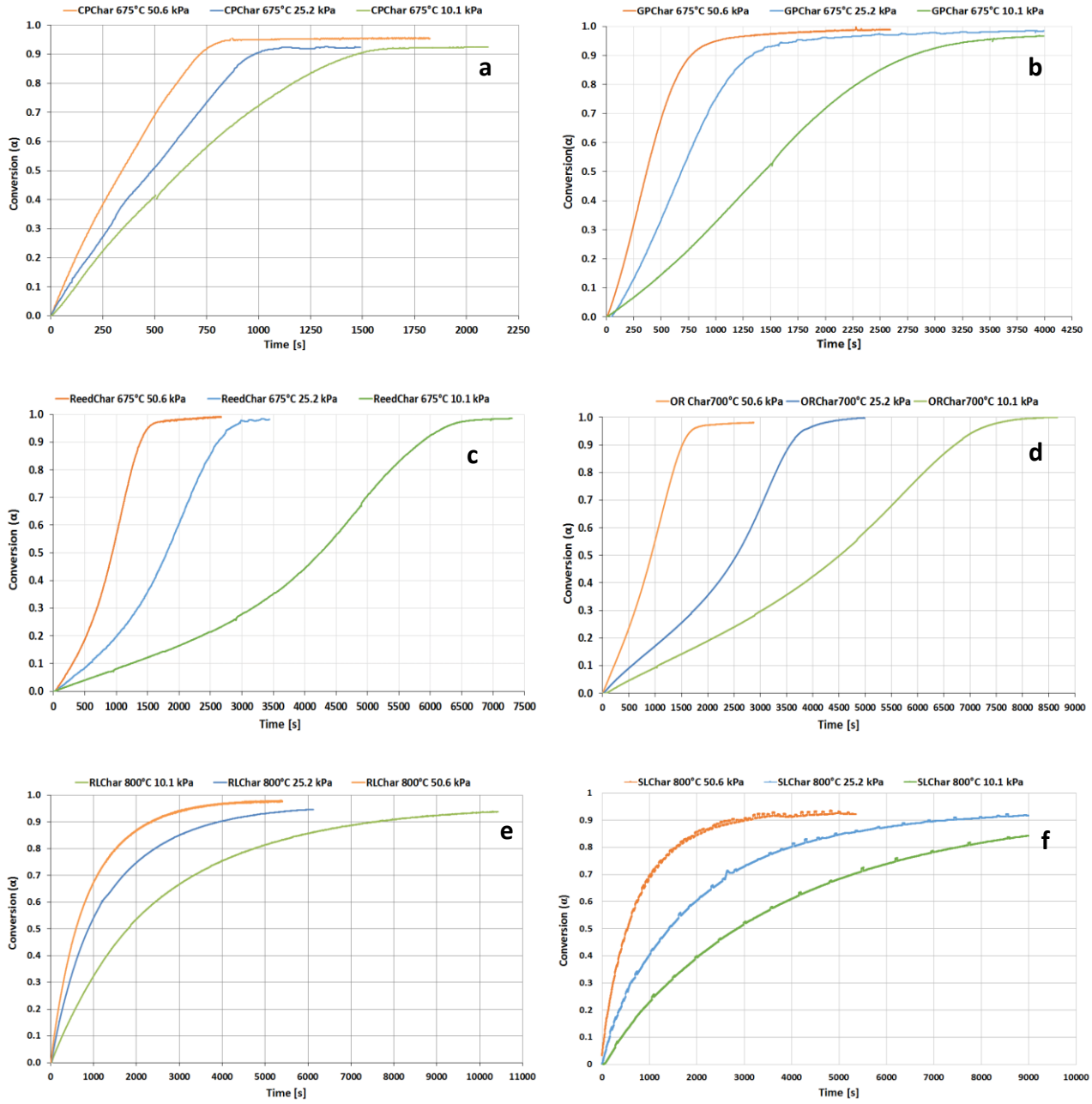

Figure 2. 10 Isothermal α vs t curves of (a) CPChar, (b) GPChar, (c) ReedChar, (d) OPChar, (e) RLChar and (f) SLChar samples.

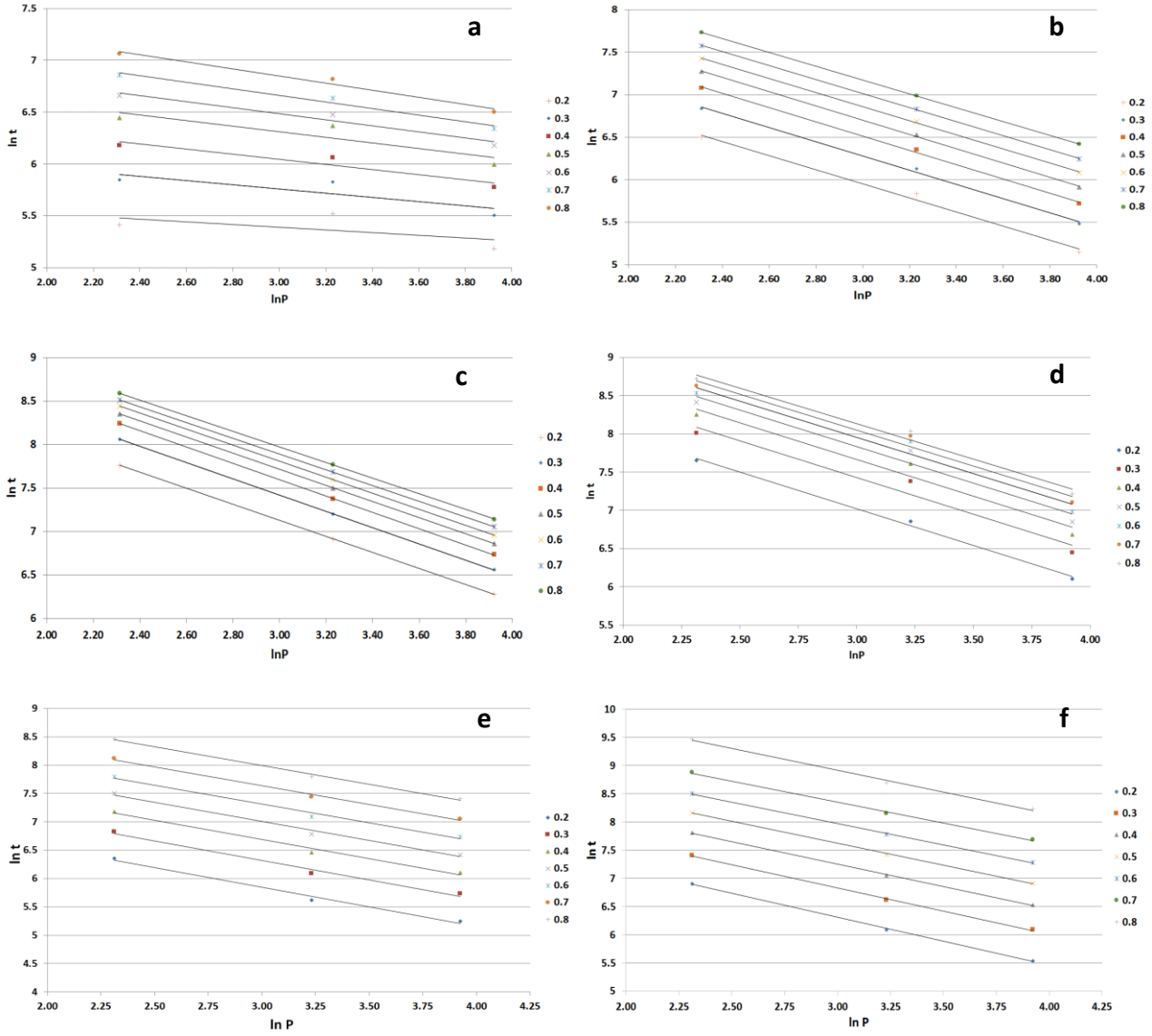

Figure 2. 11 ln t vs ln P lines of of (a) CPChar, (b) GPChar, (c) ReedChar, (d) OPChar, (e) RLChar and (f) SLChar samples.

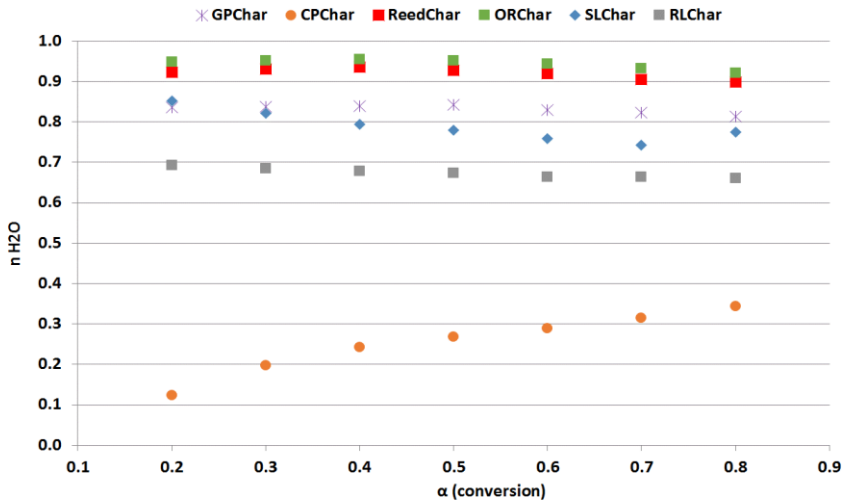

Figure 2. 12 Isoconversional reaction orders of char samples

2.3.3.3. *Pre-exponential factor calculation*

The pre-exponential factor can be calculated even with a model-free approach, making use of the compensation effect, described in section 2.1.2. In this work, an integral approach for the application of the compensation effect has been used, in order to avoid the application of differential equations to integral data. In this regard, Eq.19 was used in order to calculate the kinetic constant (k) at various temperatures and different integral reaction models $g(\alpha)$. From this equation follows that the kinetic constant can be obtained by the slope of the line which best fits the plot of $g(\alpha)$ as function of time. This plot should be obtained at least for two different reaction models, without the necessity to find the correct reaction model. After that the kinetic constant has been determined at various temperature, the plot of k *vs* T allows to obtain the pre-exponential factor (A) and the activation energy (E_a) from the intercept of the straight lines (from Eq.20), for each reaction model. After obtaining the a and b constant in Eq.(17), the isoconversional (i.e. model-free) pre-exponential factors can be obtained by substituting the isoconversional values of activation energy calculated at various degrees of conversions (α). As mentioned before, with the compensation effect method, it is not necessary to find the best fitting model, however it is important to find a model that is able to describe g(α) vs t as a straight line passing through the origin of axes, in compliance with Eq.19. In the case of citrus peel and grape pomace chars a first order and Avrami-Erofeev models had the best linear fitting, corresponding to models 6 and 9 in Table 2.1, respectively, while for reed and olive pomace chars, Avrami-Erofeev models(8 and 9) has been used. For the reed lignin and straw lignin chars a first order (6) and a second order (13) models has been selected for the rate constant determination. It is interesting to notice that these differences were coherent with the decomposition modes found in Figure 2.1 (alfa vs t). In fact, Avrami-Erofeev models, which describe sigmoidal modes, were

properly used for those samples that showed a sigmoidal mode, while the n-order models were used in the case of those samples with a marked decelerating mode. The results of the iso-conversional kinetic parameters are listed in Table 2.7 in order to summarize the results of the kinetic study.

Table 2. 7 Iso-conversional kinetic parameters for the different chars

	CPChar			GPChar			ReedChar			OPChar			RLChar			SLChar		
α	E_a [kJ/mol]	A [$s^{-1}bar^{-n}$]	n	E_a [kJ/mol]	A [$s^{-1}bar^{-n}$]	n	E_a [kJ/mol]	A [$s^{-1}bar^{-n}$]	n	E_a [kJ/mol]	A [$s^{-1}bar^{-n}$]	n	E_a [kJ/mol]	A [$s^{-1}bar^{-n}$]	n	E_a [kJ/mol]	A [$s^{-1}bar^{-n}$]	n
0.2	109.7	1.85E+03	0.12	135.8	1.33E+05	0.84	193.0	7.05E+07	0.92	161.1	5.06E+05	0.95	134.2	2.70E+01	0.69	141.0	9.91E+03	0.85
0.3	121.1	9.24E+03	0.20	135.8	1.34E+05	0.84	192.6	6.73E+07	0.93	164.2	7.40E+05	0.95	145.2	4.55E+01	0.69	145.9	1.98E+04	0.82
0.4	130.3	3.35E+04	0.24	135.8	1.34E+05	0.84	190.5	5.11E+07	0.94	163.9	7.10E+05	0.96	151.2	2.11E+02	0.68	153.1	5.46E+04	0.79
0.5	137.6	9.37E+04	0.27	136.6	1.51E+05	0.84	187.1	3.28E+07	0.93	163.0	6.41E+05	0.95	158.2	1.25E+03	0.67	157.0	9.41E+04	0.78
0.6	140.9	1.50E+05	0.29	139.7	2.45E+05	0.83	183.5	2.03E+07	0.92	161.4	5.30E+05	0.94	166.7	1.10E+04	0.66	166.5	3.61E+05	0.76
0.7	144.3	2.42E+05	0.31	138.5	2.01E+05	0.82	179.6	1.21E+07	0.91	158.8	3.84E+05	0.93	175.1	9.46E+04	0.66	175.2	1.22E+06	0.74
0.8	144.8	2.60E+05	0.34	140.1	2.61E+05	0.81	175.3	6.88E+06	0.90	156.6	2.95E+05	0.92	188.1	2.66E+06	0.66	174.6	1.13E+06	0.77

2.4. Chapter summary

Here are summarized the results concerning the kinetic study of steam-char reaction performed by means of thermogravimetric analysis data. The chars were obtained from agro-industrial residues.

Thermogravimetric analysis showed that the different chars are characterized by different reaction profiles and different reactivity. The influence of ash-forming elements with catalytic (Ca, K) and inhibiting (Si, P) character was evaluated by introducing the *Inorganic Composition Ratio* (*ICR = (Ca+K)/(Si+P)*), in order to include in one parameter both catalytic and inhibiting elements. Differently from other authors, Ca concentration could not be neglected. Indeed, a good correlation was found between *ICR* and time of half conversion. It has been noticed that samples with similar *ICR* show similar reaction profiles and comparable time of conversion. In particular, the samples with *ICR* < 1 showed marked decelerating reaction profiles, while samples with *ICR* > 1 exhibited sigmoidal reaction mode.

Regarding the kinetic parameters, activation energy values varied with the degree of conversion according to different trends for each char. The reed lignin and straw lignin chars, which exhibited a marked decelerating mode, also showed a rapid increase of activation energy with conversion. The activation energies were in the range from 127 to 189 kJ/mol. Reaction orders (n) wer almost constant, except for the orange peel char, which showed reaction order close to 0.1 at low degrees of conversion, followed by a slight increase of n as conversion increased. The results of this chapter can be considered of great interest both for reactor design optimization and for planning a proper supply chain with local residual biomass that could be valorized through steam co-gasification process. In fact, from the following study it is possible to recognize the agro-industrial residues that present similar kinetic behavior, which are suitable to be converted within the same reactor at the same processes conditions. Furthermore, it was also highlighted that preliminary evaluations about the gasification behavior may be inferred by ash composition and the *ICR* values.

References

[2.1] Dupont, C., Nocquet, T., Da Costa, J.A., Verne-Tournon, C., 2011. Kinetic modelling of steam gasification of various woody biomass chars: influence of inorganic elements. Bioresour. Technol. 102, 9743–9748.

[2.2] C. Di Blasi, Combustion and Gasification rates of lignocellulosic chars, Progress in Energy and Combustion Science 2009; 35; 121-140.

[2.3] Ollero P, Serrera A, Arjona R, Alcantarilla S. The CO_2 gasification kinetics of olive residue. Biomass Bioenergy 2003;24:151–61.

[2.4] Barrio M, Hustad JE. CO_2 gasification of birch char and the effect of CO inhibition on the calculation of chemical kinetics. In: Bridgwater AV, editor. Progress in thermochemical biomass conversion. Oxford: Blackwell Science Ltd.; 2001. p. 47–60.

[2.5] Bandyopadhyay D, Chakraborti N, Ghosh A. Heat and mass transfer limitations in gasification of carbon by carbon dioxide. Steel Res 1991;62:143–51.

[2.6] Barrio M, Gobel B, Risnes H, Henriksen U, Hustad JE, Sorensen LH. Steam gasification of wood char and the effect of hydrogen inhibition on the chemical kinetics. In: Bridgwater AV, editor. Progress in thermochemical biomass conversion. Oxford: Blackwell Science Ltd.; 2001. p. 32–46.

[2.7] Z. Huang, J. Zhang, Y. Zhao, H. Zhang, G. Yue, T. Suda, M. Narukawa, Kinetic studies of char gasification by steam and CO_2 in the presence of H_2 and CO, Fuel Processing Technology 91 (2010) 843–847.

[2.8] Laurendeau NM. Heterogeneous kinetics of coal char gasification and combustion. Prog Energy Combust Sci 1978;4:221–70

[2.9] Walker PL. Char properties and gasification. In: Bridgwater AV, Kuester JL, editors. Research in thermochemical biomass conversion. London and New York: Elsevier Applied Science; 1988. p. 485–509.

[2.10] Klose W, Wolki M. On the intrinsic reaction rate of biomass char gasification with carbon dioxide and steam. Fuel 2005;84:885–92.

[2.11] Hemati M, Laguerie C. Determination of the kinetics of the wood sawdust steam gasification of charcoal in a thermobalance. Entropie 1988;142:29–40

[2.12] Bhat A, Bheemaresetti JVM, Rao TR. Kinetics of rice husk char gasification. Energy Convers Manage 2001;42:2061–9.

[2.13] Encinar JM, Gonzalez JF, Rodriguez JJ, Ramiro MJ. Catalysed and uncatalysed steam gasification of Eucalyptus char: influence of variables and kinetic study. Fuel 2001;80:2025–36

[2.14] C. Hognon, C. Dupont, M. Grateau, M. Delrue. Comparison of steam gasification reactivity of algal and lignocellulosic biomass: influence of inorganic elements. Bioresource Technology, 2014; 164; 347-353

[2.15] Di Blasi C, Branca C, D'Errico G. Degradation characteristics of straw and washed straw. ThermochimActa 2000;364:133–42.

[2.16] Davidsson KO, Korsgren JG, Pettersson JBC, Jaglid U. The effects of fuel washing techniques on alkali release from biomass. Fuel 2002;81:137–42

[2.17] Huang, Y., Yin, X., Wu, C., Wang, C., Xie, J., Zhou, Z., Ma, L., Li, H., 2009. Effects of metal catalysts on CO2 gasification reactivity of biomass char. Biotechnology Advances 27, 568–572.

[2.18] K.O. Davidsson, J.G. Korsgren, J.B.C. Pettersson, U. Jäglid, The effects of fuel washing techniques on alkali release from biomass, Fuel 81 (2002) 137–142.

[2.19] Varhegyi G, Meszaros E, Antal MJ, Bourke J, Jakab E. Combustion kinetics of corncob charcoal and partially demineralized corncob charcoal in the kinetic regime. Ind Eng Chem Res 2006;45:4962–70.

[2.20] Marquez-Montesinos F, Cordero T, Rodriguez-Mirasol J, Rodriguez JJ. CO_2 and steam gasification of a grapefruit skin char. Fuel 2002;81:423–9.

[2.21] M. Perander, N. DeMartini, A. Brink, J. Kramb, O. Karlström, J. Hemming, A. Moilanen, J. Konttinen, M. Hupa, Catalytic effect of Ca and K on CO_2 gasification of spruce wood char, Fuel 150 (2015) 464–472.

[2.22] Vyazovkin S, Burnham AK, Criado JM, Pérez-Maqueda LA, Popescu C, Sbirrazzuoli N. ICTAC kinetics committee recommendations for performing kinetic computations on thermal analysis data. Thermochim Acta 2011;520:1–19.

[2.23] S. Vyazovkin, Kinetic concepts of thermally stimulated reactions in solids: a view from a historical perspective, Int. Rev. Phys. Chem. 19 (2000) 45–60.

[2.24] A. Garcia-Maraver, J.A. Perez-Jimenez, F. Serrano-Bernardo, M. Zamorano, Determination and comparison of combustion kinetics parameters of agricultural biomass from olive trees, Renewable Energy 83 (2015) 897-904.

[2.25] S. Vyazovkin, N. Sbirrazzuoli, Isoconversional kinetic analysis of thermally stimulated processes in polymers, Macromol. Rapid Commun. 27 (2006) 1515–1532.

[2.26] Akahira T, Sunose T. Joint convention of four electrical institutes. Sci Technol 1971;16:22–31

[2.27] Kissinger H. Variation of peak temperature with heating rate in differential thermal analysis. J Res Nat Bur Stand 1956;57:217–21.

[2.28]Salla JM, Ramis X (1996) Comparative study of the cure kinetics of an unsaturated polyester resin using different procedures. Polym Eng Sci 36:835–851.

[2.29] Roman F, Calventus Y, Colomer P, Hutchinson JM (2013) Isothermal curing of polymer layered silicate nanocomposites based upon epoxy resin by means of anionic homopolymerisation. Thermochim Acta 574:98–108.

[2.30] S. Vyazovkin, Isoconversional kinetic of thermally stimulated processes, Springer International Publishing Switzerland, 2015.

[2.31] S. Vyazovkin, C. A. Wight, Model-free and model-fitting approaches to kinetic analysis of isothermal and nonisothermal data, Thermochimica Acta 340-341 (1991) 53-68.

[2.32] Uzun B., Apaydin-Varol E., Ates F., Özbay N., Pütün A. Synthetic fuel production from tea waste: Characterisation of bio-oil and bio-char. Fuel, 2010, 89, 176-184.

3. Energy valorization of citrus peel by Air-Steam Gasification – SOFC: a simulation tool for energy assessment

3.1. Chapter Introduction

The object of this chapter is the investigation of the energy sustainability of a Combined Heat and Power (CHP) system, in which a solid oxide fuel cell has been combined with Citrus Peels (CP) gasification (using air and steam as oxidants). This study has been developed by mean of Aspen Plus simulation software, which allows developing evaluations about process feasibility and optimization of process parameters, in order to maximize the efficiencies, without the necessity to involve commercial-scale facilities. While the previous chapter's target was to obtain useful information for reactors design, based on kinetic study of steam gasification, the main goal of this chapter is to realize a useful simulation tool that is able to give preliminary information for the design of CHP systems using CP from citrus juice production process. Among the various agro-industrial residues that have been analyzed in this thesis, CP have been selected because they are local agro-industrial wastes of the Italian territory and very challenging to manage. As reported in the introduction chapter (§1.2), CP represents a typical residue of small and medium size enterprise in Sicily, whose share is > 50% of the Italian citrus production capacity [3.1-3.2]. This kind of agro-industrial residue is characterized by a huge water content (>75%), thus making its management, valorization and disposal more complicated and very expensive [3.3-3.4]. Furthermore, involving small size enterprise, the proposed solution for residues valorization could be exploited for distributed renewable energy production. For this reason, the simulation of a small size gasification-SOFC CHP process has been proposed.

Figure 3.1 shows a simplified flowsheet of the citrus juice production process (black lines), in which the gasification-SOFC system is integrated (blue lines). The citrus residues leave the juice extraction process with water content between 75-85%. A mechanical drying, such as a biomass pressing, reduces the water content to the value of about 65%. This is followed by thermal drying in order to reduce the moisture in the solid residue to 20%. Then, biomass is ready to enter the gasification unit where hydrogen rich syngas is produced to feed the SOFC unit. The scope of the following feasibility study is to determine the energy balance of the process and verifying the possibility of self-producing the heat required for the drying step, being this the most energy-demanding one. A zero-dimensional simulation model, using Aspen Plus simulation software, was used to analyze the combined system. Mathematical model of the gasification unit was experimentally validated by lab-scale experiments, while the SOFC model was validated with data available in literature. After the stand-alone models validation, the two units' models were integrated in order to simulate the syngas production process combined with the syngas utilization through a SOFC unit.

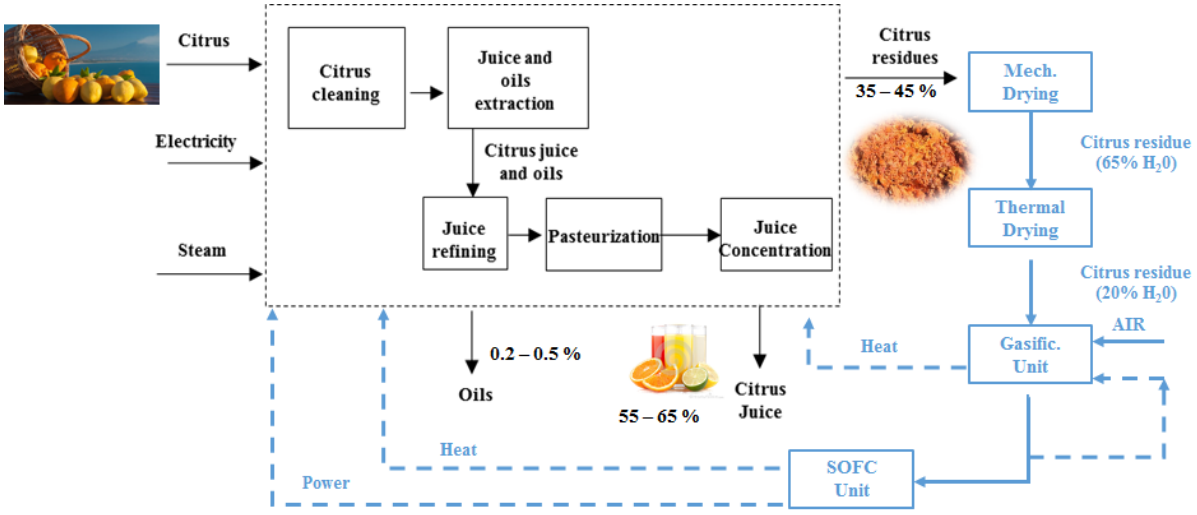

Figure 3. 1 Simplified flowsheet of citrus juice production process (black lines) and proposed residues valorisation process (blue lines).

The simulation software has also been used for the system scale-up in order to simulate a 120 kW DC gasification-SOFC CHP plant. Moreover, optimal operative conditions and integration options were investigated and maximum theoretical overall efficiency of the system was calculated.

The experimental activity consisted in the biomass characterization for ultimate and proximate analysi and in the gasification model validation through a bench-scale fluidized bed gasification reactor, installed in the laboratories of the CNR-ITAE, in Messina (Italy).

3.1.1. ASPEN Plus simulation software

Aspen Plus is a software widely used in the field of process and chemical engineering for the simulation of chemical processes. It is used to simulate and predict performances of a process that can be split in basics fundamental steps. Some of the most common uses of this software relate to the assessment of the effects of changes in operating parameters. It is also an easy tool for the feasibility study of process in variety of industrial scales. ASPEN Plus makes use of unit operation blocks that model specific operations, such as pumps, compressors, heat exchangers, reactors, etc. Material and energy streams connect the different unit operation blocks. In each material stream, it is possible to specify the stream classes, allowing the user to handle different substreams, named as the MIXED, CISOLID, and NC. The first is used to model conventional components in gaseous or liquid phases, while CISOLID allows handling solid components. NC substreams model non-conventional components, that is, components that have a complex structure that cannot be represented by a standard component that is in the software database. The non-conventional components are defined by mean of the components attributes, i.e. proximate and ultimate analysis.

In this work the selected stream class was the MIXCINC, made by MIXED, CISOLID and NC substreams. As an alternative, a MCINPSD class can be selected if particle size distribution of solid and non-conventional components is known. As expected, the biomass is modeled by a non-conventional component because it is not possible to give a unique accepted composition. Therefore the BIOMASS component is modeled in a NC substream, while water, gasification mediums and the gaseous products are modeled in the MIXED substream. The non-conventional components are converted in the sum of their elements (CHNS/O), indicated in the ultimate analysis, in order to consider their participation in the chemical reactions and in the phase and equilibrium calculations.

Through Aspen Plus software it is also possible to select a proper property method, which defines the thermodynamic calculations. Many authors consider the Peng-Robinson equation of state with Boston-Mathias modifications as the recommended for fuel applications, power generation systems and coal/biomass gasification [3.5;3.6]. However, in this study just negligible variation in the syngas composition has been verified when using the Ideal property method.

Various reactors models are available in the ASPEN Plus software in order to simulate different transformations mechanisms, depending on the knowledge's degree of the user regarding the specific reactions. The RSTOIC reactor models systems if reaction stoichiometry and fractional conversions are known, while in RCSTR reactors stoichiometry and kinetic parameters are specified. REQUIL and RGIBBS reactors are based on the equilibrium approach. The first is used when the equilibrium composition is obtained from the reaction stoichiometry, while for the RGIBBS reactor the calculation are based on the Gibbs free energy minimization, without the need to specify each reaction stoichiometry. Considering the complexity of biomass thermochemical processes, gasification reactors are usually modeled by RGIBBS reactors. The RYIELD reactor needs the reaction yields to be known, and it is used in order to convert the non-conventional component in its elements. The latter are the inputs for the RGIBBS reactor.

3.2. Simulation models description

ASPEN Plus simulation software was selected for creating the simulation model of the scaled up gasification-SOFC integrated system. For this work, the simulation was based on a steady state equilibrium model for both gasification and fuel cell units. The following assumptions have been taken into consideration:

(1) Steady state equilibrium process.
(2) Zero-dimensional process.
(3) Every stage of the gasification process (drying, pyrolysis, gasification and combustion) is considered as isothermal process.
(4) Pressure drop are neglected.
(5) The pyrolysis stage is modeled according to a regressive approach based on experimental yields.
(6) Gas cleaning section is neglected in the model.
(7) Heat exchanger are considered as ideal (100% efficiency).

The simulation model was developed with the aim of simulating the virtual scale-up of the gasification-SOFC system to be applied in a real industrial context, designed to promote waste valorization. The model consists of three main units: (i) biomass pretreatment (drying), (ii) biomass gasification and (iii) SOFC unit for combined heat and power production. Gasification and SOFC unit models were individually validated and then they were integrated in order to simulate the complete system. The gasification model was experimentally validated by mean of the lab-scale fluidized bed reactor described in section 3.3.1.

3.2.1. Drying and Gasification model

In order to assess the gasification model reliability, the lab-scale gasification facility was developed at first, in which the input feedstock was a dry biomass. After its validation, the scaled-up model was developed with the introduction of the drying sections and the heat exchangers for the heat recovery from a three-steps syngas cooling, while the proper gasification section remained unchanged with respect the lab-scale model.

Figure 3.2 shows the Aspen Plus flowsheet of the scaled-up gasification model. The pretreatment unit simulates the drying process of the raw biomass (RAWBIOM stream), where the water content is reduced from about 65% to 20%. Waste heat from the fuel cell could supply the heat for this purpose. As an alternative, the heat produced in SOFC unit could be decoupled by the drying step and used for

the juice extraction process. A RYield reactor block dissociate a desired amount of water from the raw biomass. Within this block an additional mixed substream, containing water, has been created. The water amount that leaved the unconventional substream of RAWBIOM stream, was determine by mean of an external calculator block, which allowed to define the dry biomass and water yields, according to the following Fortran equations:

DRYBIOM = (STREAMIN * 0.35 / 0.8) / STREAMIN

H2OOUT = 1 – DRYBIOM

where DRYBIOM is the mass yield of the BIOMASS unconventional component, STREAMIN is the wet biomass inlet stream (70% w/w of water content), called RAWBIOM, in the RYIELD block, while H2OOUT is the block variable representing the water yield. The new proximate composition of the biomass in the RAWBIOM2 stream was indicated using a calculator block. Water heating and evaporation in the mixed substream was modeled by a heat exchanger. The specific drying heat ("Q_{dry}" in kJ/kg) was calculated according the following equation:

$$Q_{dry} = \left[c_{p-biom} \cdot DM \cdot \Delta T_1 + c_{p-H2O} \cdot (1 - DM) \cdot \Delta T_2 + (h_{383v} - h_{373l}) \cdot x_{ev}\right] / \eta_{dry} \qquad (1)$$

where cp-biom and cp-H2O are the specific heat [kJ/kgK] of dry biomass and water, respectively, while DM is the dry matter fraction [wt/wt]; ΔT1 (105 K) and ΔT2 (85 K), are the temperature variations from room temperature (288 K) for solid and water fraction in the wet biomass, respectively; h_{383v} and h_{373l} are the steam enthalpy at 383 K and the water enthalpy at 373 K [kJ/kg], x_{ev} , is the evaporated water fraction of the original wet biomass. A typical dryer efficiency, η_{dry} , was also considered to be about 70% [3.7]. Then, the physical separation of evaporated water from biomass was modeled by a separator block.

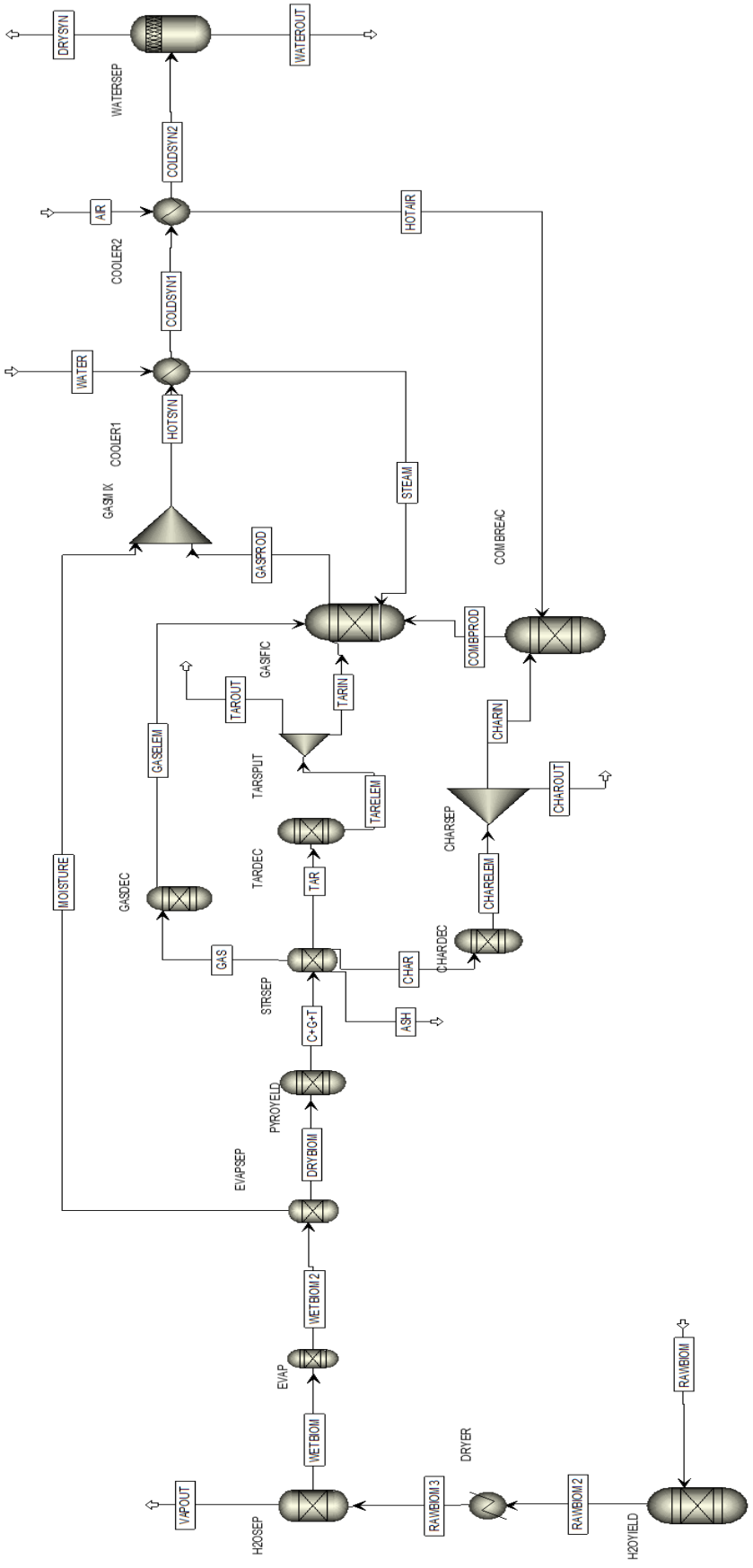

Figure 3. 2 Aspen Plus flowsheet of the scaled-up gasification model

The gasification unit is described by a semi-regressive method. Inside the reactor, the biomass is subjected to different thermal steps, the first of which is the complete drying, passing from 20% of water content to 0%. Hence, the water evaporation that takes place inside the reactor is modeled by means of a RYield and Separator block, using the same method explained for the external drying section. Then, the non-conventional dried biomass is separated in three different non-conventional streams: TAR, CHAR and GAS. Yields, ultimate and proximate analysis of char and tar components were obtained from previous experimental analysis during pyrolysis tests, whose results are reported in Table 3.1, while gas yield and composition were obtained from the difference between biomass composition and char and oil composition. Hence, the composition and yields of the new unconventional stream were inserted as input through a Fortran calculation block. In this work, the pyrolysis of 600°C has been selected.

Table 3. 1 Citrus Peel Pyrolysis yields obtained in a bench-scale packed bed reactor

Citrus peel pyrolysis yields [%w/w]			
Temperature [°C]	**Char**	**Oil**	**Gas[a]**
400	37.0	39.0	24.0
450	30.6	41.6	27.8
500	29.9	41.9	28.2
550	25.7	47.3	27.0
600	26.3	44.5	29.2

[a] by difference

These streams were directed to their respective RYield blocks, in order to decompose the non-conventional components in their elements, according to the ultimate analysis. The decomposed streams TARELEM and CHARELEM were directed into two splitters, in order to separate the unreformed tars and the unreacted char from the main streams. The split ratios were experimentally determined, according to results obtained in the experimental part described in section 3.3.1. The char fraction that was converted in syngas, passed through the COMBREAC reactor, where the combustion reactions took place. This section was modeled thorough a RGibbs reactor, that allows to obtain the product composition by minimizing the Gibbs free energy at the specified temperature and pressure conditions. The feeding air was calculated in order to reach a specific equivalence ratio (ER) by mean of a Fortran calculator block. The ER used for the gasification model validation was set to 0.3. Combustion products, constituted by mixed stream of carbon, carbon monoxide and carbon dioxide, were directed into GASIF reactor block, along with gas products from the pyrolysis step and the converted fraction of tars, where the gasification products where calculated by mean the free Gibb's energy minimization. This block was operated at 750°C, while the combustion block was set at 100°C higher than the gasification reactor temperature [3.8]. The scaled-up system design

contemplates a syngas cooling section, consisting of two heat exchangers. The first (COOLER) models a steam generator system, suppling heat for steam production for the gasification block. Water flow rate was calculated by a Fortran calculation block in order to reach the desired steam to biomass ratio (S/B), supposing to feed steam at 220°C. The second heat exchanger (COOLER2) was installed in the model in order to reach the desired water content in vapor phase in the syngas stream COLDSYN2. Condensed water is then separated from the syngas stream through a flash separator. The second cooler has the further scope to preheat the air at about 250°C before the gasification inlet.

3.2.2. Solid Oxide Fuel Cell model

The third unit models a SOFC developed by SIEMENS and it is based on a typical layout used in literature [3.8-3.12]. As reported in Figure 3.3, in this study the recirculation unit was modified inserting a heat exchanger in order to heat up the syngas until 800°C and maximizing the heat production at the same time. This choice was motivated by the large amount of heat required in the drying unit. It is an obvious consequence that the higher is the syngas temperature after the compressor block, the lower is the amount of recirculated gas from the anode. In order to maximize the thermal output from the SOFC unit, an additional heat exchanger for syngas preheating, fed by flue gas from the SOFC, was placed once after the compressor (COMPSYN stream) and once before the compressor (DRYSYN stream). The latter is the case reported in Figure 3.3, where the additional heater is represented by the SYNHEAT block. Both scenarios have been analyzed in order to verify the effects on the thermal and global performances. The effect of the current density has been evaluated as well. In Aspen Plus environment it is not possible to model the semi-reactions, thus the overall reaction of water formation is modeled in the anode block, modeled by a Gibb's reactor. The cathode is modeled by a separator, where the amount of oxygen that is split into the anode is calculated on the base of the fuel utilization factor, i.e. the ratio between the hydrogen consumed in the reaction and the hydrogen flow rate in the syngas, as reported in the following equations:

$$nH_{2,in} = nH_{2,syngas} + nCO_{syngas} + 4nCH_{4,syngas} \quad (2)$$

$$U_f = \frac{nH_{2,consumed}}{nH_{2,in}} \quad (3)$$

$$nO_{2,consumed} = 0.5\, nH_{2,consumed} \quad (4)$$

$$O_{2,split} = \frac{nO_{2,consumed}}{nO_{2,in}} \quad (5)$$

In the above equations nX_{in}, nX_{syngas}, $nX_{consumed}$ and $O_{2,\ split}$ are the molar flows [kmol/h] of the chemical species that are fed in the SOFC unit, the molar flows in the syngas stream, the consumed

molar flows in the SOFC unit and the oxygen molar fraction that is split from the cathode to the anode, respectively. Voltage calculations, obtained as function of current density j (mA/cm^2), were performed applying the Nernst equation, in order to obtain the Nernst potential (V_N), and subtracting voltage losses, which comprise Ohmic (V_{Ohm}), Activation (V_a) and Concentration losses (V_c), the cell voltage can be obtained as follow:

$$V = V_N - V_{Ohm} - V_a - V_C =$$

$$= V_N - \left(V_{Ohm_A} + V_{Ohm_C} + V_{Ohm_E} + V_{Ohm_{Int}}\right) - j \cdot \left(R_{act_A} + R_{act_C}\right) - \left(V_{conc_A} + V_{conc_C}\right) \qquad (6)$$

The terms of the above equations, related to voltage losses, were calculated according to equations available in literature for these tubular SOFC systems [3.8-3.13], which are shown in Table 3.2.

Table 3. 2 Voltage loss calculations

Ohmic loss	
Anode	$V_{Ohm\_A} = \frac{j \cdot \rho_A (A \cdot \pi \cdot D_m)^2}{8 \cdot t_A}$
Cathode	$V_{Ohm\_C} = \frac{j \cdot \rho_C (\pi \cdot D_m)^2}{8 \cdot t_C} \cdot A[A + 2(1 - A - B)]$
Electrolyte	$V_{Ohm\_E} = j \cdot \rho_E \cdot t_E$
Interconnection	$V_{Ohm\_Int} = j \cdot \rho_{Int} (\pi \cdot D_m) \frac{t_{Int}}{w_{Int}}$
Activation loss	
Anode	$\frac{1}{R_{Act\_A}} = \frac{2 \cdot F}{R_g \cdot T_{op}} \cdot k_A \left(\frac{P_{H_2}}{P^0}\right)^m \exp\left(\frac{-E_A}{R_g \cdot T_{op}}\right)$
Cathode	$\frac{1}{R_{Act\_C}} = \frac{4 \cdot F}{R_g \cdot T_{op}} \cdot k_C \left(\frac{P_{O_2}}{P^0}\right)^m \exp\left(\frac{-E_C}{R_g \cdot T_{op}}\right)$
Concentration loss	
Anode	$V_{Conc\_A} = -\frac{R_g \cdot T_{op}}{2 \cdot F} \ln\left[\frac{1 - (R_g \cdot T_{op}/2 \cdot F)(t_A / D_{An(eff)}) \cdot y^0_{H_2} \cdot P_{SOFC}) j}{1 + (R_g \cdot T_{op}/2 \cdot F)(t_A / D_{An(eff)}) \cdot y^0_{H_2O} \cdot P_{SOFC})) j}\right]$
Cathode	$V_{Conc\_C} = -\frac{R_g \cdot T_{op}}{4 \cdot F} \ln\left\{\frac{(P_{SOFC}/\delta_{O_2}) - [(P_{SOFC}/\delta_{O_2}) - y^0_{O_2} \cdot P_{SOFC}] \exp[(R_g \cdot T_{op}/4 \cdot F)(\delta_{O_2} \cdot t_C / D_{Cat(eff)}) \cdot P_{SOFC})] j}{y^0_{O_2} \cdot P_{SOFC}}\right\}$

Doherty et al. [3.8] extensively described the calculations of voltage losses in eq. (6), as well as the details of SOFC geometric, physical and material properties, as reported in Table. 3.3

Table 3. 3 Fuel Cell properties

Geometry [19,34–36]	
Cell length/diameter (m)	1.5/0.022
Anode thickness t_A (m)	0.0001
Cathode thickness t_C (m)	0.0022
Electrolyte thickness t_E (m)	0.00004
Interconnection thickness t_{Int} (m)	0.000085
Interconnection width w_{Int} (m)	0.009
Material properties	
Anode resistivity ρ_A (Ω m) [14]	$2.98 \times 10^{-5} \exp(-1392/T_{op})$
Cathode resistivity ρ_C (Ω m) [14]	$8.114 \times 10^{-5} \exp(600/T_{op})$
Electrolyte resistivity ρ_E (Ω m) [14]	$2.94 \times 10^{-5} \exp(10\,350/T_{op})$
Interconnection resistivity ρ_{Int} (Ω m) [19]	0.025
Ohmic loss [23]	
A/B	0.804/0.13
Activation loss [24,32]	
Pre-exponential factor k_A/k_C (A/m^2)	$2.13 \times 10^8/1.49 \times 10^{10}$
Slope m	0.25
Activation energy E_A/E_C (J/mol)	110 000/160 000
Concentration loss	
Electrode pore radius r (m) [25]	5×10^{-7}
Electrode porosity ϵ/tortuosity ξ [37]	0.5/5.9

In the SOFC unit model, ASPEN Plus was used for mass and heat balance calculations, while the electrical operating conditions were determined by mean of an EXCEL external calculator. Then, the cell model reliability were validated with data obtained in literature [3.8]. Once the desired DC Power, current density, cell active area and cell voltage are specified, the total cells number and current *I* were calculated. Hence it was possible to calculate the hydrogen molar flow rate ($nH_{2,in}$) and fuel molar flow rate ($nFuel_{in}$) as follow:

$$nH_{2,in} = \frac{I \times 3600}{2FU_f \times 1000} \tag{7}$$

$$nFuel_{in} = \frac{nH_{2,in}}{xH_2 + xCO + 4xCH_4} \tag{8}$$

where $nH_{2,in}$ and $nFuel_{in}$ are expressed in kmol/s, while F and *x* are the Faraday constant (C/mol) and the molar fraction of gaseous components, respectively.

The principal model input consists in the biomass ultimate and proximate analysis, expressed on total dry bases. The following table shows the proximate and ultimate analysis of citrus peel, used as input for the simulation model.

Table 3. 4 Ultimate and Proximate analysis of citrus peels

Ultimate Analysis (%)						
	C	H	N	S	O[a]	Ash
Total Dry Basis	43.0	6.3	1.3	0.1	40.8	8.5
	Proximate Analysis (%)			**HHV**	**LHV**	
Moisture	VM	FC	Ash	(MJ/kg)	(MJ/kg)	
20.0	71.9	19.6	8.5	14.41	13.84	

a. by difference

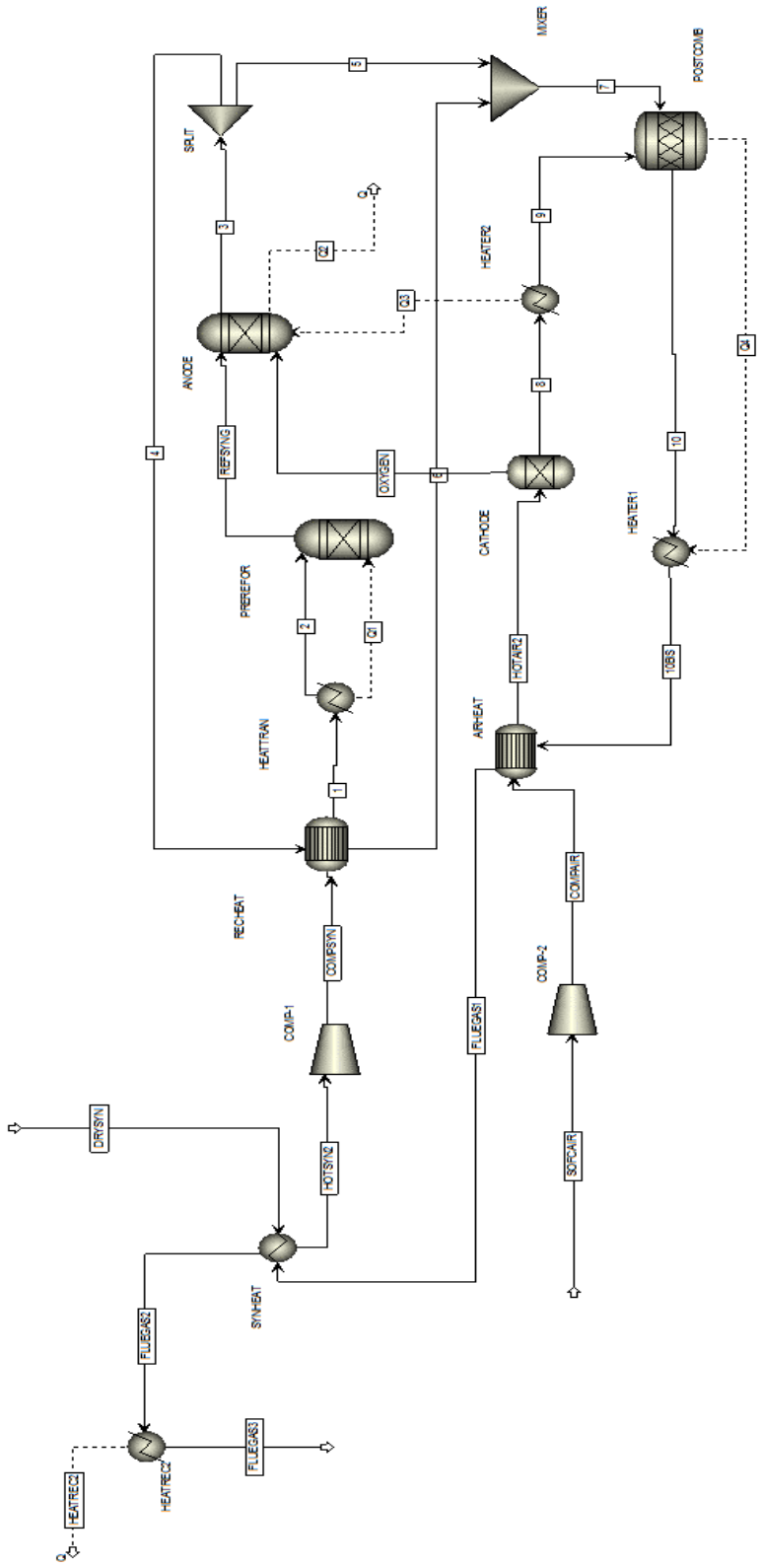

Figure 3. 3 Aspen Plus flowsheet of the Solid Oxide Fuel Cell simulation model

3.3. Gasification model validation and experimental activity

The gasification model was validated by mean of a lab scale fluidized bed reactor, installed in the laboratories of CNR-ITAE, in Messina, Italy. It is an atmospheric air/steam blown continuous system where biomass feeding rate ranges approximately from 0.3 to 1.5 g/min, depending on the specific biomass density. The reactor is 700 mm high with an internal diameter of 27 mm in the bed zone, while the free board has a dimeter of 50 mm. The reactor bed used in this work was a pure silica sand, with particle size $0.4 < d < 0.6$ mm. The gasification system consists of five main sections:

- The biomass feeding section, consists in a stirred storage vessel (1), with internal volume of 1 l, and a screw feeder (2). The vessel is filled with nitrogen in order to apply a counter-pressure and avoid oxygen or syngas intake.
- The fluidized bed reactor (3).
- The hot syngas transfer line (4), kept at 300°C with a cyclone/filter (4') and a hot box (5) at 220°C for streams heating and for the optional syngas upgrading through a smaller reactor (6).
- The syngas cooling section (7) for liquid-gas separation and subsequent syngas outlet.
- The gasification agents supply section, consisting in the HPLC pumps for water supply (8), heating coils (9) in the hot box, the air supply unit (10) and the feeding gas transfer line (11) kept at 300°C.

The bench scale gasification system is equipped with several thermocouples and temperature controller in order to monitor and regulate temperatures of different zones. In particular, the reactor is equipped with three thermocouples. One monitors the upper part of the freeboard, while another thermocouple is used to control the temperature inside the reactor's bed. The third thermocouple is positioned in contact with the external surface of the reactor, between the furnace and reactor. Furthermore, pressure controller are installed in order to monitor the pressure on the top and the bottom of the reactor, the ΔP in the reactor, to control the pressure inside the storage vessel and the plant global pressure. The biomass feeding rate is controlled by mean of the power control of the motorized screw feeder, after a preliminary calibration with the specific biomass, while gas flow rate is regulated through mass flow controllers. Final syngas composition and flow were evaluated with a MicroGC and a flow meter, respectively. Two chillers set at 3°C are used in order to keep the screw feeder (2) cold and to condensate the produced liquids (water + tar) in the liquid-gas separation section (7). Such a small scale is a rare configuration to find for continuous fluidized bed reactors, which allows for easy and not expensive biomass testing, with or without the use of a catalyst, in situ or in a following syngas upgrade.

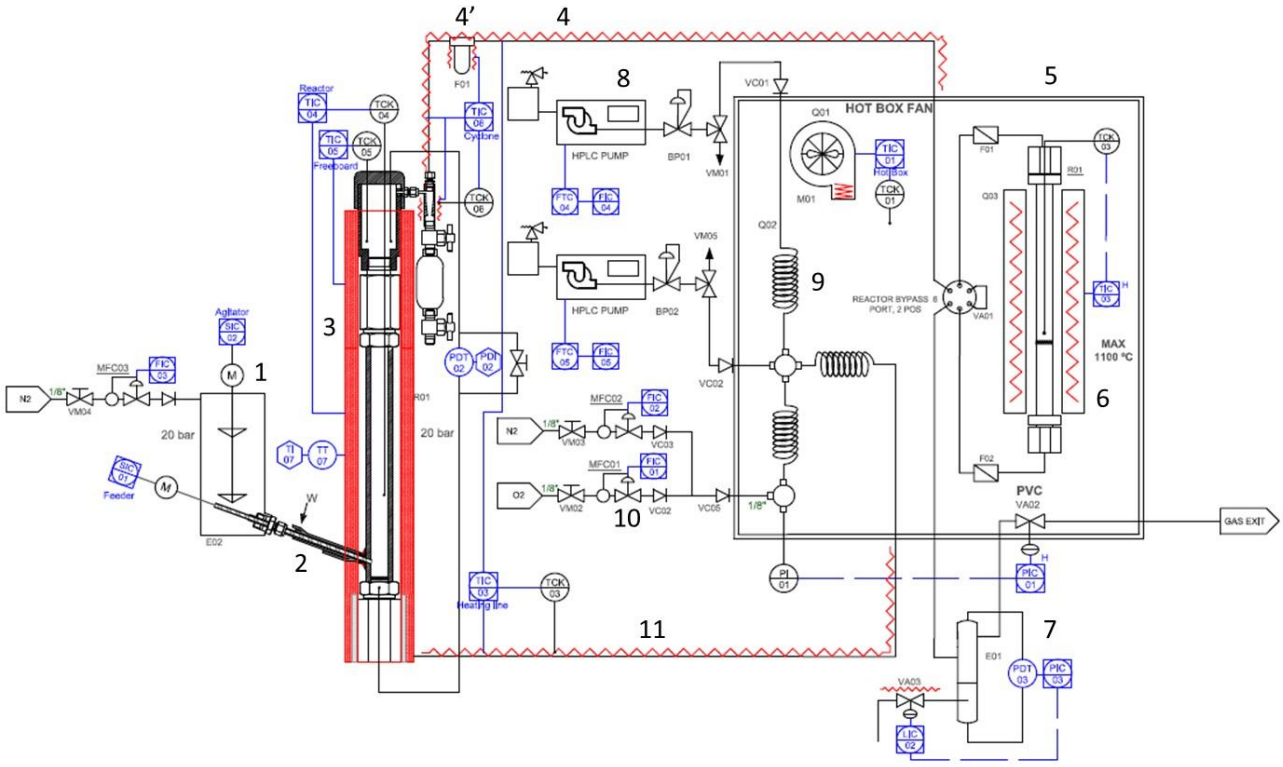

The gasification reactor operated at ambient pressure and at 750°C. The ER value was a compromise between the optimum biomass feeding rate and the adequate air flow rate necessary to ensure the fluidization conditions. The minimum fluidization conditions were calculated according to the following equations:

$$Re_{mf} = \frac{U_{mf} d_p \rho_g}{\mu} = [C_1^2 + C_2 \cdot Ar]^{0.5} - C_1 \quad (9)$$

$$Ar = \frac{\rho_g(\rho_p - \rho_g) g d_p^3}{\mu^2} \quad (10)$$

where U_{mf} is the gasifying agent's minimum fluidization velocity at which the bed become fluidized. It is strongly dependent on the bed particle diameter d_p and the difference between particle and gas density (ρ_p and ρ_g). The values of empirical constants, C_1 and C_2, are 27.2 and 0.0408, respectively [3.14], while μ is the gas viscosity. By the substitution of tabulated parameters in equations (9) and (10), the minimum fluidization velocity was equal to 0.0530 m/s that, for a cross section of 5.7*10-4 m2, leads to an air flow rate of 521 ml/min, re-calculated at room temperature. Then, the minimum fluidization air flow rate was multiplied by a factor of 2.5 in order to ensure better fluidization conditions, leading to an optimum flow rate of about 1300 ml/min. A biomass feeding rate of 1.03 g/min has been chosen in order to reach an ER = 0.3 for 1350 ml/min of air, while the steam to biomass ratio was in the range from 0.5 to 1.25.

Table 3. 5 Data for the fluidization calculations

Parameter	Unit	Value
ρ(g) (1000K)	kg/m^3	0.3482
ρ(p)	kg/m^3	1500
d(p)	m	5.00E-04
μ (1000K)	10^7 x N s/m^2	4.24E-05
g	m/s^2	9.81
C1	-	33.3
C2	-	0.0408

3.3.1. Gasification model validation results

Figure 3.4 shows the simulation results compared with experimental data for syngas composition at four different steam to biomass ratios. It is possible to observe that H_2 percentage increases with S/B ratio for both experimental and simulation tests. The decrease of the carbon monoxide with the steam increase was attributed to the water-gas shift reaction [23ATI], that favors the increase of CO_2 percentage. For these species a good agreement between experimental and simulated data was found at steam to biomass ratios higher than 0.5. This result was expected because the higher is the steam flow rate, the higher is the steam partial pressure, and the higher is the reaction kinetics. It follows that at higher S/B the experimental behavior is closer to the thermodynamic one, modeled in the simulation software. The analysis of mean error data for syngas composition is shown in Table 3.6, showing good agreement between simulated and experimental data [3.15;3.16]. It should be noticed from Figure 3.4 that the mean errors could be considerably reduced if only S/B > 0.5 will be considered.

Table 3. 6 Mean Errors of the main syngas components and syngas yield obtained at different S/B

	Mean Error [%]			
	H_2	CO	CO_2	Syngas Yield
Gas composition versus S/B	14.8	18.6	8.1	0.6

The mean error of methane, i.e. the species that showed the larger differences between simulated and experimental data, was not reported because thermodynamic results showed a negligible amount of it. This result can be explained with the complete steam reforming of methane in the simulation model, which does not consider the reaction kinetics, but just the Gibbs free energy minimization. In fact, at the gasification conditions, the methane formation is disadvantaged from a thermodynamic point of view.

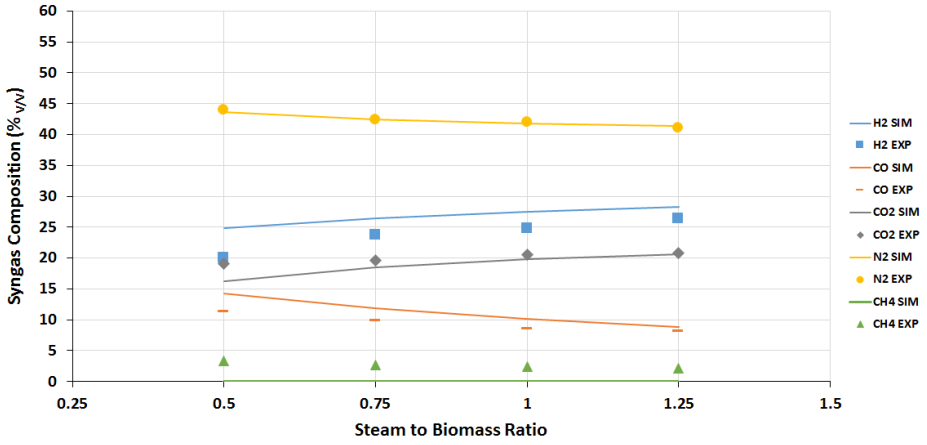

Figure 3. 4 Comparison between experimental (dots) and simulated (lines) syngas compositions at 750°C, ER=0.3.

Another important output result to be considered in gasification processes is the syngas yield, expressed as the syngas flow rate per kg of biomass, which is shown in Figure 3.5a, where experimental and simulated data are compared, showing good agreement. In solid oxide fuel cells applications, the H_2 and CO flow rates are others important parameter that have to be considered for the selection of the best operating conditions. In fact, the higher is the concentration of these components in the syngas, the lower is the syngas required to feed the SOFC unit and the higher is the global efficiency of the system. The H_2+CO yield (Nm^3/kg_{biom}) has been reported in Figure 3.5b, comparing experimental and simulated data. It can be noticed that the experimental H_2+CO yield appreciably increase with the S/B ratio, while in the simulation model the trend is almost flat and the values result to be quite overestimated. It should be underlined that according to Eq.8, the syngas low rate is also dependent on the methane concentration, that is negligible in the simulation results. This imply that the risks of performances overestimations for the simulation model are minimized, precisely because of the higher concentration of methane in the experimental runs.

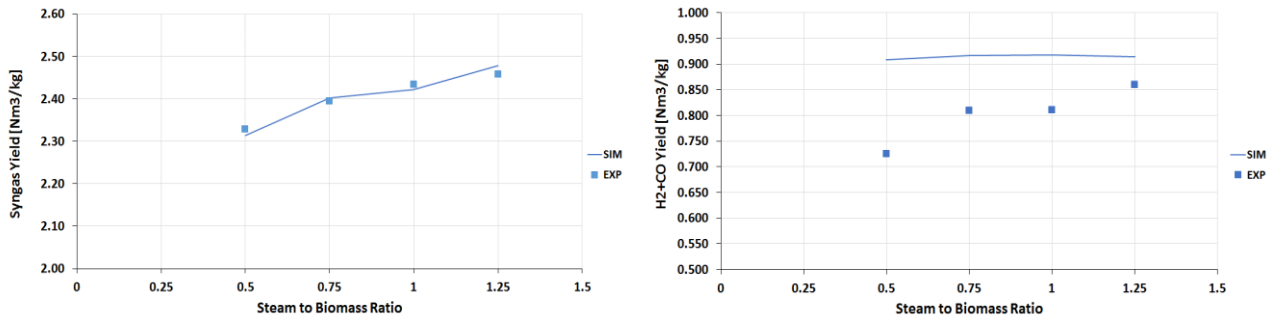

Figure 3. 5 Syngas yield (a) and H_2+CO yield (b) for simulated (lines) and experimental runs (dots) at 750°C, ER = 0.3.

3.3.2. SOFC stack model validation results

Electrical performances of the SOFC model were validated with data available in literature [3.8]. Figure 3.6 shows the comparison between the polarization curve obtained by Doherty and the one that has been replicated in this work, using the same operating conditions, cell characteristics and syngas composition available in [3.8].

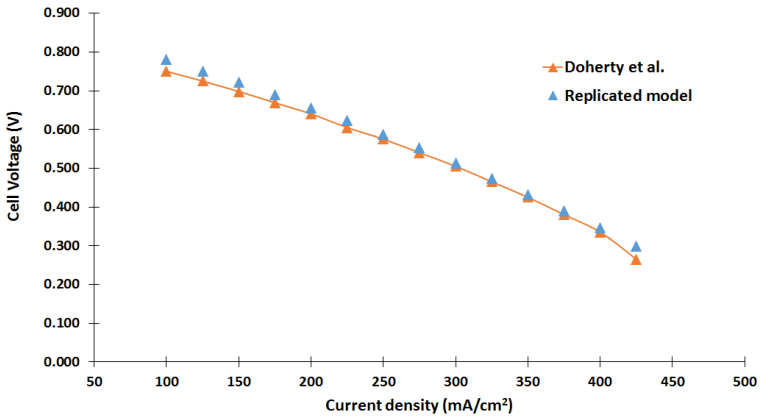

Figure 3. 6 Polarization Curves for SOFC mathematical model validation from literature data

The results show good agreement between the Doherty model and the replicated one. After SOFC model validation, the fuel cell unit was run with the specific syngas compositions obtained in the following section. Furthermore, the integration of the two models was then realized for the scaled-up system, in order to give a feasible tool for technical assessment of the application of residues gasification-SOFC in a citrus juice company.

3.3.3. Integrated model simulation results

After the standalone models validations, the simulation models were then integrated in a single model. As shown in Figure 3.8, the DRYSYN stream (gasification outlet) has been connected to the SOFC. The gasification section in the integrated model has been run using the following operative conditions: S/B= 0.75, ER = 0.23, T = 750°C. As explained in the experimental section (see §3.3), the conditions of the gasification model validation have been selected according to the best operative condition of the experimental set-up, which showed some limitations because of the very small scale. The S/B ratio (0.75) has been selected according to a compromise between the hydrogen and carbon monoxide yields and the necessity to reduce the steam supply, which can negatively affect the energy performance of the system. At the light of the relatively low gasification temperature, a lower ER than the one used in the validation section has been selected in order to improve the system performances, while ensuring proper operative conditions ($0.19 < ER < 0.3$) [3.15-3.17].

Syngas composition obtained by the integrated model is shown in Table 3.7, in which both dry and wet syngas compositions are listed. The latter was considered because the syngas that enters the SOFC should contain a certain amount of water vapor in order to avoid carbon deposition in the anode and for the syngas reforming reactions. The optimized water content in the syngas that enters the SOFC unit is 13.4%.This value was calculated using a so called "optimization block" in Aspen Plus, setting the H_2 partial pressure maximization at the anode inlet stream (REFSYNG) as target. An optimization block allows maximizing or minimizing a target variable through the variation of one or more variables.

Table 3. 7 Wet and Dry Syngas composition obtained from the integrated model

	Wet syngas [$\%_{vol}$]	Dry syngas [$\%_{vol}$]
H_2	29.6	34.2
CO	13.5	15.6
CO_2	15.7	18.1
N_2	27.8	32.1
H_2O	13.4	0.0

The new syngas composition was used as input for the SOFC voltage calculations, in order to determine the new polarization curve. Figure 3.7 shows the effect of current density on DC power density (mW/cm^2), cell voltage (mV) and AC efficiency (%). It is well established that there must be a trade-off between current density, power density and efficiency, that implies a compromise between capital and operating costs [17,18]. As inferred from the AC efficiency trend, that has been calculated based on syngas LHV, the cell efficiency decreases from 0.59 to 0.17, as the current density increases

from 100 to 475 mA/cm^2. Typical values of current density, for this type of fuel cells, are from 150 to 300 mA/cm^2 [17,18]. In this study, a current density of 200 mA/cm^2 was considered, corresponding to cell voltage and DC power density values of 0.745 V and 149 mW/cm^2, respectively. In order to assess the effect of higher current density on the energy performances, a current density of 300 mA/cm^2 was also considered. The compared results are shown in section 3.5, where energy performances are discussed. The SOFC unit was operated under the above mentioned conditions and the required amount of syngas has been calculated according to equations (7) and (8).

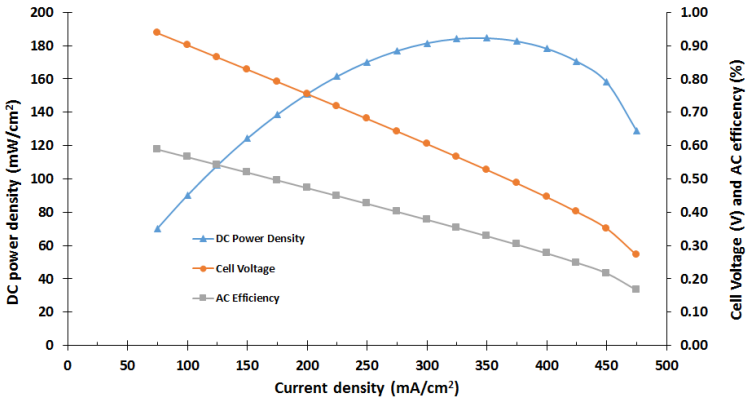

Figure 3. 7 Electrical performances of the SOFC fed by the simulated syngas composition of the 120 kW DC scale system

Simulation results showed that 8.1 kmol/h of syngas is necessary to produce 120 kW DC at 200 mA/cm^2. The two models were integrated and the gasification unit model was also equipped with a so called “design specification block” (i.e., a block that allows finding the value of a variable that returns a specific value of another target variable) available in Aspen Plus in order to determine the biomass feeding rate that was necessary at the specified syngas flow rate. The required feedstock rate was about 96 kg/h and 220 kg/h for biomass with 20%$_{wt}$ and 70%$_{wt}$ of moisture, respectively. As explained in the mathematical model description section, the SOFC unit was mainly developed for the energy and mass balance.

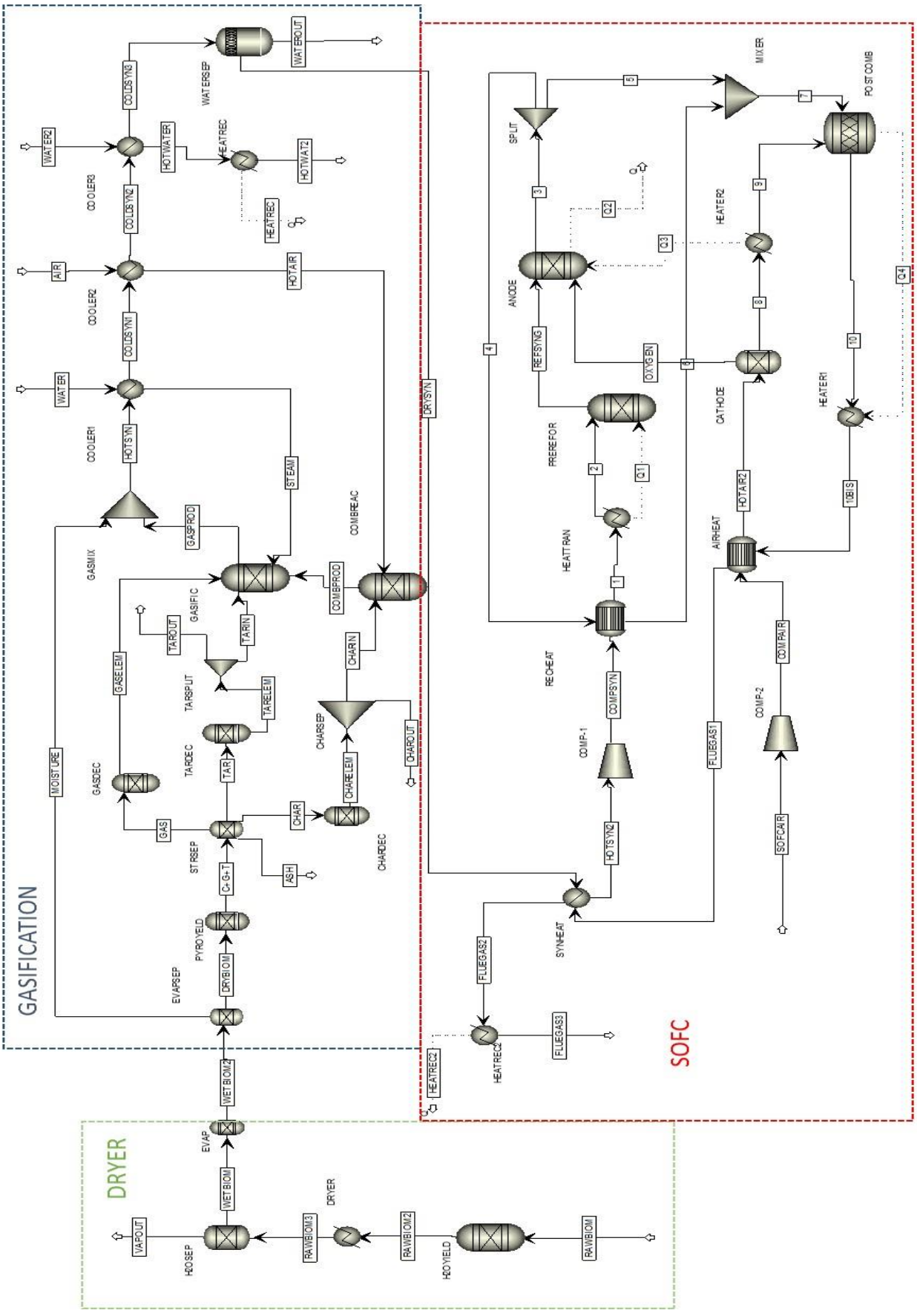

Figure 3. 8 Aspen Plus flowsheet of the integrated model for the system scale up (120 kW DC)

3.4. Performances evaluation

Gasification performances are measured in terms of both quality and quantity of gas produced [3.17], considering the total amount and the calorific values of product gas. The most widely used efficiency parameter is the so-called cold-gas efficiency, expressed as the potential power output over the power input [3.17]:

$$\eta_{cg} = \frac{Q_g M_g}{LHV_f M_f} \quad (9)$$

where Q_g is the *LHV* of syngas that has a M_g mass flow, and M_f and LHV_f are the mass flow input of biomass and the biomass lower heating value, respectively.

Another useful parameter for the gasifier efficiency description is the carbon conversion efficiency, which represents the capacity of the system to convert the carbon in the biomass feedstock. This can be expressed as follow:

$$\eta_c = \frac{m_{Csyngas}}{m_{Cbiom}} \quad (10)$$

In Eq.(10) $m_{Csyngas}$ and m_{CBiom} are the mass of carbon leaving the reactor (in the form of syngas) and the mass flow rate of carbon entering the reactor (in the form of biomass).

The fuel cell efficiency was calculated through the SOFC AC efficiency, which is expressed by the ratio between the AC power output over the syngas power input. Then, it is possible to distinguish between gross and net AC efficiency. The latter also considers the internal consumption, primarily due to compressors.

$$\eta_{ACgross} = \frac{P_{AC}}{Q_g M_g} \quad (11)$$

$$\eta_{ACnet} = \frac{P_{AC} - P_{cmp}}{Q_g M_g} \quad (12)$$

where P_{AC} and P_{cmp} are the AC electrical power output and the compressor power consumption, respectively, while $Q_g M_g$ is the same potential power possessed by the syngas expressed in Eq.(9).

The global plant efficiency is an important parameter that has to be taken into account in order to assess the potential of citrus waste gasification for renewable and efficient energy production. According to this, the plant net combined heat and power (CHP) efficiency can be calculated considering the SOFC power (P_{AC}) and thermal output (P_{th}), the internal consumption (P_{cmp}) and the thermal power required for the drying step (P_{dry}), as reported in Eq.(13):

$$\eta_{CHPnet} = \frac{P_{AC}+P_{th}-P_{cmp}-P_{dry}}{LHV_f M_f} \quad (13)$$

The thermal power output includes the heat recovered from the SOFC unit and the heat that can be eventually recovered from the syngas cooling section. In this work, the recovered heat is considered as the maximum recovered heat, i.e. cooling the fluids up to 25°C, without considering the specific uses or thermal efficiency of the heat exchange units, which depends on the specific heat exchanger.

In order to assess and compare the environmental performances between the proposed system and the state of things of the existing power supply system from the national electrical grid an emission factor of 326.78 gCO_2/kWh [3.18] has been considered for the electric power to the final user of the Italian national grid. Furthermore, biomass has been considered as carbon neutral fuel, and operational year (h) of 7000 *h/year*, the CO_2 savings (CS) can be calculated as follow:

$$CS = P_e \times h \times 326.78 \times 10^{-6} \ [\frac{t}{year}] \quad (14)$$

where P_e is the net AC Power.

3.5. Results and discussion on energy assessment

Table 3.8 shows results of the simulated Gasification-SOFC system, modeled for three different configurations. In the first case, the effect of the current density variation has been evaluated for a standard configuration without the additional syngas preheating (SYNHEAT block). The current density values in the standard configuration were 300 mA/cm^2 (Case 1) and 200 mA/cm^2 (Case 2a). Although higher current density implies lower cell number and lower capital costs, it causes a drastic reduction of system efficiency. The reduction of current density to 200 mA/cm^2 implies the reduction of the biomass input to the system, involving the combined reduction of biomass thermal input from 468 to 362 kW and heat demand necessary for biomass drying, allowing an increase of the plant net CHP efficiency from 0.43 (Case 1) to 0.55 (Case 2a).

Table 3. 8 Main results of the 120 kW DC scale simulated system

Parameter	Case 1	Case 2a	Case 2b
Current Density (mA/cm^2)	300	200	200
Cell voltage (mV)	595	745	745
Internal power consumptions (kW)	32.9	25.8	33.6
Net AC Power	83.5	90.6	82.8
SOFC AC gross efficiency	0.37	0.48	0.48
SOFC AC net efficiency	0.27	0.37	0.34
Dry Biomass flow rate (kg/h)	97.5	77.2	77.2
Biomass thermal input (kW)	469	369	369
Drying thermal input (kW)	179	140	140
Max. recoverable heat (SOFC flue gas/syngas cooling) (kW)	167/128	135/116	143/116
Carbon Conversion Efficiency	0.85	0.85	0.85
Cold Gas Efficiency	0.68	0.68	0.68
Plant net CHP efficiency (LHV basis)	0.43	0.55	0.55

In the second case (case 2b), the additional syngas preheating from up to 300°C before the SOFC inlet (SYNHEAT block), by mean of the heat exchange with the SOFC flue gas, implies that the recoverable heat from the SOFC flue gas increases from 135 to 143 kW. This effect is negatively compensated by the increased power demand of the syngas compressor, thus increasing the total internal power consumption from 25.8 to 33.6 kW. As it is possible to observe from Table 3.8, the additional preheater does not influence the plant CHP efficiency, but the advantage relies in the possibility to completely satisfy the drying thermal demand because of the increased thermal output. The latter is due to the possibility to increase the temperature of the syngas up to 530°C in the flowsheet section between the compressor (COMP-1) and heat exchanger of the anode recirculation (RECHEAT). When using the preheater after the compressor (Case 2a), the compressor's power is reduced but the maximum syngas temperature that can be reached is about 300°C, instead of 533°C

in the Case 2b. The use of a higher temperature after the compressor reduces the amount of anode recirculation and leads to higher amount of hot syngas to the post combustion block, allowing for more heat recovery from the SOFC unit. In this way, it also possible to satisfy the heat required in the drying section. The gasification efficiencies are also reported in Table 3.8, in terms of cold gas efficiency (CGE) and carbon conversion efficiency (CCE), being 0.68 and 0.85, respectively. The obtained CCE values is consistent with data reported elsewhere in literature and determined at the same conditions [3.19-3.22], T=750°C and ER = 0.23. It can be further observed that as the current density decreased from 300 to 200 mA/cm^2, the gap between the drying heat and the heat recovered from the SOFC is halved, leading to a self-sustainable process when it is included the additional syngas pre-heating in Case 2b. Another important information obtained from the simulation results is the biomass required to feed the system. Results in Table 3.8 show that in Case 2a-b 77.2 kg/h of dry biomass (0% H_2O) are required in order to produce the syngas necessary to produce 120 kW DC of electrical power from the SOFC unit. This result implies that 96.5 and 220.6 kg/h of citrus peel with 20% and 65% of water content, respectively, are required to feed the system. If 7,000 h of operational year are considered, the total amount of wet citrus peel with 82% of water content (as it comes out from the extraction process and before the mechanical drying) will be about 429 kg/h and 3,003 t/year, with the possibility to produce 579.6 MWh_e. Hence, these results provide important information about the potential of energy production from a single citrus juice company, whom specific energy potential is 0.193 MWh_e/t. From Eq.14 it was possible to calculate the amount of CO_2 savings, that is about 189 t/year, considering biomass as a carbon neutral fuel [3.17].

With the use of the simulation software, it was possible to understand the potential of citrus residues valorization, process sustainability and some of the operative conditions were optimized. The sensitivity analysis of the steam to biomass ratio has been developed in order to verify its effect on both the syngas composition and the simulation reliability. It was also determined the best wet syngas composition in order to maximize the hydrogen concentration, i.e. partial pressure, in the anode.

References

[3.1] Censimento ISTAT Agricoltura 2010. http://dati.istat.it/Index.aspx?DataSetCode=DCSPCOLTIVAZ/

[3.2] Patto di sviluppo del distretto produttivo Agrumi di Sicilia, http://www.distrettoagrumidisicilia.it/writable/allegati/patto+sviluppo276.pdf/

[3.3] Volpe M, Panno D, Volpe R, Messineo A. Upgrade of citrus waste as a biofuel via slow pyrolysis. J. of Analytical and Applied Pyrolysis 2015;115:66-76.

[3.4] Crawshaw R. Co-product feeds: animal feeds from the food and drinks industries. Nottingham: Nottingham University Press; 2004.

[3.5] Kuchonthara P, Bhattacharya S, Tsutsumi A. Combinations of solid oxide fuel cell and several enhanced gas turbine cycles. Journal of Power Sources 2003;124:65.

[3.6] Ramzan N, Ashraf A, Naveed S, Malik A. Simulation of hybrid biomass gasification using Aspen plus: A comparative performance analysis for food, municipal solid and poultry waste. Biomass and Bioenergy 2011;35:3962.

[3.7] G. Haarlemmer. Simulation study of improved biomass drying efficiency for biomass gasification plants by integration of the water gas shift section in the drying process, Biomass and Bioenergy 2015;81:129-136.

[3.8] W. Doherty, A. Reynolds, D. Kennedy. Computer simulation of biomass gasification-solid oxide fuel cell power system using ASPEN Plus, Energy 2010;35:4545-4555

[3.9] W. Doherty, A. Reynolds, D. Kennedy. Process simulation of biomass gasification integrated with a solid oxide fuel cell stack. Journal of Power Sources 2015;277:292-303.

[3.10] Song TW, Sohn JL, Kim JH, Kim TS, Ro ST, Suzuki K. Performance analysis of a tubular solid oxide fuel cell/micro gas turbine hybrid power system based on a quasi-two dimensional model. Journal of Power Sources 2005;142:30-42.

[3.11] Achenbach E. Three-dimensional and time-dependent simulation of a planar solid oxide fuel cell stack. J of Power Sources 1994;49:333-48.

[3.12] Zhang W, Croiset E, Douglas PL, Fowler MW, Entchev E. Simulation of a tubular solid oxide fuel cell stack using AspenPlusTM unit operation models. Energy Conversion and Management 2005;46:181-96.

[3.13] Anderson T, Vijiai P, Tade M.O. An adaptable steady state Aspen Hysys model for the methane fuelled solid oxide fuel cell. Chemical Engineering Research and Design 2014;92:295–307.

[3.14] P. Basu, Combustion and Gasification in Fuidized beds, Taylor & Francis Group, 2006.

[3.15] M.B. Nikoo, N. Mahinpey, Simulation of biomass gasification in fluidized bed reactor using ASPEN PLUS, Biomass Bioenergy 32 (12) (2008) 1245-1254.

[3.16] J.H. Pauls, N. Mahinpey, E. Mostafavi, Simulation of air-steam gasification of woody biomass in a bubbling fluidized bed using Aspen Plus: A comprehensive model including pyrolysis, hydrodynamics and tar production, Biomass and Bioenergy 95 (2016) 157-166.

[3.17] P. Basu, Biomass Gasification, Pyrolysis and Torrefaction - Practical Design and Theory – Second Edition, (Oxford: Academic Press Elsevier 2013).

[3.18] A. Caputo, C. Sarti, Fattori di emissione atmosferica di CO2 e sviluppo delle fonti rinnovabili nel settore elettrico, ISPRA – Istituto Superiore per la Protezione e la Ricerca Ambientale - Rapporti 212/15.

[3.19] X. T. Li, J. R. Grace, C. J. Lim, A. P. Watkinson, H. P. Chen, and J. R. Kim, "Biomass gasification in a circulating fluidized bed," *Biomass and Bioenergy*, vol. 26, pp. 171-193, 2004.

[3.20] L. Zeng and A. R. P. Van Heiningen, "Carbon gasification of kraft black liquor solids in the presence of TiO2 in a fluidized bed," *Energy and Fuels*, vol. 14, pp. 83-88, 2000.

[3.21] A. Gomez-Barea, R. Arjona, and P. Ollero, "Pilot-plant gasification of olive stone: A technical assessment," *Energy and Fuels*, vol. 19, pp. 598-605, 2005.

[3.22] P. M. Lv, Z. H. Xiong, J. Chang, C. Z. Wu, Y. Chen, and J. X. Zhu, "An experimental study on biomass air-steam gasification in a fluidized bed," *Bioresource Technology*, vol. 95, pp. 95-101, 2004.

4. Conclusions

The aim of this study was to provide fundamental data that are necessary for the development of steam gasification systems for the energy valorization of biomass from agro-industrial residues. Two approaches were applied in order to face this topic. The first was to compare the gas-solid reaction kinetics of steam gasification of different chars obtained from residual biomass. With such approach, it has been determined the effect of the temperature on the reaction profile and the effect of steam partial pressure. Then, the kinetic parameters were obtained according to an iso-conversional approach (model free method). The variation of kinetic parameters with conversion has been investigated, observing different trends for different samples. Thermogravimetric analysis in steam-nitrogen atmosphere showed that the different chars are characterized by different reaction profiles and different reactivity. The influence of ash-forming elements with catalytic (Ca, K) and inhibiting (Si, P) characters was evaluated by introducing the *Inorganic Composition Ratio* (*ICR* = *(Ca+K)/(Si+P)*), in order to include in one index both catalytic and inhibiting elements. A good correlation was found between *ICR* and time of half conversion. It has been noticed that samples with similar *ICR* show similar reaction profiles and comparable time of conversion. In particular, the samples with $ICR < 1$ showed marked decelerating reaction profiles, while samples with $ICR > 1$ exhibited sigmoidal reaction mode.

It was further determined that, unlike to other authors, the presence of calcium could not be neglected in order to find an acceptable correlation between kinetic behavior and ash composition, which is the biomass characteristic that has the most influence on the char gasification kinetics. The kinetic study of various feedstocks is not only fundamental for reactor design optimization, but it is also an important tool for planning a proper supply chain for steam co-gasification of local residual biomass. For instance, it was highlighted that in terms of conversion kinetic, the best feedstock integration for co-gasification could be made with orange peels and grape pomace. In addition, both residues from second-generation bioethanol showed a very similar reactivity.

The second tool, that has been intended to provide fundamental information for agro-industrial residues valorization, was the development of a simulation model used for the evaluation of the sustainability of a Combined Heat and Power (CHP) system. The CHP system that has been studied consisted in the combination of Solid Oxide Fuel Cell (SOFC) with citrus peel gasification (with air and steam as oxidants), which used residues from the citrus juice production process as fuel. Aspen Plus simulation software allowed realizing the optimization of some operative conditions, the evaluation of process energy self-sustainability and the potential of the proposed application. It was found that air-steam gasification of such residues could be potentially combined with SOFC in order to achieve good efficiency of energy conversion in small-scale applications. The issue related to the

management of such a wet residual biomass was covered by using the heat recovered from the CHP system. It should be pointed out that the consequent reduction of the CHP efficiency due to the drying step is counterbalanced by the fact that the feedstock is free of costs for a citrus juice company, since it is a residue of the same process.

Improvements of the current study could deal with the development of a detailed kinetic based simulation model. These detailed models could be very useful for the design of reactors for co-gasification of more agro-industrial residues, with the aim of local residues and wastes valorization, in order to improve short supply chains of small-scale gasification processes. Indeed, Aspen Plus simulation software allows to develop basic reactors design when kinetic reactors are employed in the system description. Another interesting topic, may be to compare energy performances of traditional gasification systems with a system were the different steps are split in more reactors, or the addition of biomass pretreatment for the reduction of the water content, in order to increase the energy density of the feedstock in a more sustainable way.

From the experimental activities of citrus peel gasification, it was evident the issue of ash agglomeration because of the very high ash content and the presence of low melting elements. This is a challenging issue to face with and maybe the biggest limitation for the application of these technologies to agro-industrial residues. It follows that a deep research on reactor design is needed. An important finding of this research activity is that some of the residues investigated in this study, such as orange peel and grape pomace, could be gasified at lower temperatures than traditional biomass (wood) and lignin reach residues. Of course this fact is helpful for the reduction of the ash agglomeration issue.

With regard to the kinetic study, addition improvement could be related to the further investigation of biomass kinetic behavior, by deepening the evolution of macro and mesopores during conversion, even in different reactive environments, and expanding the types of selected residues.

The potential for the exploitation of bio-residues and bio-wastes in Sicily is huge, due to the variety of agricultural products that this land is able to offer. Considerations about the industrial network and its products volume should steer bio-energy policies towards the promotion of small plants spread in the territory, in combination with an integrated waste management from the different processing activities, if the aim is the achievement of sustainable supply chains. Such an approach could be also of fundamental importance for the economic recovery of local agricultural or agro-industrial activities.